DISSERTATION

THE THERMOPHYSICAL AND MICROSTRUCTURAL EFFECTS OF AN ARTIFICIAL ICE LAYER IN NATURAL SNOW UNDER KINETIC GROWTH METAMORPHISM

Submitted by

Ethan M. Greene

Geosciences

In partial fulfillment of the requirements

For the Degree of Doctor of Philosophy

Colorado State University

Fort Collins, Colorado

Spring 2007

COLORADO STATE UNIVERSITY

December 8, 2006

WE HEREBY RECOMMEND THAT THE DISSERTATION PREPARED UNDER OUR SUPERVISION BY ETHAN MARSHAL GREENE ENTITLED THE THERMOPHYSICAL AND MICROSTRUCTURAL EFFECTS OF AN ARTIFICIAL ICE LAYER IN NATURAL SNOW UNDER KINETIC GROWTH METAMORPHISM BE ACCEPTED AS FULFILLING, IN PART, REQUIREMENTS FOR THE DEGREE OF DOCTOR OF PHILOSOPHY.

Committee on Graduate Work

Edward Adams

Karl Birkeland

Roger Pielke

Martin Schneebeli

Advisor—Freeman Smith

Co-Advisor—Kevin Elder

Department Head—Sally Sutton

ABSTRACT OF DISSERTATION

THE THERMOPHYSICAL AND MICROSTRUCTURAL EFFECTS OF AN ARTIFICIAL ICE LAYER IN NATURAL SNOW UNDER KINETIC GROWTH METAMORPHISM

The macrostructure of a seasonal snow cover evolves with each new weather event. With wind and precipitation, layers of snow coat the old snow surface and the microstructure within these layers develops as a function of the environmental conditions. The thermal, mechanical and optical properties of snow are highly dependent on its microstructure. Many researchers have investigated metamorphism in homogenous snow, but little is known of snow metamorphism at the interface of two layers. In this study I observe the thermal and microstructural evolution of layered and non-layered samples of natural snow in kinetic growth metamorphism. The layered samples contain a 4 mm thick ice layer, which creates a large gradient in thermal conductivity and porosity.

I collected samples of natural snow with a density range of 150 – 290 kg m^{-3} from the mountains of northern Colorado. In a cold laboratory, I subjected paired, treatment (layered) and control (non-layered), samples to a vertical temperature gradient of 60 -110 K m^{-1} for a period of 5 days. During the experiment I measured the heat flux at the boundaries and the temperature profile within the sample. At the end of each experiment I cast the snow samples and performed serial sectioning and three-dimensional reconstruction of the snow microstructure. I also used the thermophysical data and microstructural data to simulate the evolution of the microstructure and the thermal state at the end of the experiment.

The temperature profiles show snow in a steady-state thermal environment. There is no consistent signal from the ice layer in the temperature data. The microstructure within the snow samples undergoes a dramatic change during the experiments. In the control samples vertical chains of faceted and hollow particles develop and are responsible for transporting most of the thermal energy in the sample. Faceted structures grow off the bottom of the ice layer, while the upper surface erodes and becomes smooth and round. The presence of the ice layer affects thermal, mechanical and optical properties of the snow, these effects occur within several particles of the interface and would be difficult to detect with standard field techniques.

Ethan M. Greene
Geosciences
Colorado State University
Fort Collins, Colorado
Spring 2007

This work is dedicated to my grandfather, Harry Gray.

ACKNOWLEDGEMENTS

This project spanned six years, three organizations and two continents. Along the way, there were plenty of opportunities for people to contribute to this work. I am very lucky that so many people took an interest in me and this project, and offered their help. Without their interest, encouragement and assistance, I certainly would not have completed this work.

The original funding for this work came from a series of small grants from the American Avalanche Association, American Alpine Club and the Colorado Mountain Club. I would like to thank Russ Johnson and Doug Chabot for their help with these organizations. Mazamas, a mountain club based in Portland, Oregon, also awarded a not so small grant from their graduate research program. The main funding for this project came from a Dissertation Enhancement grant from the International Division of the National Science Foundation (NSF-0406468). The USDA-Rocky Mountain Research Station and Swiss Federal Institute for Snow and Avalanche Research provided facilities, equipment and research support.

Each member of my graduate committee contributed to this project. Dr. Freeman Smith agreed to be my graduate adviser after I had been in the Department of Geosciences for several years. I am grateful to him for being a great advocate, sheparding me through the Ph.D. process and continuously pushing me to complete the work while always being supportive. Dr. Roger Pielke encouraged me to pursue my own

ideas through my entire graduate school experience. He has been a consistent supporter and given me lots of good advice, even though I did not always follow it. Dr. Ed Adams was very helpful during the design phase of this project. He also helped me step out of my scientific ruts and look at topics from a different perspective. Ed is a very thoughtful scientist. He will always be my teacher, but has also become my friend. Dr. Karl Birkeland has encouraged me to study snow and avalanches since my first semester in college. Over the years I have spent countless hours with Karl discussing our experiences in the field and our understanding of snow. Karl has always dissected my ideas in a way that sent me searching for more information. He is an excellent scientist and a wonderful friend. Dr. Martin Scheebeli literally changed how I look at snow. Martin's approach to snow science was uninhibited by many paradigms that confined my perspective of snow metamorphism. He taught me to respect the work of our predecessors, but not to be confined by their approach and assumptions. He opened his office, lab and home to me. I have come to respect him as an original thinker and wonderful person. Without Dr. Kelly Elder I never would have started this work, let alone complete it. It is hard to describe the advocate Kelly has been for me over the last six years. He gave me room to explore my ideas, but was always there to help me through the hard times. Time after time he stuck up for me and helped me get the resources I needed, even when it made his own job more difficult. I have gained the utmost respect for Kelly as a person and a scientist.

While working on my dissertation I worked at three different facilities: Colorado State University (CSU), USDA-Rocky Mountain Research Station (RMRS) and the Swiss Federal Institute for Snow and Avalanche Research (SLF). At each location I met

some wonderful people that offered me their help and support. At CSU Julie Orwick helped me navigate the NSF and state requirements to spend research money. Drs. Jeff and Carol Wilusz gave me access to their staff, laboratory and equipment. At RMRS, Dr. Chuck Rhoades, Dr. Rob Hubbard, Marian Lathrop, Gus Goodbody, Jean Wheeler and Andrew Grosheider helped me laugh at my predicament, kept my motivation up and loaned or helped me acquire equipment. John Frank helped me design and build the control circuits for the heat exchangers. Rudy King and Laurie Porth helped with the statistics. At SLF I would like to thank Dr. Michael Lehning, Daniela Schmid, Bernd Pinzer, Dr. Thomas Kaempfer, Dr. Margret Matzl, Reto Kolas and Reto Wetter for their help. Madeleine Oberhänsli helped me obtain the necessary permits to be a visiting scientist in Switzerland. Dr. Christine Pielmeier, Julia Wessel and Dr. Thomas Wiesinger helped me make the most of my time in Switzerland and cope with the long absences from home. In addition to these groups, Dr. Lee Dexter and Dr. Matthew Sturm gave me encouragement and very helpful suggestions and Larry Scott created the schematics in Chapter 3.

Last I would like to thank my family. Without the love and support of my mother, Reggie Gray, I would never have had the confidence to pursue my own ideas and interests. She help me through many turbulent years in the public school system and supported me during my nontraditional career path. My father, Bruce Greene, allowed me to set and pursue my own goals. My wife, Dr. Dana Greene, gave me the confidence to accept difficult challenges and the determination to follow them to a logical conclusion. Without her unconditional love and support, I would have never completed this project. Recently my daughter, Elona Greene, has given me a completely new perspective on life. I love you all and cannot thank you enough.

TABLE OF CONTENTS

LIST OF FIGURES

LIST OF TABLES

LIST OF SYMBOLS

AT	air temperature (ºC)
C_p	specific heat of ice at constant pressure (J K^{-1} kg^{-1})
D_w	diffusion coefficient for water in air (m^2 s^{-1})
E	root mean squared error, or measurement error
E_{UB}	root mean squared error with constant bias removed
Gr	Grashof number
g	acceleration due to gravity (m s^{-2})
I	number of intersections of a stereological probe and structural component
k	thermal conductivity (W m^{-1} K^{-1})
k_e	effective thermal conductivity (W m^{-1} K^{-1})
L	latent heat of vaporization (J kg^{-1})
l	length of a stereological probe
l	length measurement, characteristic length
P	count of point in a stereological grid
p	grid point in a stereological grid
$\boldsymbol{q}$	heat flux vector (W m^{-2})
q	heat flux (W m^{-2})
$\hat{S}_V$	estimated surface density

SSA_i	specific surface area with respect to ice
T	temperature (K or °C)
T_{sfc}	surface temperature (K or °C)
T_{sur}	surrounding temperature (K or °C)
$\hat{V}_V$	estimated volume fraction
Y	component of a structure in stereology
z	vertical coordinate
α	probability rejection crierion for hypothesis testing
β	volume coefficent of expansion for gas
ε	emissivity (dimensionless)
ϕ	predicted value
ϕ_{obs}	observed value
ϕ_0	mean of observed or predicted value
μ	dynamic viscosity
ρ	mean snow density
ρ_v	water vapor mass concentration (kg m^{-3})
σ	Stefan-Boltzmann constant (W m^{-2} K^{-4}), standard deviation

Chapter 1

INTRODUCTION

1.0 Introduction

Snow and ice on the ground account for a significant portion of the Earth's fresh water and play critically important roles in the hydrologic cycle. Up to 10% of the Earth's land surface is covered by perennial snow and ice formations and over 30% is covered by seasonal snow (Dozier, 1989). In addition, monthly averages of land area covered by snow in the Northern Hemisphere range from 7 to 40% annually, making snow cover the most rapidly varying large-scale surface feature on Earth (Hall, 1988). Through surface energy fluxes, snow cover distributions affect atmospheric temperatures and mesoscale circulation patterns (Segal et al., 1991; Leathers et al., 1995; Taylor et al., 1998). Although these feedbacks occur on the mesoscale, the surface energy exchange that drives them occurs at a much smaller spatial scale.

Previous studies of snow metamorphism generally consider a snow cover with homogenous properties. Although this greatly simplifies heat and mass transfer problems, it does not adequately represent what is observed in the field (Colbeck, 1991; Pielmeier and Schneebeli, 2003). In nature, a series of accumulation and ablation events combine to form a layered structure within a given snow cover. The interactions between these layers and their effect on snow microstructure have been examined from a theoretical perspective (Adams and Brown, 1990; Colbeck, 1991; Colbeck and

Jamieson, 2001). However, field and laboratory studies to confirm or disprove these theoretical results have not been completed.

In this study I conducted a series of laboratory experiments and model simulations to investigate the effects of layering on snow microstructure. I focused on a stratigraphy where a thin layer of ice creates a large gradient in density and porosity. Paired snow samples, homogenous snow samples and samples that contain an artificial ice layer, were subjected to a thermal gradient in a controlled environment. I then analyzed the microstructure of the snow with serial planar sections and stereological techniques and conducted numerical simulations of the experiments. The results of this study have implications for atmospheric and hydrological modeling efforts, as well as cold regions research and avalanche research programs.

1.1 The Significance of Snow Microstructure

Sensible and latent energy are transferred through a snow cover by a combination of conduction, convection, and diffusion processes (Armstrong, 1985). The efficiency of these processes is governed by environmental conditions, boundary conditions, and the microstructure of the snow. Metamorphic processes within a snow cover create a complicated matrix of ice, water, water vapor, and air. The characteristic size, shape, and number of ice bonds between grains vary with different metamorphic processes. Snow microstructure impacts energy transfer within the snow because the geometry of the ice grains, bonds, and pore spaces dictate how heat and mass move through the snow. The effects of microstructure on energy transfer cannot be directly correlated to bulk snow properties such as density because the number and size of ice

bonds can vary in snow samples of similar density (Kry, 1975; Sturm et al, 1997; Adams and Sato, 1993).

Advances in remote sensing have allowed us to collect important information about the cryosphere. These techniques have provided a wealth of data that support both modeling and observational studies in a variety of fields. Although our knowledge of interactions between electromagnetic waves and ice has greatly increased, these interactions remain complex. Microstructural parameters such as grain shape and size have a large effect on the electromagnetic response of snow (Dozier, 1989; Davis et al., 1987; Grenfell et al., 1994; Grenfell and Warren, 1999; Matzler, 2002), yet we still know little about the evolution of microstructural parameters. A better understanding of how snow microstructures develop will benefit efforts to collect snow cover data remotely (Carsey, 1992). Matzl (2006) showed the complexity of snow microstructure in profiles using near infrared photography and discussed the link between microstructural parameters (specific surface area with respect to ice) and optical properties (optical diameter).

In mountainous regions, property and transportation arteries are threatened by the destructive power of snow avalanches. Avalanche accidents are increasing as more people venture into the backcountry for winter recreation and as human settlements move into mountainous environments (Atkins and Williams, 2000). In the United States, avalanches cause more fatalities than many other natural hazards including earthquakes (Voight, 1990) and the annual number of fatalities due to avalanches has increased from less than 10 in the 1970's to over 30 since the 2001/2002 winter (Figure 1.1). Avalanches have an economic impact on society by destroying infrastructure, delaying

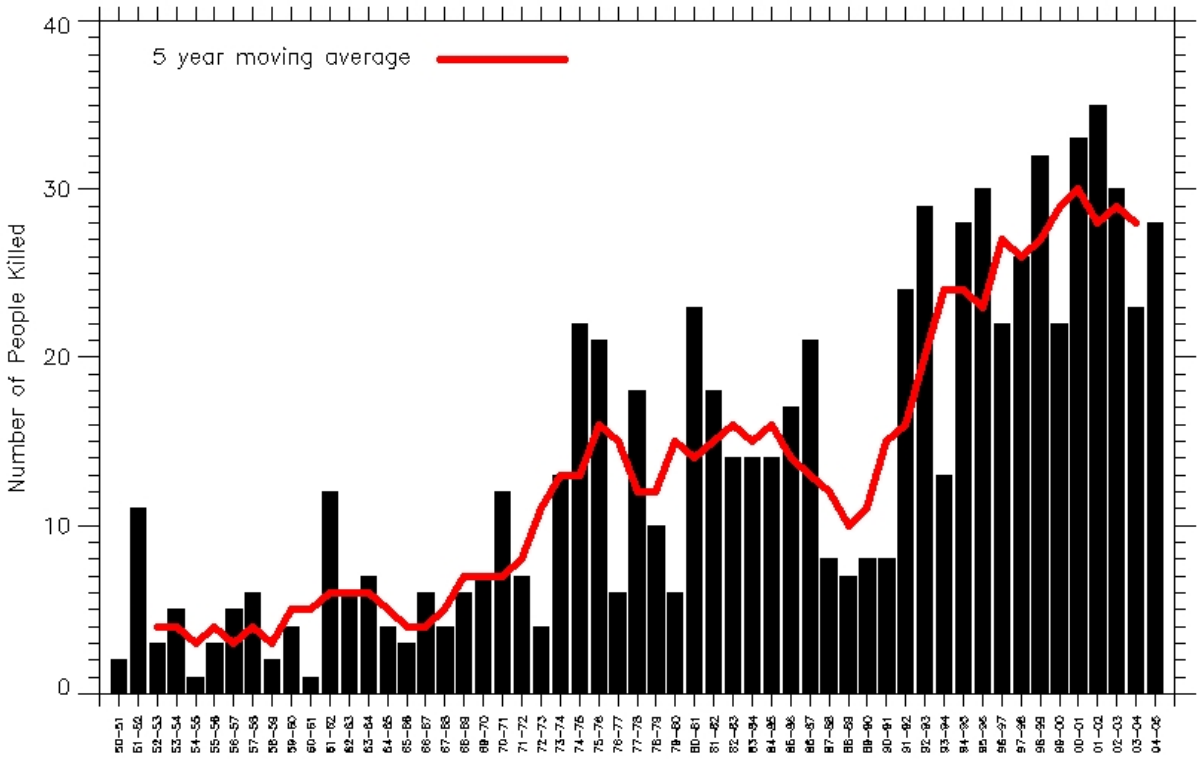

Figure 1.1: Number of people killed in the United States by avalanches from 1950 through 2005 (Courtesy of the Colorado Avalanche Information Center and Dale Atkins).

the transportation of goods, and increasing the need for wilderness rescues. An estimated $750,000 in revenue is lost each hour that Interstate-90 through Snoqualmie Pass in Washington State is closed by avalanches (Moore et al., 2003). By increasing our understanding of snow and how metamorphism affects its physical properties we can improve avalanche forecasts, saving lives and reducing property damage.

1.2 Heat Transport in Snow

In nature, heat can be transported within the snowpack and between the snowpack and its environment by all three transport mechanisms: conduction, convection, and radiation. In a laboratory setting, transport by one or more of the

mechanisms can be limited or in some cases completely removed. By stating the different heat transport components and examining their relative magnitudes, we can obtain a better understanding of the experiment and how the results presented in this document can be applied to snow covers in nature.

The transport mechanisms have five components that move heat into or through a natural snow cover: 1) conduction through the ice matrix, 2) conduction through air in the pore spaces, 3) convection through the pore spaces, 4) long wave radiation exchange, and 5) short wave radiation exchange. In addition, latent heat is transported through snow as water mass sublimates off of an ice crystal, diffuses through the pore space, and deposits on an adjacent ice grain.

If the total internal energy within the system is U, and the internal energy per unit mass is u, then ρu is the internal energy per unit volume. Neglecting any mechanical effects, the sum of the energy generated within the control volume and any energy that moves into that control volume is equal to the amount of energy contained within the control volume, or

$$\frac{d}{dt}\int_V \rho u dV = -\int_S \boldsymbol{q}\cdot\boldsymbol{n} dS + \int_V \rho r dV \tag{1.1}$$

where $\boldsymbol{q}$ is the heat flux, $\boldsymbol{n}$ is the unit vector normal to the surface of the control volume and r represents any energy generated within the control volume. Using the divergence theorem this becomes

$$\frac{d}{dt}\int_V \rho u dV = -\int_V \nabla\cdot\boldsymbol{q} dV + \int_V \rho r dV \tag{1.2}$$

and if the volume of the system does not change, it reduces to

$$\int_V \left(\frac{d}{dt} \rho u + \nabla \cdot \boldsymbol{q} - \rho r \right) dV = 0 \tag{1.3}$$

For an arbitrary volume, the conservation equation becomes

$$\frac{d}{dt} \rho u + \nabla \cdot \boldsymbol{q} - \rho r = 0 \tag{1.4}$$

For this discussion, we are interested in the thermal energy contributions to u, and if u is a function of temperature only then

$$u = c_p T \tag{1.5}$$

where c_p is the specific heat of snow at a constant pressure. If we neglect any processes that generate thermal energy within the control volume, our energy conservation equation becomes

$$\rho c_p \frac{dT}{dt} = -\nabla \cdot \boldsymbol{q}_{total} \tag{1.6}$$

The right side of Equation 1.6 represents the heat flux. As described above, heat flux in snow includes: conduction through the ice matrix, conduction through the air in the pore spaces, convection through the pore spaces, radiative flux of long and short wave energy, and latent heat from water mass changing phase. The total heat flux is the sum of all of the contributions from each component.

$$\boldsymbol{q}_{total} = \boldsymbol{q}_{condution\_ice} + \boldsymbol{q}_{conduction\_air} + \boldsymbol{q}_{convection} + \boldsymbol{q}_{LW} + \boldsymbol{q}_{SW} + \boldsymbol{q}_{latent\_heat} \tag{1.7}$$

The conductive heat flux in ice can be described by *Fourier's Law* (Incropera and De Witt, 2002)

$$\boldsymbol{q}_{conduction} = -k\nabla T \tag{1.8}$$

Snow is composed of both air and ice and conduction through each component must be considered separately. However, since the thermal conductivities of ice (k_{ice} = 2.4 W m^{-1} K^{-1}, (Petrenko and Whitworth, 1999)) and air (k_{air} = 0.024 W m^{-1} K^{-1}, (Wallace and Hobbs, 1977)) differ by a factor of 100, heat conduction through the air in snow is typically neglected ($\boldsymbol{q}_{air} << \boldsymbol{q}_{ice} \therefore \boldsymbol{q}_{air} \approx 0$) (Kaempfer et al., 2005).

The contribution of convection to heat transfer in natural snow covers has been debated for many years. Although it is generally accepted that air flow through snow would have dramatic effects on snow metamorphism (Bell, 1993; Clark and Waddington, 1991; Colbeck, 1989), the conditions under which convection could occur remain ill-defined (Sturm and Johnson, 1991; Powers et al., 1985a, b; Palm and Tveitereid, 1979; Akitaya, 1974). Sturm and Johnson (1991) observed convective cells in the natural subarctic snowpack with updraft and downdraft size on the order of 1 and 0.3 m respectively (i.e. cells on the order of 1.3 m). They concluded that convection does occur in snow, but that their results may not apply to snow in other climates where the permeability and thermal gradients are much smaller. Laboratory results are also less than conclusive. Akitaya (1974) concluded that convection could occur in snow with a high permeability that was under a large thermal gradient (≥ 200 °C m^{-1}). Powers et al. (1985a, b) observed convection in the laboratory with snow that had a grain size of 1.5 mm and was under a temperature gradient in excess of 500 °C m^{-1}. It is unlikely that convection was a significant heat transfer mechanism in the experiments described in

this document (see Chapter 4, section 4.1). Therefore the heat flux contribution from convection can be neglected (i.e. $\boldsymbol{q}_{convection} \approx 0$).

Radiation is an important heat transfer mechanism in natural snow covers. The upper portion of the snowpack is heated by incoming solar radiation and cooled as it radiates into the atmosphere in the infrared bands. Although $\boldsymbol{q}_{SW}$ and $\boldsymbol{q}_{LW}$ are important source and sink terms in nature, they play minor roles in this study. Snow metamorphism occurred in a dark cold room and therefore heating from incoming short wave radiation was not possible. The temperature of adjacent ice grains within a snowpack differ by a fraction of a degree and therefore radiative heat transfer between grains is negligible. In addition, the surface of the experimental snow samples was covered by an aluminum plate whose temperature was very close to the temperature of the snow surface. Therefore radiative exchange in both the short and long wave bands can be neglected in these experiments (i.e. $\boldsymbol{q}_{SW} \approx 0$ and $\boldsymbol{q}_{LW} \approx 0$).

In addition to conduction, convection, and radiation, latent heat is transported through the snowpack as water mass diffuses through the pore spaces. This mechanism was described by Yosida and colleagues (1955) as “hand-to-hand” transport of heat and mass is now recognized as an important component of the total heat transfer in snow. The flux of latent heat can be described by including latent heat in Fick’s first law of diffusion

$$\boldsymbol{q}_{latent\_heat} = -LD_w \nabla \rho_v \tag{1.9}$$

where L is the latent heat of vaporization, D_w is the diffusion coefficient of water vapor in air, and ρ_v is the water vapor mass concentration within a given control volume.

After considering the laboratory conditions and the relative magnitudes of each component of heat transfer, we need to represent both conduction through the ice matrix and latent heat exchange. Therefore the total rate of heat gain within the control volume that includes conduction through the ice matrix and latent heat exchange becomes

$$\rho c_p \frac{\partial T}{\partial t} = -\nabla \cdot (\boldsymbol{q}_{ice\_conduction} + \boldsymbol{q}_{latent\_heat}) \tag{1.10}$$

Since the lateral flow of heat within these laboratory experiments is much smaller than the vertical flow, we can neglect heat flux in all but the vertical direction. Combining equations 1.8, 1.9 and 1.10 yields the rate equation

$$\rho c_p \frac{\partial T}{\partial t} = \frac{\partial}{\partial z}(k \frac{\partial T}{\partial z}) + L_w D_w \frac{\partial^2 \rho}{\partial z^2} \tag{1.11}$$

which describes the transport of heat within the snow samples used in these laboratory experiments. However, temperature and heat flux were the only parameters measured. With these fields we cannot differentiate the contribution of conduction from the contribution of diffusion. Therefore, it makes sense to combine these effects into one term. With this simplification the rate equation becomes

$$\rho c_p \frac{\partial T}{\partial t} = \frac{\partial}{\partial z}(k_e \frac{\partial T}{\partial z}) \tag{1.12}$$

where k_e is the effective thermal conductivity. The effective thermal conductivity represents the contributions of conduction through the ice matrix and latent heat transfer by diffusion. However, in reality it also represents the sum of all active heat transport

mechanisms. Therefore, it becomes a simplistic method for representing heat transfer components that cannot be explicitly represented in the rate equation.

1.3 Research Objectives

The objective of this study is to investigate the effects of temperature gradients on an ice layer buried in snow. To limit the scope of the investigation, I focus on snow in the kinetic growth regime. Kinetic growth is characterized by high crystal growth rates and an environment with a large temperature gradient. The specific methodology is presented in Chapter 3. The research questions I address in this study are:

1. Is there a consistent effect on the thermophysical properties of the snow sample from the presence of the ice layer?

2. Is there a local increase in the temperature gradient due to the ice layer?

3.Is there a consistent difference between the structures that develop in the homogenous and layered samples?

4. Is there a consistent difference between the structures that develop along the upper and lower interfaces of the ice layer?

5. Can current numerical models of snow metamorphism simulate the evolution in the thermophysical properties we observed?

1.4 Terminology

The terminology in snow science is fairly well established, but there are aspects of this study that are not completely addressed by the current vernacular. Therefore, clarification of terms used throughout this document is necessary. Snow microstructure is generally described by snow grain characteristics. Snow grains are defined as:

> The obvious subunit in snow on the ground. In snow research, this term does not have the same meaning as the term in metallography. (Sommerfeld, 1976)
>
> The smallest characteristic subunit of snow texture recognizable with a hand lens (e.g.10x); it can consist of one or more crystals of ice. (Colbeck et al., 1990)
>
> The smallest distinguishable ice component in a disaggregated snow cover. Usually synonymous with crystal in snow applications. The term grain can be used to describe polycrystal formations when the crystal boundaries are not easily distinguishable with a field microscope. (Greene et al., 2004)

Each of these definitions describes disaggregated snow crystals. However, the thermal, optical and structural properties of snow are governed by the intact microstructure and disaggregating the crystals destroys much of the vital information sought by researchers. In this study I examine the intact microstructure and therefore discussion of grains, as previously defined, is inadequate. Instead I propose and use the following terms:

> *Particle* – The smallest discernable but repetitive unit of snow. Particles within a snow layer are repetitive in shape but not necessarily in size.
>
> *Structure* – A connected portion of ice in snow containing one or more particles.

The SNOWPACK model uses the conceptual model of grains and the snow grain classification to represent the snow. In that section I use the traditional snow grain terminology.

Chapter 2

PREVIOUS WORK

2.0 Introduction

The scope of this study encompasses several different topics within the scientific literature. In order to address issues relevant to the proposed study, the following review will focus on: field observations of faceted snow near an ice crust, investigations of snow layering and metamorphism, investigations of snow microstructure, stereology and snow, thermal conductivity measurements of snow, and the modeling of snow covers.

2.1 Field Observations of Faceted Snow near Ice Crusts

In nature, faceted snow layers have been observed both above and below dense snow layers or crusts (McClung and Schaerer, 1993). This stratigraphy may have been first recorded by Seligman (1936) and has been well documented in the Arctic and Antarctic regions (Palais, 1984; Alley, 1988; Steffen et al., 1999; Domine et al., 2002). Faceted snow layers near ice crusts have also been observed in mid-latitude regions. Moore (1982) described the formation of faceted grains above a hard ice layer in the Cascade Mountains of Washington. LaChapelle (1970) and Armstrong (1985) observed faceted layers near sun crusts in the San Juan Mountains of Colorado. Fierz (1998) describes the formation of faceted grains below a surface ice crust in the Swiss Alps. Jamieson et al. (2001) describe two separate events where layers of faceted snow grains

formed above an ice crust in the Columbia Mountains of British Columbia. Greene and Johnson (2002) observed the formation of faceted snow grains both above and below an ice crust in the Wasatch Mountains of northern Utah. Moore (1982), Jamieson et al. (2001), and Greene and Johnson (2002) all describe significant avalanche cycles associated with the crust-facet combination. Although these authors observed and described microstructural changes around buried ice layers, none of these studies quantified the effects of an ice lens on the microstructure. Jamieson (2006) presents a comprehensive review of snow metamorphism around freezing wet layers and how it pertains to avalanche formation.

2.2 Investigations of Snow Layering and Metamorphism

Previous investigations on the effects of layering on snow metamorphism can be divided into three groups: 1) theoretical explanations, 2) modeling investigations, and 3) laboratory studies. Theoretical explanations describe how changes in the permeability and thermal conductivity of snow layers affect the movement of heat and mass through a snow cover (Colbeck, 1983a; Colbeck, 1991). The presence of a denser and less permeable layer disrupts the flow of water vapor, causing a local increase in condensation and therefore, crystal growth rates. The denser layer also has a higher thermal conductivity than the surrounding snow. The difference in thermal conductivity between the high and low density layers causes an increased temperature gradient at the layer interface. The larger thermal gradient in turn causes crystal growth rates to increase. As the growth rates increase the morphology of the crystals will change from rounded equilibrium forms to faceted kinetic forms. Numerical models using classical

and continuum approaches have been applied to heat and mass transport problems in layered snow covers (Adams and Brown, 1983; Adams and Brown, 1990). These studies predict a locally higher vapor flux near the boundaries of a dense snow layer, which contributes to the formation of faceted snow grains.

Colbeck and Jamieson (2001) examined a situation where a wet layer freezes, releasing latent energy and forming a crust. Their results show an increase in growth rates up to 27 hours, which may be beyond the time required for the latent heat, released as the crust forms, to disperse. Jamieson and van Herwijnen (2002) conducted laboratory experiments to observe this process. They constructed a layered sample of wet snow sandwiched between two dry snow layers. As the wet layer froze, faceted grains formed near the wet-dry snow interface and in the upper dry snow layer. Jamieson and Fierz (2004) present a combined laboratory and modeling study of heat transfer and metamorphism around a wet snow layer as it freezes. They describe an evolution in the thermal state of the snow as the wet layer freezes and then the snow reaches a quasi-steady-state temperature profile. They also note that the strong thermal gradients that exist around the wet layer, before and while it freezes, are conducive for kinetic growth and the formation of faceted snow. Fierz (1998) followed the development of a faceted snow layer in the field and then modeled its progression. Near-surface processes heavily influenced the metamorphism of this layer, but he noted that the model was limited by its representation of grain texture. Adams and Brown (1982) subjected heterogeneous snow samples, composed of newly fallen and old rounded snow, to a large temperature gradient. Their results showed a slight increase in strength

above, and a decrease in strength below, a dense layer. The snow below the dense layer continued to lose strength for up to a week.

2.3 Investigations of Snow Microstructure

Numerous researchers have recognized the significance of microstructural characteristics on the thermal and mechanical properties of snow. Seasonal snow covers are typically quite fragile; hence a preparation method is required so that snow samples can be characterized using standard material science techniques. Commonly used methods rely on capillary action or vacuums to draw a supercooled liquid through the porous snow. The liquid is then frozen producing a solid block of snow and filler material. Previous research into preparation methods have used a variety of filler liquids: tetrabromoethane (Bader et al., 1939), ethyl laurate (Bader et al., 1939), diethyl phthalate (de Quervain, 1950; Matzl, 2006), a water-detergent mixture in thin film-coated snow (Fuchs, 1956), aniline (Kinosita and Wakahama, 1959), different types of acid and cinnamate solutions (Watanabe, 1974), dimethyl phthalate (Perla, 1982; Good, 1989), and phtalic acid diethyl ester (Good, 1982; Brzoska et al., 1998). Perla (1982) offers a thorough discussion of the chemical properties of several appropriate filler liquids.

Once the fragile quality of the sample has been reduced, thin sections or planar sections of the snow sample are cut with a microtome and the two-dimensional plane is sampled via photography and evaluated using stereological methods. Thin sections can be observed with either transmitted or reflected light. Previous researchers have used thin sections to observe crystallographic orientation (Bader et al., 1939), changes in

grain boundaries (Yosida, 1963), texture or grain size and shape distributions (Fuchs, 1959; Keeler, 1969; Akitya, 1974; Gow, 1975; Kuroiwa, 1975; Good, 1980; Good, 1982; Good, 1987; Nakamura et al., 1998), and liquid water content (Brzuska et al., 1998). Planar sections can only be observed with reflected light. Planar sections have been used extensively to characterize the microstructure of snow (Narita, 1969; Narita, 1971; Good, 1980; Sommerfeld, 1983; Perla and Doizer, 1984; Perla, 1985; Perla and Ommanney, 1985; Akitaya, 1986; Davis et al., 1987; Shi et al., 1993; Sato et al., 1997; Pfeffer and Mrugala, 2002; Pielmeier and Schneebeli, 2003; Sethi et al., 2002) and compare it to topological parameters (Good, 1975). Results from section analysis have also been used to determine mechanical properties of snow (Dozier et al., 1987; Good, 1987; Davis et al., 1996; Davis et al. 1998; Fohn et al., 1998) and to examine the properties of bonds and the connectivity of grains (Kry, 1975; Gubler, 1978; Alley, 1986; Hansen and Brown, 1986; Edens and Brown, 1991; Brown and Edens, 1991; Edens and Brown, 1992; Davis et al., 1996; Davis et al., 1998). To my knowledge there has been limited use of microstructural sections to investigate thermal properties of snow (Murakami and Maeno, 1989; Sato et al., 1994).

Serial sectioning is the process of taking successive planar sections in order to gain information about a material in three dimensions. This technique has been widely used in biological sciences and has also been applied to material science problems (Dehoff, 1983). However, the number of sections required, combined with time required to prepare each planar section, has limited its application in snow microstructural studies (Perla et al., 1986). Previous studies that used serial sectioning have focused on techniques (Perla et al., 1986; Good, 1987; Good, 1989; Schneebeli, 2000; Coleou et al., 2001), validation of two-dimensional models (Edens and Brown, 1992), or observations of structure and mechanical properties (Fohn et al.,

1998). The recent construction of a coupled sectioning and imaging facility at the Swiss Federal Institute for Snow and Avalanche Research allows for automation of the serial sectioning process (Schneebeli, 2000). Once serial sections have been obtained, a three-dimensional model of the sample can be reconstructed.

Recently several research groups have used electromagnetic imaging to observe the microstructure of snow. Two-dimensional images and three-dimensional reconstruction have been accomplished via X-ray tomography (Coleou et al., 2001; Flin et al., 2001), computed tomography (CT-scan) (Lundy and Adams, 1998; Lundy et al., 2002; Schneebeli and Sokratov, 2004), and magnetic resonance (MR) imaging (Ozeki et al., 2000; Ozeki, et al., 2003). Changes in specific surface area have been investigated with optical and electron microscopy (Dominé et al., 2001; Dominé et al., 2003; Legagneux et al., 2003; Legagneux et al., 2004). Although these techniques show some promise, they are all limited by the expense of the equipment needed. In addition, MR imaging of snow is a destructive technique since a contrasting agent must be placed in the pore spaces to resolve the boundaries of ice grains (Ozeki et al., 2003), and spatial resolution of MR images are currently insufficient for studying the bonds between ice grains in a snow cover (Constable and Henkelman, 1991; Grönemeyer and Lufkin, 2000).

2.4 Stereology Applied to Snow Microstructure

Stereology is a group of mathematical methods used to calculate and/or estimate properties of a three-dimensional structure from measurements made on a two-dimensional plane. These methods can be divided into first-order techniques (estimates of means and total counts of quantities) and second-order techniques (spatial distribution of quantities) (Howard and Reed, 1998). Previous authors have used first-order techniques to characterize the

microstructural properties of snow (Sommerfeld, 1983; Perla and Ommanney, 1985; Davis et al., 1987; Shi et al., 1993; Pfeffer and Mrugala, 2002; Pielmeier and Schneebeli, 2003; Matzl, 2006), investigate mechanical properties of snow (Kry, 1975; Gubler, 1978; Perla et al., 1986; Good, 1987; Edens and Brown, 1991; Davis et al., 1996; Davis et al., 1998), and examine the properties of bonds between ice grains (Kry, 1975; Gubler, 1978; Alley, 1986; Hansen and Brown, 1986; Edens and Brown, 1991; Brown and Edens, 1991; Davis et al., 1996; Davis et al., 1998).

One of the basic tenets of stereology is the assumption that elements of the material are isotropic, uniform, and randomly distributed (IUR) (Howard and Reed, 1998). Although these assumptions are valid for many materials, snow can be highly anisotropic due to the formation of features in the direction of water vapor flow. One approach to characterizing anisotropic materials is to sample on planes with a randomly selected orientation (Howard and Reed, 1998; Russ and Dehoff, 2000). This requirement is nearly unattainable with destructive sampling. However, stereological techniques can be applied to anisotropic materials provided the orientation of the section is fixed and perpendicular to isotropic features in the structure and the position is random (assumption of VUR) (Howard and Reed, 1998; Baddeley et al., 1986). Estimates from VUR sections are equivalent to estimates from IUR sections if cycloid probes are used instead of line probes.

2.5 Thermal Conductivity Measurements of Snow

The transport of heat through a snow cover is a complex process that involves conduction through the ice structure and pore spaces, convection and radiation within the ice network, and latent heat transported by the diffusion of water through the pores. In most cases,

previous researchers have not attempted to measure the actual thermal conductivity of snow, but rather an effective thermal conductivity. An effective thermal conductivity includes the combined effects of two or more transport processes. A common methodology is to limit as many of the transport mechanisms as possible, and allow the measured value to represent those that remain. The thermal conductivity cannot be easily estimated by bulk characteristics such as density or grain size and shape (Sturm et al., 1997). The heat transfer properties of snow are highly dependent on the nature of its microstructure as well as the temperature and liquid water content of the material (Sturm et al., 1997; Singh, 1999; Sturm et al., 2002; Schneebeli and Sokratov, 2004).

Sturm et al. (1997) provide a detailed review of 27 studies where the thermal conductivity of snow was measured. According to their analysis, methods used in snow measurements generally fall into three categories: Fourier methods, steady-state methods, and transient methods. Fourier methods involve measuring the temperature at various levels in the snow and calculating the thermal diffusivity from the attenuation of the thermal wave. The thermal conductivity is the product of the thermal diffusivity, specific heat, and density of a material (Incropera and DeWitt, 2002). Steady-state methods involve exposing a snow sample to a constant and known heat source until it reaches thermal equilibrium. Temperatures within the sample are then measured and the thermal conductivity calculated as the quotient of the heat flux and the temperature gradient within the sample (Incropera and DeWitt, 2002). Transient heat methods involve exposing a sample in thermal equilibrium to a point heat source. The timing of the snow's thermal response is recorded and the thermal conductivity can be calculated by a modification of Fourier's heat equation that accounts for latent heating (Sturm and Johnson, 1992).

2.6 Modeling of Snow Covers

In order to simulate the microstructural development of a snow cover, a model that represents the thermal and mechanical properties of a heterogeneous snow cover is required. Brun et al. (1989 and 1992) developed a one-dimensional heat and mass transport model that was capable of simulating a layered snow cover (CROCUS). CROCUS has also been coupled to an atmospheric model (SAFRAN) and an expert system (MEPRA) for avalanche forecasting applications (Durand et al., 1999). In addition Crocus has been coupled to a global climate model to improve global climate simulations (Brun et al., 1999), used for hydrological applications (Etchevers et al., 2001), and used to simulate sublimation during surface hoar development and depletion (Hachikubo, 2001).

Jordan (1991) created a one-dimensional heat and mass transfer model to investigate snow surface temperatures (SNTHERM). SNTHERM has been used to investigate a wide array of snow related phenomena including spectral properties (Davis et al., 1993), snowmelt (Rowe, et al., 1995; Cline, 1997), and surface energy balance (Cline, 1997; Davis et al., 1997; Gustafsson et al., 2001).

A collaborative effort between scientists at the Swiss Federal Institute for Snow and Avalanche Research, Montana State University, and the Snow and Avalanche Study Establishment (Manali, India) has created a sophisticated snow cover model for research and operational avalanche forecasting (SNOWPACK) (Bartelt and Lehning, 2002; Lehning et al., 2002; Lehning et al., 2002). The model uses rate equations to predict grain size, bond size, and two grain-shape parameters (dendricity and sphericity). These equations are a combination of mixture theory, classical physical relations, and empirical relations. SNOWPACK has been used in research applications (Fierz and Baunach, 2000) and is currently used for an operational

avalanche forecasting program in Switzerland. Bartelt et al. (2004) developed a model that uses nonequilibrium equations for heat and mass transport in snow. The model treats the ice and air components of the snow separately allowing the model to diagnose entropy production, but also requiring initial condition information on the thermal state of each component.

Miller (2002) used a set of differential equations coupled through a phase change to represent dry snow metamorphism. His two-dimensional equations for energy and mass transfer were used to represent a one-dimensional snow cover. To my knowledge this is the first model that is capable of representing equilibrium and kinetic growth as well as the transition between them. This model has only been used to simulate homogenous snow covers, but is flexible enough to represent a more complex stratigraphy.

Kaempfer et al. (2004) adapted a model of elastic stress in bone structures to simulate the thermal state of an ice structure. The model requires a three-dimensional representation of the ice structure of snow as well as the temperature at the boundaries. It solves a stationary energy equation to determine the temperature distribution within the ice matrix. The model does not account for heat transfer in the pore spaces and does not evolve through time.

Chapter 3

RESEARCH METHODOLOGY

3.0 Laboratory Experiments

The laboratory experiments in this study were designed so that I could reproduce the experiment multiple times with comparable results. Samples were collected in the field, stored and used in experiments in a systematic manner. The complete laboratory protocol is listed in Appendix A.

3.0.1 Snow Sample Collection

The snow samples used in the laboratory experiments were collected at one of three sites in the northern mountains of Colorado: 1) Rabbit Ears Pass, 2) Buffalo Pass and 3) Fool Creek (Figure 3.1). The sampling locations at each site were high in elevation (above 2700 m a.s.l.), near level, devoid of trees or large vegetation, and sheltered from the wind. The snow was collected in blocks approximately 28 x 43 x 16 cm in dimensions. The blocks were cut from a single layer of the snowpack and placed in cardboard boxes (Figure 3.2). The boxes of snow were placed in large coolers and packed in snow and dry ice. The coolers were placed on an air mattress in the bed of a pickup truck, covered in insulation, and transported to the Rocky Mountain Research Station (RMRS) in Fort Collins (1250 m a.s.l.). The maximum temperature

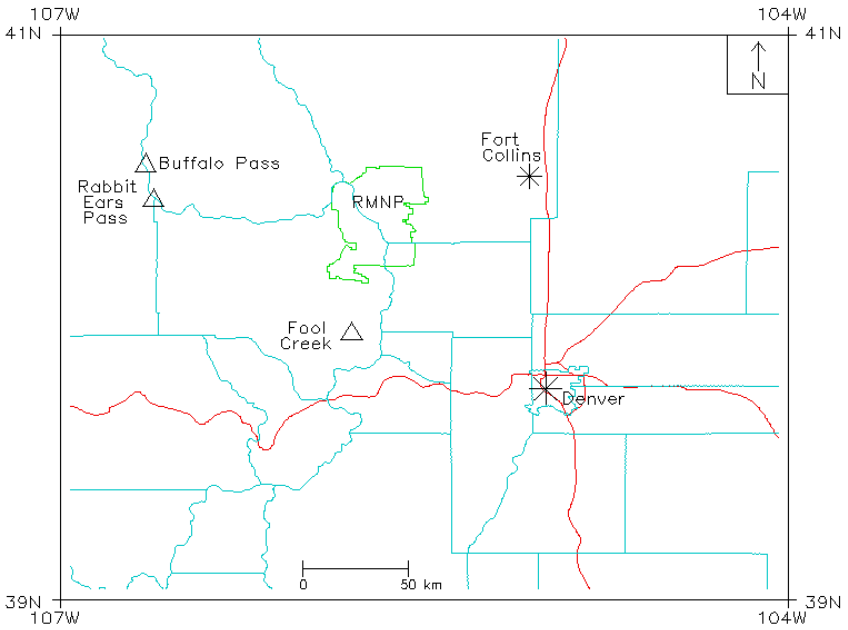

Figure 3.1: Map north-central Colorado. The snow collection sites are marked as well as the Rocky Mountain Research Station in Fort Collins. The red lines are Interstate highways and the blue lines are the county boundaries. Rocky Mountain National Park is outlined in green.

inside each cooler was recorded during transportation to insure that the cold temperature integrity was not compromised in transit. At the RMRS, the boxes were removed from the coolers and stored at -25 °C.

Snow with specific physical properties was collected for the laboratory experiments. Each sample had to: 1) have a high porosity (between 0.7 and 0.85), 2) be from a single snowpack layer at least 15 cm thick, and 3) have grains that were more round than angular. The most important property considered in sample selection was porosity; however, in the field it is much easier to measure snow density. Although sample location and timing were carefully considered, the type of snow selected was primarily controlled by availability. A savvy field observer might know the best place to collect samples on a given day, but in general the density of the snow used in these

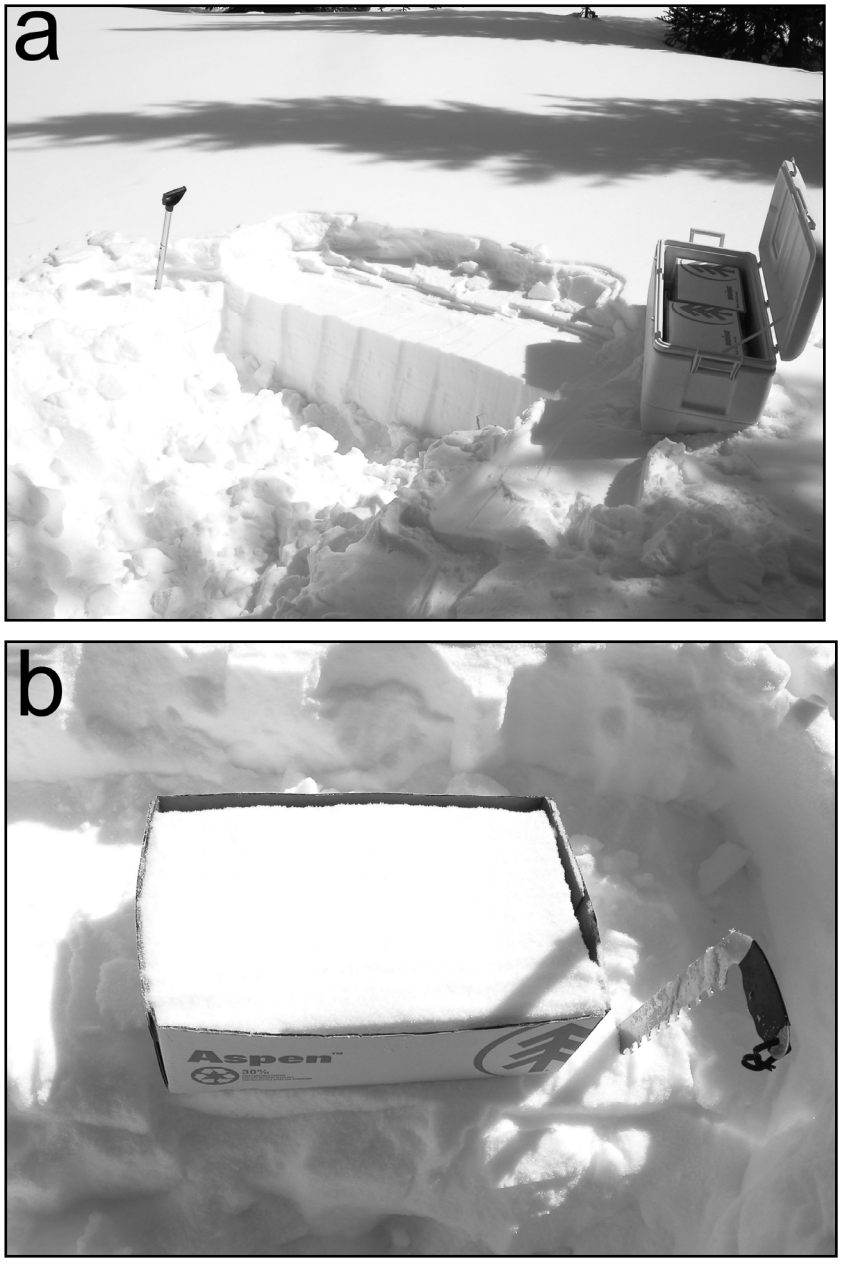

Figure 3.2: Snow sample collection site: a) snow sample preparation. b) a harvested snow sample.

experiments was controlled by Mother Nature. Ideally snow with a density equal or less than 200 kg m^{-3} was selected. However, at times snow samples with densities in excess of 250 kg m^{-3} were sampled. Samples in this study ranged from 153 to 274 kg m^{-3}.

3.0.2 Introducing Artificial Ice Layers to Natural Snow

Ice layers of various thickness and porosity form in natural snow covers. These hard layers or crusts typically form during precipitation or melt-freeze events. This study focused on a particular type of ice layer, a thin crust that might form during a very light precipitation event such as a mist or a surface melting event of short duration. The result is a nearly solid layer of ice a few millimeters thick.

Several methods for creating an ice layer were investigated. The goal of this investigation was to find a reproducible process that created a relatively uniform and level ice layer. The criteria for the method and resulting ice layer were: 1) the method had to create ice layers of similar thickness over multiple iterations, 2) the process must not introduce contaminants into the sample, 3) the process should have limited effect on the existing snow morphology.

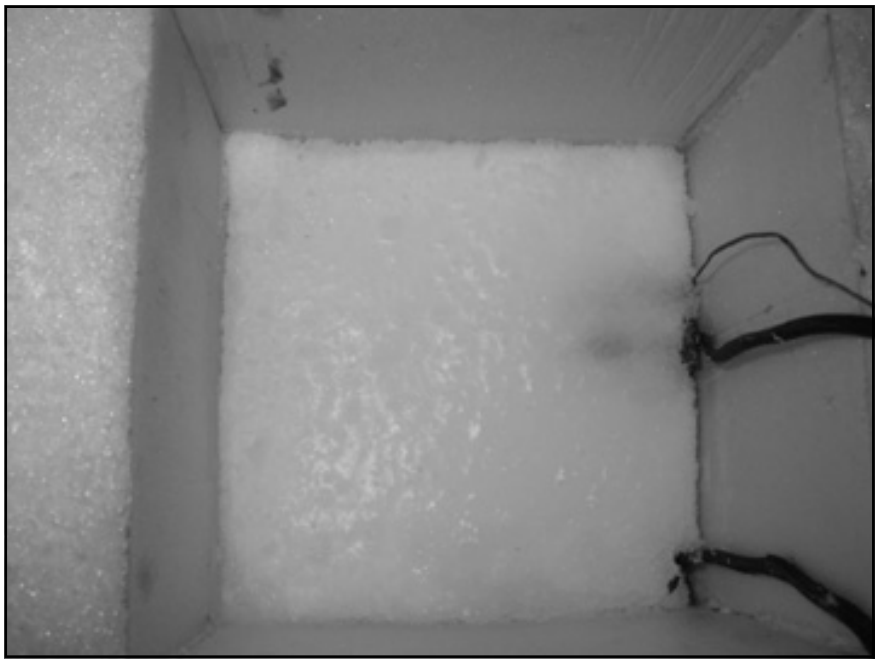

Figure 3.3: An artificial ice layer inside of a sample box. The photograph is taken looking down into the box after the lower half of the sample was assembled.

I investigated several different methods of creating ice layers in natural snow. The method I selected involved a light mist of deionized water sprayed on the snow surface. A plastic sheet is then placed on top of the wet layer, which is immediately frozen with finely crushed dry ice. After the misted water freezes, the plastic and dry ice are immediately removed. Six iterations of this process creates an ice layer three to four millimeters thick (Table 3.1) (Figure 3.3). Rapid freezing of the liquid water from above reduces the amount of released latent heat that could conduct into the snow matrix (L. R. Dexter 2000, personal communication) and prevents vertical channels from forming

Table 3.1: Crust thickness measurements (n=40 for each iteration).

Iteration	r^2	Maximum (mm)	Minimum (mm)	Mean (mm)	Standard Deviation (mm)
1	0.18	4.5	2.6	3.6	0.4
2	0.28	4.8	2.4	3.5	0.6
3	0.22	5.6	2.5	3.7	0.8
4	0.064	4.4	2.5	3.3	0.5
5	0.025	5.5	3.0	4.2	0.6
6	0.092	6.6	3.4	4.5	0.8
7	0.035	4.5	2.5	3.2	0.4
8	0.21	4.0	2.2	2.9	0.5

(C. C. Lundy 2000, personal communication). This method produced ice layers with a mean thickness of ± 1 mm over multiple iterations (Table 3.1). To determine if the method consistently produced thick or thin regions in the sample location, a rectangular grid was placed on eight test layers and the thickness measured at randomly selected points. Linear regression of thickness measurements shows a low correlation between the x and y coordinates (Table 3.1). Therefore, the method is without a measurable bias and does not consistently produce thick or thin regions in the same location.

3.0.3 Inducing Temperature Gradients in Snow

The factors that control the recrystallization rate of snow are porosity, mean temperature, and temperature gradient, which is equivalent to the vapor pressure gradient (Sokratov, 2001). Issues regarding the physical properties of the snow, such as porosity, were addressed in Section 3.0.1. The remaining factors are controlled by the laboratory environment and equipment. In order to produce conditions conducive for kinetic metamorphism, the target thermal environment for these experiments had a mean sample temperature between -5 °C and -10 °C and a temperature gradient much greater than 10 °C m^{-1}, which is considered to be the minimum temperature gradient for depth hoar development by many field workers (Armstrong, 1985). To better mimic the natural conditions of seasonal snow covers, samples in the cold laboratory were heated

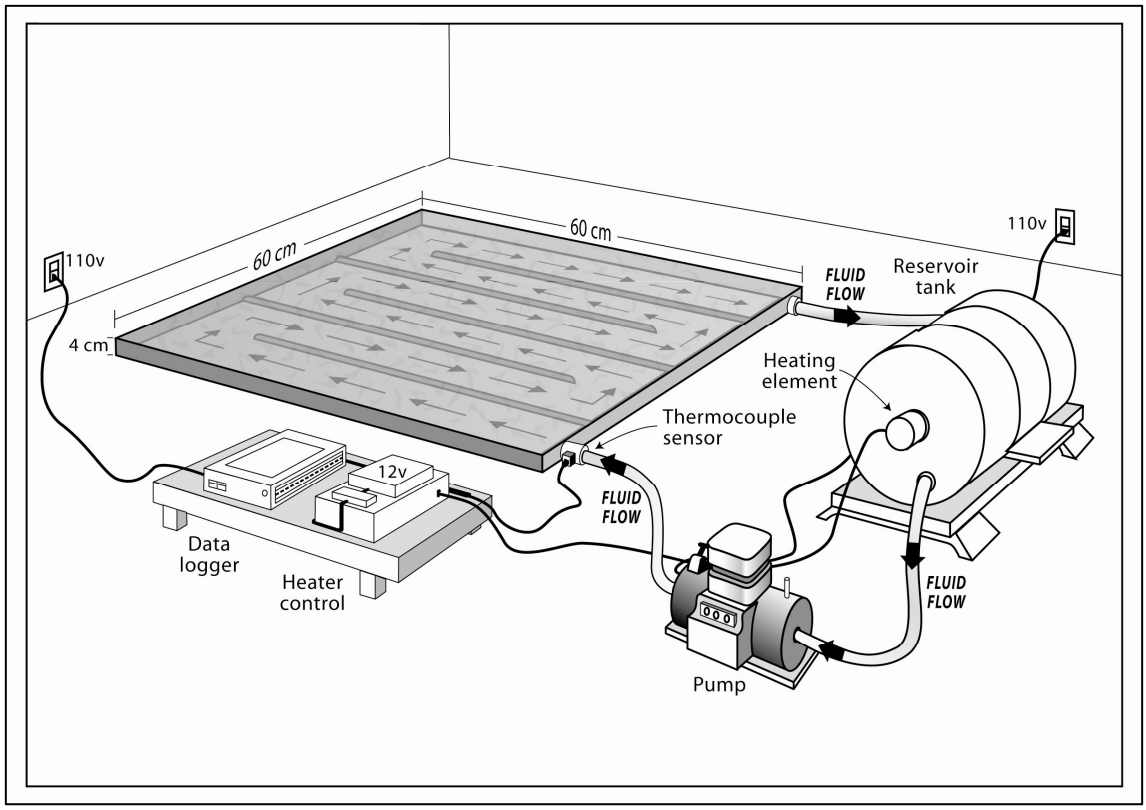

Figure 3.4: Schematic of the heat exchanger system.

from the bottom with a heat exchanger and cooled at the top by the ambient temperature of the laboratory. Although heat was introduced into the samples from the bottom, the entire sample remained below 0 °C.

Two heat exchangers similar to ones used for metamorphic experiments at Montana State University were constructed (Adams and Brown 2000, personal communication) (Figure 3.4). Each exchanger was composed of a 60 x 60 x 3 cm baffled aluminum tank with an ethylene glycol and water mixture circulating through eight fluid channels. Fluid circulated from a reservoir into the aluminum tank and back at a rate of approximately 18 L min^{-1} (March magnetic pump, model AC-2CP-MD). The reservoir and pump were connected by 0.95 cm ID vinyl tubing and the pump, aluminum tank, and return were connected by 0.6 cm ID tubing. The fluid temperature

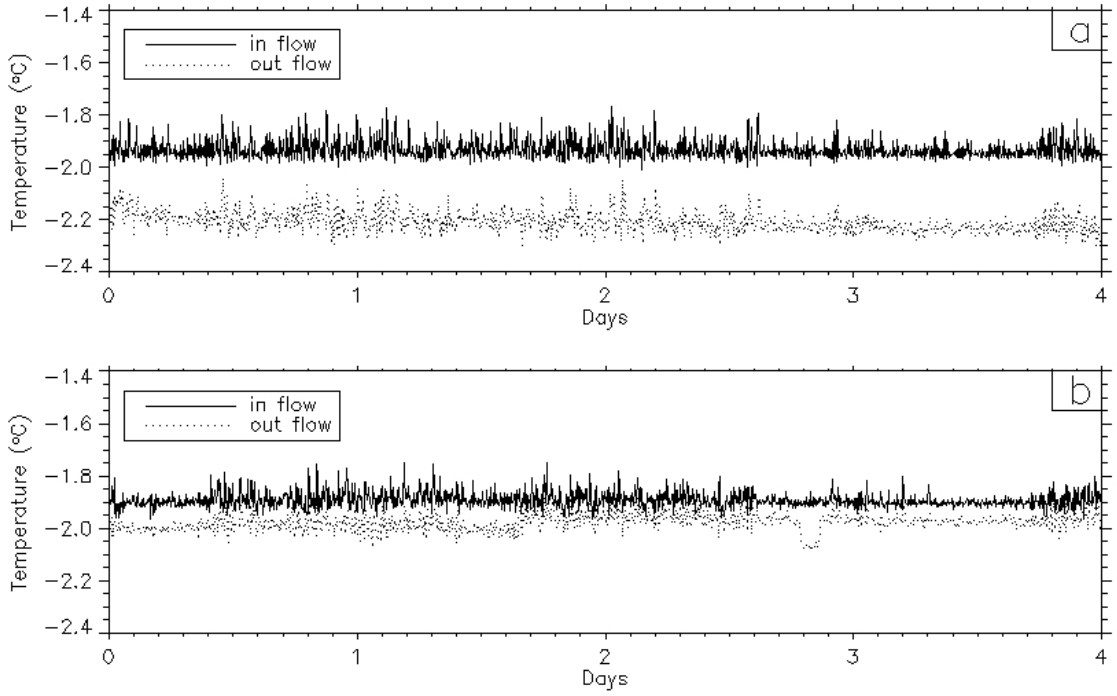

Figure 3.5: Temperature of the fluid into and out of each heat exchanger plate during a performance test of the system: a) upper heat exchanger, b) lower heat exchanger.

was monitored at the inlet and outlet of the aluminum tank by 24 AWG type T thermocouples. A Campbell Scientific CR10X data logger recorded the temperature and turned the heating element on and off based on the inlet fluid temperature. A 1500 W heating element in the reservoir increased the temperature of the fluid. The reference temperature for the thermocouples was measured with a CR10XTCR. The CR10X was programmed to turn on the heating element when the fluid temperature fell below -2 °C

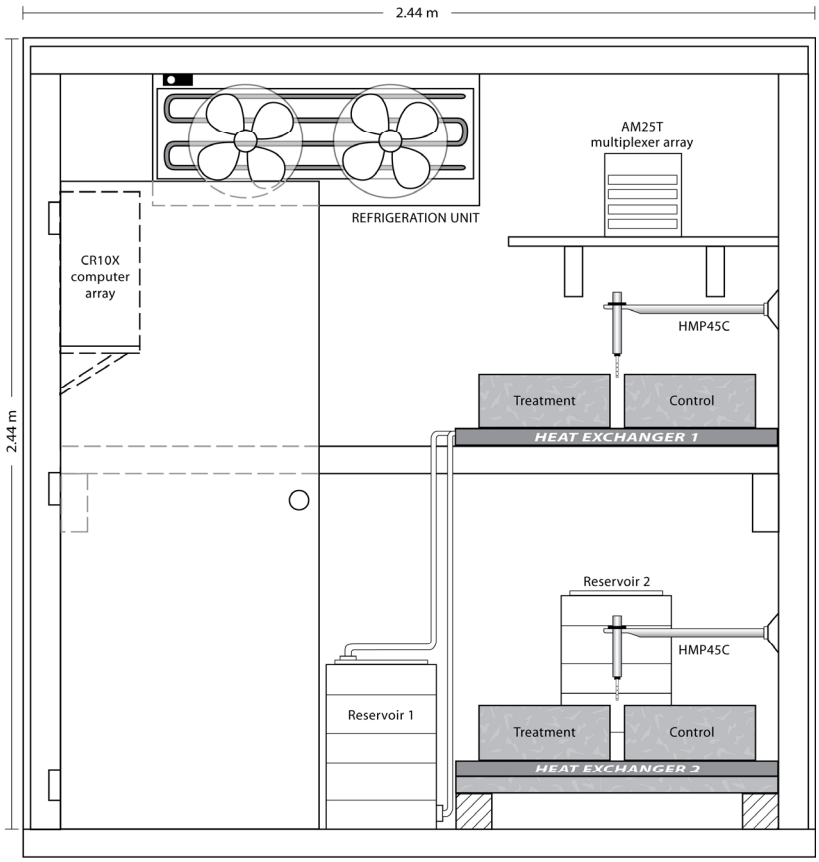

Figure 3.6: Schematic of the cold laboratory at the Rocky Mountain Research Station.

and turn it off when the temperature reached -1.99 °C. A five day test of the thermal stability of both units was performed before the laboratory experiments began. The inlet temperatures in both units did not vary significantly over the course of the test period

(Figure 3.5); however the outlet temperatures vary by about 1 °C. This difference was due to the thermal environment of the two units. Due to space constrains, the first unit sat on a bench in the cold laboratory about midway between the floor and the ceiling, while the second unit was about 10 cm above the floor (Figure 3.6). During the experiments the ambient air temperature at each unit differed by about 5 °C and thus the cooling rate of the fluid was not the same in each unit. These differences were not significant in the experimental results.

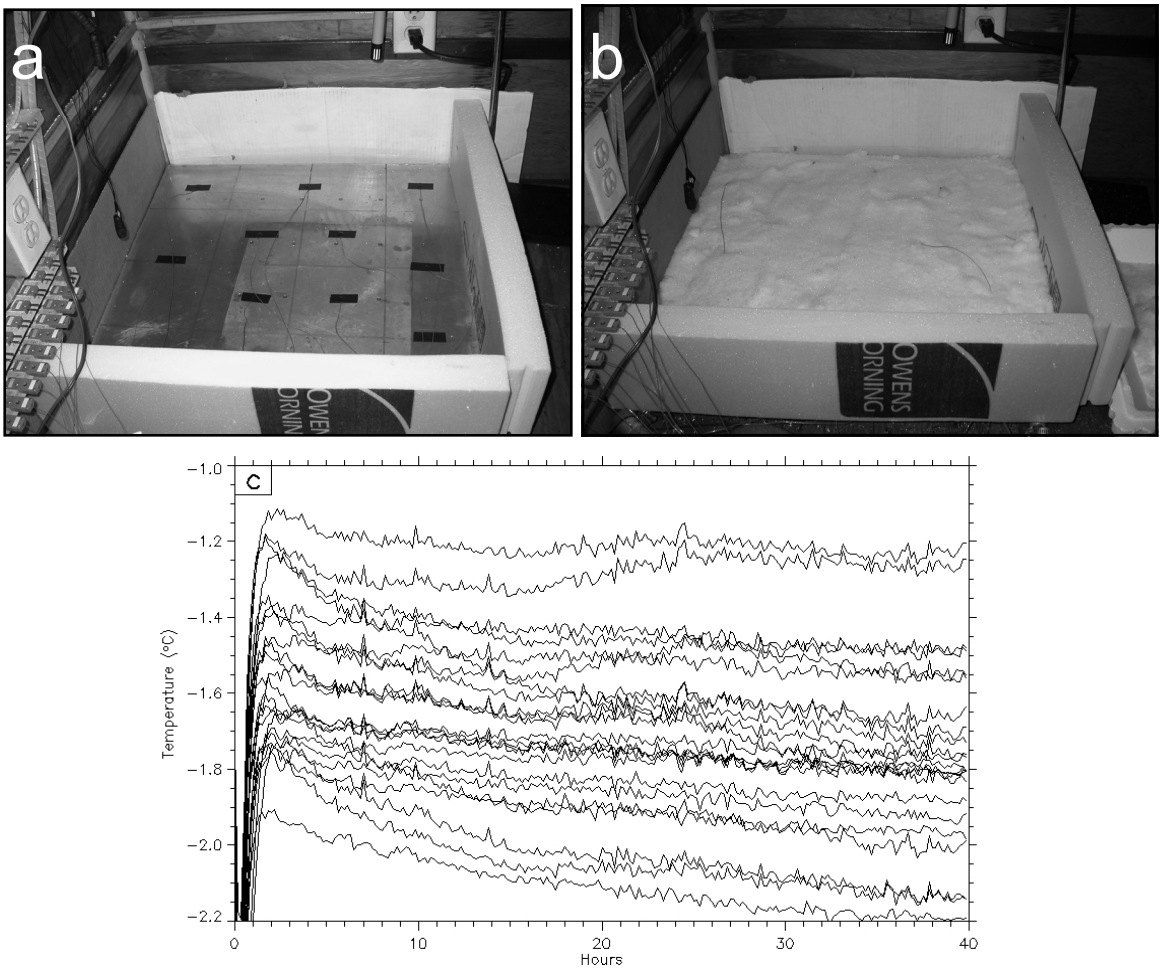

Figure 3.7: Heat exchanger surface temperature test: a) thermocouple sensors attached to the heat exchanger's surface, b) heat exchanger covered with an insulating layer of snow for the test, c) temperature distribution on the surface of the heat exchanger during the test. Each line is the temperature in the center of a 400 cm^2 area.

The spatial distribution of surface temperature for each heat exchanger is shown in Figure 3.7. This test was conducted by fixing 30 AWG type T thermocouples in a checkerboard pattern to the surface of each unit with electrical tape. The thermocouples were then buried in approximately 10 cm of snow to reduce the influence of air temperature fluctuations on the measurements. The surface temperature fluctuated less than 1 °C across each unit, while average surface temperature of each unit differed by less than 0.5 °C.

The cold laboratory available for this project was not designed to maintain a constant temperature over a period of several days. A substantial amount of work was required to control the amount of thermal noise within the laboratory environment. Eventually a steady temperature throughout the room was achieved (Figure 3.8).

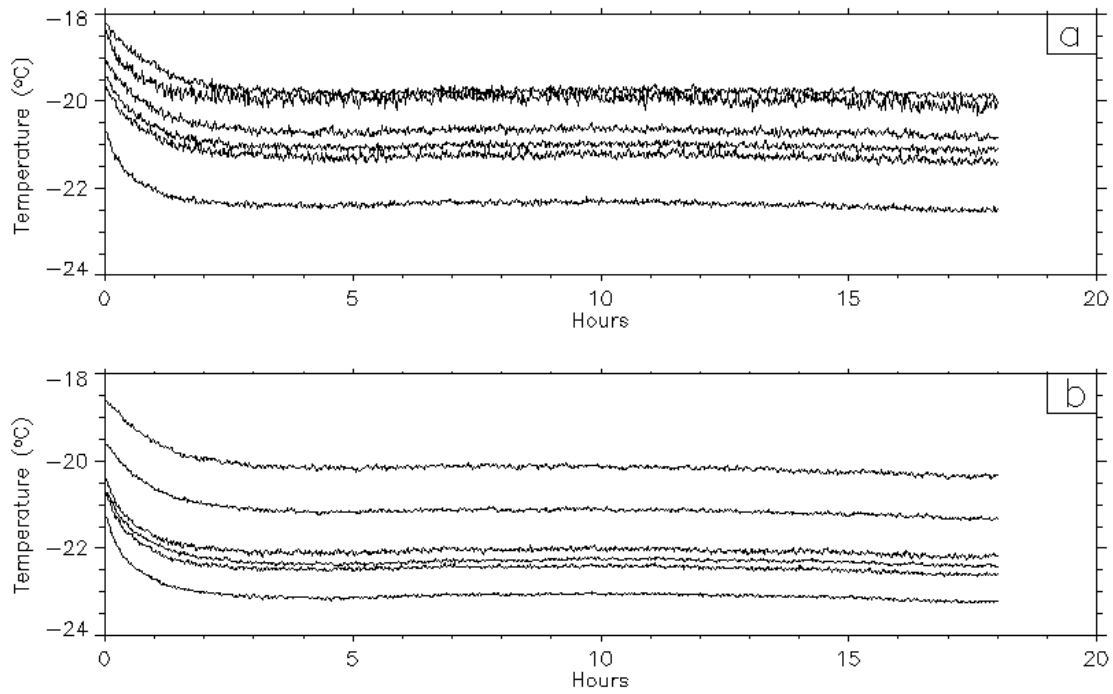

Figure 3.8: Spatial distribution of temperature in the cold laboratory: a) the horizontal temperature distribution, b) the vertical temperature distribution.

Effectively controlling the ambient temperature created two problems. First, the cold room door had to be sealed during each experiment. Second, the defrost cycle had to be turned off during the course of the experiment. Without the defrost cycle, ice would gradually build on the coils of the cooling unit and decrease its efficiency. This constraint limited the length of the experiment to approximately 5 days. Limiting the length of the experiments did not completely solve the problem. In several experiments a gradual but steady increase in the ambient air temperature was observed.

The test of the thermal environment in the cold laboratory showed a small horizontal (0.8 ºC m^{-1}) and vertical temperature gradient (1.25 ºC m^{-1}) (Figure 3.8). This test was conducted with no additional equipment running in the laboratory. Once both heat exchangers were operational a pronounced vertical temperature gradient was apparent. During the experiment the air temperature difference between the upper and lower heat exchangers was about 5 °C.

3.0.4 Sample Box Design

Specialized containers were needed to house the snow samples during the metamorphic portion of the laboratory experiments. In order for each step of the experiment to succeed, the boxes had to meet the following criteria: 1) facilitate building an artificial ice layer, 2) maintain a one-dimensional heat flow, 3) allow placement of the thermocouple probes, and 4) allow the introduction of casting fluid and removal of the sample at the end of the experiment. These criteria seemed straight forward at first, but proved to be mutually exclusive at times.

All box designs were constructed out of 5 cm thick sheets of Owens Corning Foamular 250 insulation (k=0.026 $Wm^{-1}K^{-1}$). Several boxes with alternate designs were built and tested. These designs were created to address criteria 1, 3, and 4. However they were all rejected due to their poor performance on criterion 2. It became apparent that one-dimensional heat flow had to be the primary design criterion, and that seemingly small gaps or cracks in the insulating walls significantly compromised uniformity in the heat flux field.

Eventually a simple box design was selected; however, additional components were added to the "experimental box system" (EBS) to satisfy all of the design criteria. The box itself was composed of eight pieces of insulation bound together with urethane glue (Figure 3.9). The top and bottom of the box were covered with two pieces of 3 mm aluminum sheet (Figure 3.9). The aluminum sheet was attached to the insulated walls by two layers of a duct sealing compound (Gardner Bender model DS-130). A Plexiglas sleeve and plunger made of wire and thin plastic sheeting were added to the system to

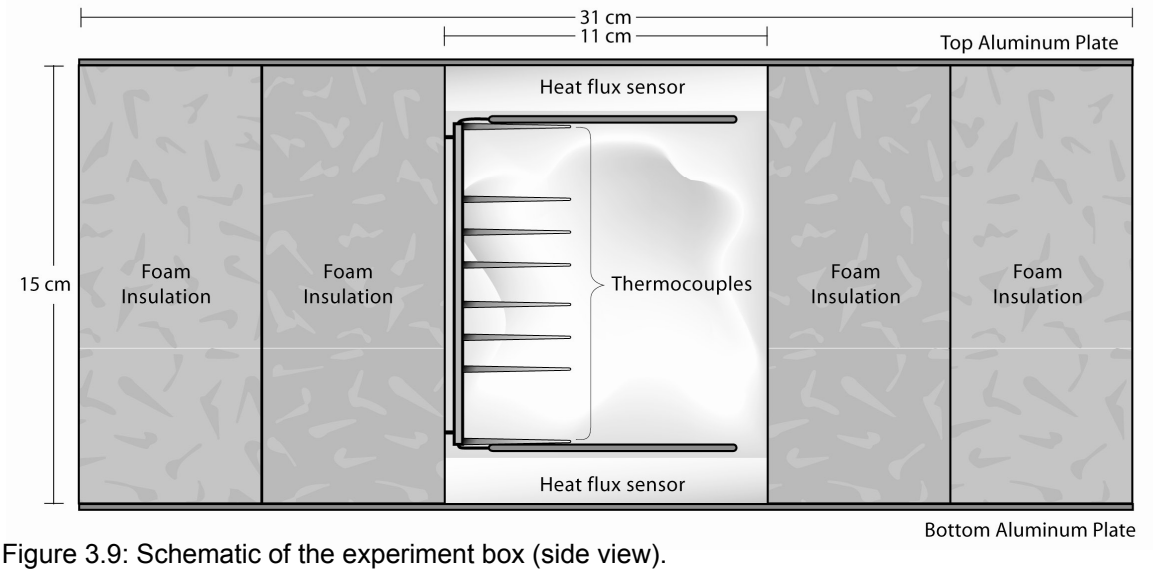

Figure 3.9: Schematic of the experiment box (side view).

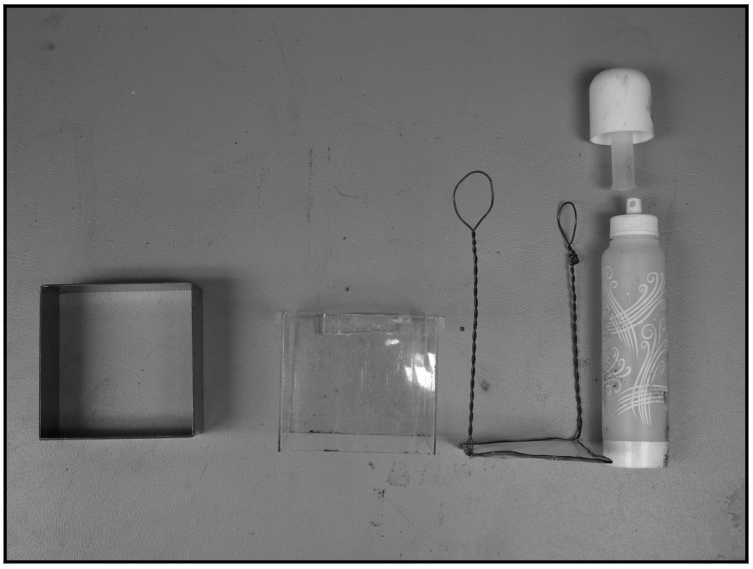

Figure 3.10: Equipment used to create artificial ice layers. From left to right, snow sample cutter, Plexiglas sleeve, dry ice holder and atomizer.

facilitate building the ice layer (Figure 3.10). Prior to casting, the aluminum plates were removed and replaced with 0.6 cm thick sheets of clear Plexiglas. Input holes and vents were cut into the sides of the insulated box with cylindrical plug cutters.

The EBS allowed completion of all portions of the laboratory experiment with a reasonable degree of accuracy and repeatability. Unfortunately the necessity of destroying the box during each experiment meant that four insulated boxes needed to be built for every experimental repetition.

3.0.5 Thermophysical Measurements

Measurements of the thermophysical conditions of the snow samples during each laboratory experiment included: 1) air temperature above the snow sample, 2) relative humidity above the snow sample, 3) vertical temperature profile of the snow sample, and 4) heat flux into and out of the snow sample. Campbell Scientific CR10X

data loggers and AM25T multiplexes housed in an insulated enclosure collected and recorded these data.

Vaisala HMP-45C probes (AT_{error} = ± 0.4 °C at -20 °C, RH_{error} = ± 2% from 0 to 90% at 20 °C, no RH error is given for subfreezing conditions) measured air temperature and relative humidity in the cold room approximately 30 cm above each heat exchanger. The instruments were sampled every 5 sec and 10 min averages were stored.

An array of type T thermocouples measured the vertical temperature profile of the snow samples. The thermocouple probes were constructed from 30 AWG Special Limits of Error wire. The length of the thermocouple leads on heat exchangers one and two were 2 m and 2.5 m respectively. The probes were connected to the data logger system with type T miniature thermocouple connectors (Omega, SMP-T-MF). Each spool of wire was tested for accuracy by methods that conformed to ISO 10012-1, ISO 9001 Section 4.11, and ANSI/NCSL Z540-1-1994. Special Limits of Error wire is typically accurate to ± 0.5 °C. The calibration showed that the wire used was within 0.16 °C of the actual test temperature. Given the wire error and the measurement system, the estimated absolute temperature measurement error is ± 0.3 °C.

Specialized thermocouple forks were built to facilitate the temperature measurements (Figure 3.11). The main support of each fork was made from 3 mm PTFE sheet (k = 0.25 W m^{-1} K^{-1}). The prongs of the forks were made from 1.5 cm long sections 3 mm OD graphite tubing with an additional 1.5 cm length of 1.58 OD PFA tubing (k = 0.26 W m^{-1} K^{-1}). The thermal conductivity of graphite can range between 10 and 2000 W m^{-1} K^{-1} depending on the crystallographic orientation. The exact thermal

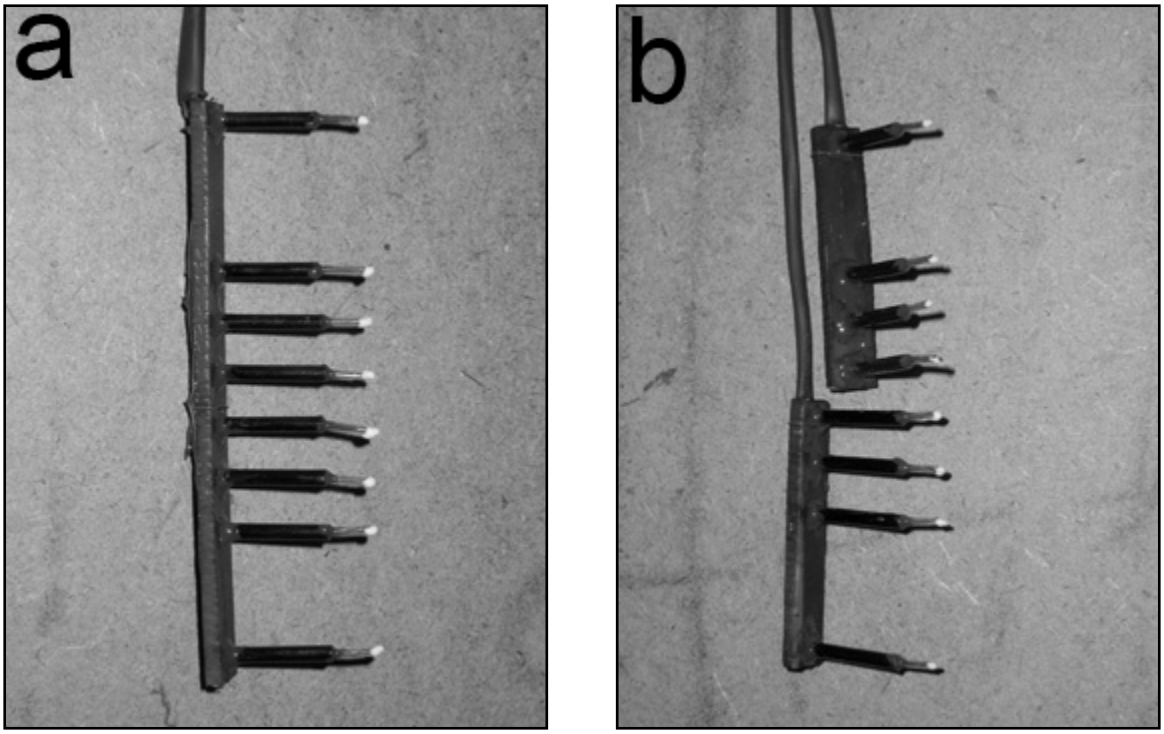

Figure 3.11: Thermocouple arrays used in the laboratory experiments: a) thermocouple fork for a control sample, b) thermocouple fork for a treatment sample. The fork for the treatment sample has two pieces so the thermocouples can be carefully inserted above and below the ice layer.

conductivity of the graphite components used in these experiments is unknown, but since they are very small and surrounded by materials with a very low thermal conductivity, measurement contamination from this factor is probably very small. The thermocouple pairs were soldered together (Kerlin, 1999) and coated with an epoxy with a high thermal conductivity (Omegabond 101, k = 12.5 W m^{-1} K^{-1}). Armstrong A-12 epoxy held the components of the fork together.

Heat flux into and out of each sample was measured with TNO PU43 heat flux sensors. The sensors have a sensitive area of 25 x 25 mm with a disk-shaped guard 10 cm in diameter and 3 mm thick. For these experiments the guard was extended to 11 x 11 cm with 3 mm thick PTFE sheet (k_{guard} = 0.25 W m^{-1} K^{-1}, k_{PTFE} = 0.25 W m^{-1} K^{-1}).

Output voltage from the sensors was recorded by the multiplexer/data logger array. Factory obtained calibration constants were used to convert the voltage to heat flux with a measurement error of ± 5%.

3.0.6 Casting

Once the metamorphic portion of the laboratory experiment was finished, the samples were cast with a supercooled mixture of dimethyl phthalate ($C_{10}H_{10}O_4$, Fisher Scientific) and Sudan Black ($C_{29}H_{24}N_6$, Sigma-Aldrich) in a ratio of 200:1 (M. Schneebeli 2003, personal communication) (Figure 3.12). Prior to casting, the fluid was cooled to -3 °C while mixing on a magnetic stirrer. The supercooled mixture was then placed in a carboy and stirred occasionally until it again cooled to -3 °C. The carboy

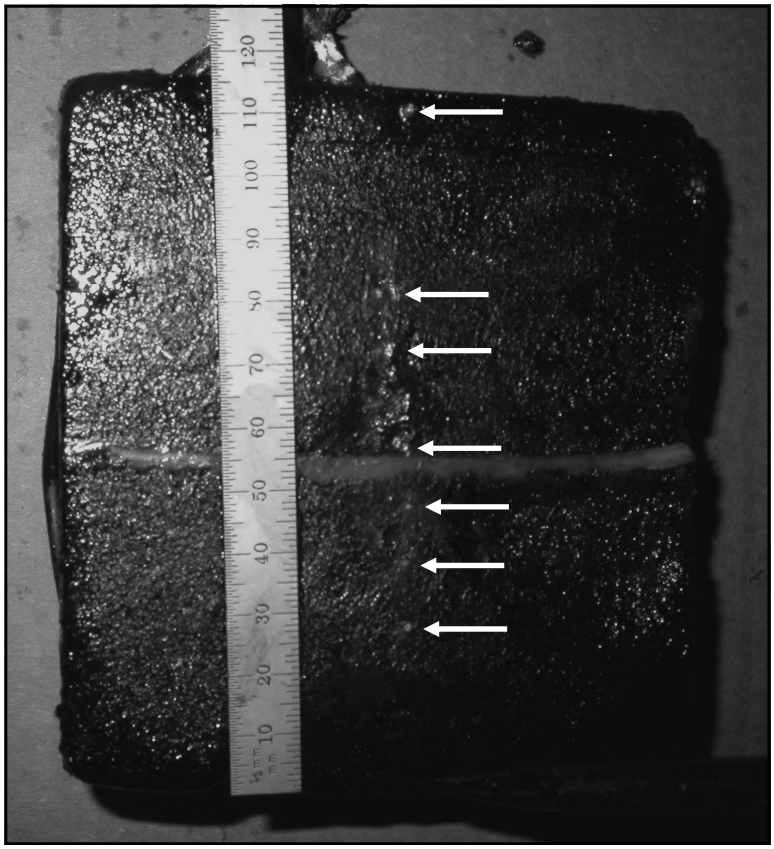

Figure 3.12: Cross section of a cast treatment sample. The arrows show the location of several thermocouple probes. The ice layer is at approximately 55 mm.

was then connected to the sample box and fluid was allowed to flow into the bottom of the box until the sample had become saturated (~10 – 15 min). Inlet and vent holes were then plugged with duct seal and the cast sample was placed in a -35 °C freezer to freeze the pore filler material.

After the casting fluid was frozen the sides of the insulated box and the heat flux sensors were removed. A vertical cut was made about 3.5 cm from the main support of the thermocouple fork. The cut face was melted by contact with an aluminum plate at room temperature until the tips of the thermocouple probes were exposed. The distance between the lower heat flux sensor and the tip of the probe was measured for each probe. Then the remaining portion of the sample was labeled and wrapped for storage at -70°C. Storage at this cold temperature decreases the recrystallization rate of the dimethyl phthalate (M. Schneebeli 2003, personal communication).

3.1 Microstructural Analysis

3.1.1 Serial Sectioning

Serial sectioning was performed at the Swiss Federal Institute for Snow and Avalanche Research in Davos, Switzerland. The serial sectioning apparatus was composed of a PC with National Instruments-Lab View, a Reichert-Jung polycut sledge microtome, and a VDS Vosskühler CCD-4000/C 4 MPixel ultra-high resolution progressive-scan camera with LCD flash (Figure 3.13). Then the center portion of each sample was cut out with a band saw (Figure 3.14). Vertical section planes parallel to the temperature gradient were sampled. Images of a 25 x 25 mm portion of the planes were photographed and stored as 12 bit signed integer images (81.92 pixels mm^{-1}). Each cut

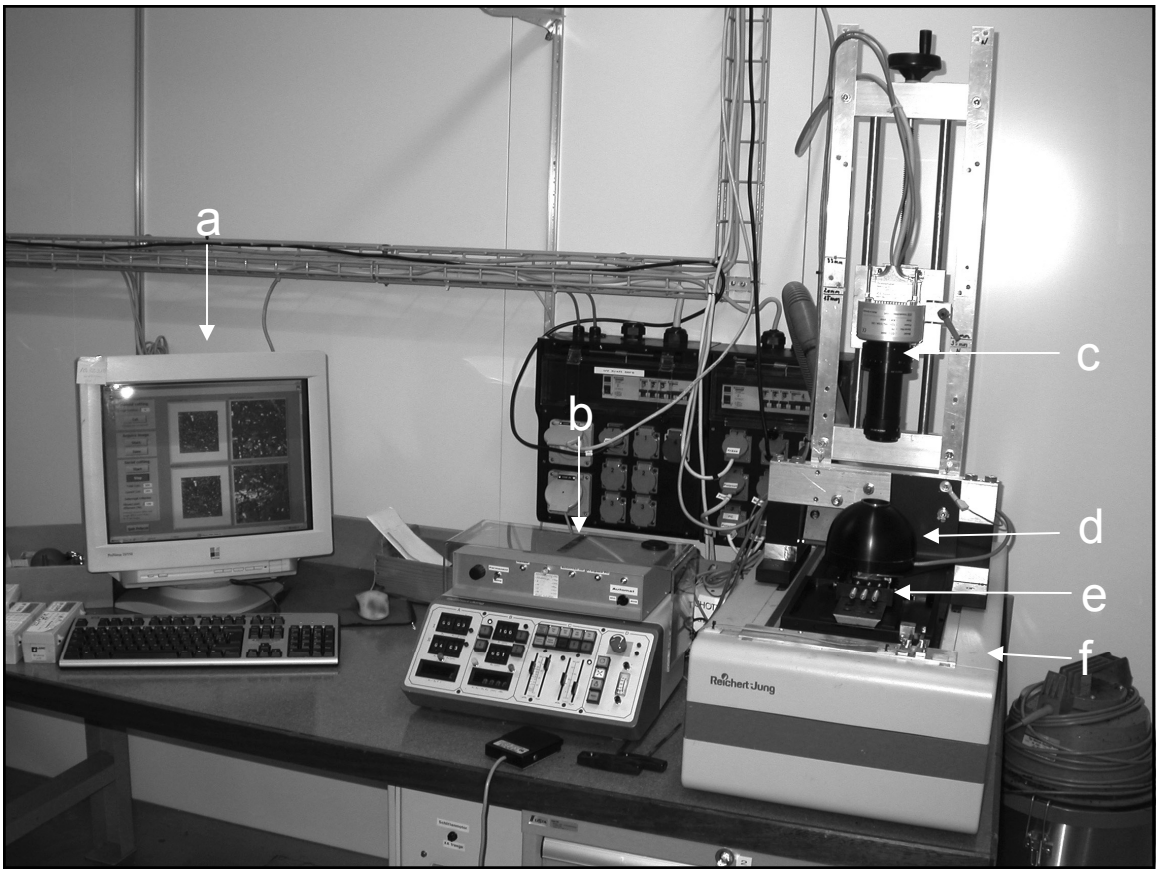

Figure 3.13: The polycut machine at the Swiss Federal Institute for Snow and Avalanche Research: a) control and image acquisition PC, b) microtome control unit, c) CCD camera, d) LCD flash, e) sample holder, f) polycut sledge microtome.

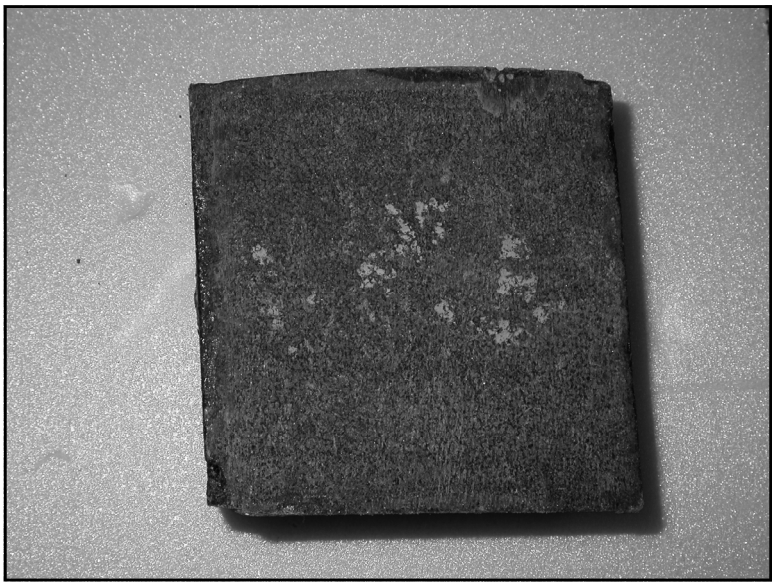

Figure 3.14: A control sample cast prepared for serial sectioning. The white areas are holes in the cast.

on the microtome was 3 μm deep and images were acquired every four cuts for a horizontal spacing of 12 μm. Between 400 and 1000 images were acquired for each sample depending on the type (experimental or initial conditions) and quality of the sample.

3.1.2 Stereological Analysis

Most stereological techniques are based on the assumption that the analyzed section is randomly selected from a uniform, isotropic material (assumption of IUR) (Howard and Reed, 1998; Russ and Dehoff, 2000). By applying linear probes to a IUR section we can obtain a set of measurements from an unbiased sample of the population of line orientations in three-dimensional space (Howard and Reed, 1998; Russ and Dehoff, 2000).

When the primary direction of heat and mass transport in snow is one-dimensional, the microstructure of snow can be anisotropic or transitory isotropic. Stereological techniques can be applied to anisotropic materials provided the vertical axis of the section is perpendicular to isotropic features in the structure and the position is random (assumption of VUR) (Howard and Reed, 1998; Baddeley et al., 1986). A common example is a section perpendicular to the layers of a layered structure. Estimates from VUR sections are equivalent to estimates from IUR sections if cycloid probes are used instead of line probes. Since the orientation of the section is fixed, we need an unbiased set of line probes in three-dimensional space to make estimations equivalent to those obtained under the IUR assumptions. If the section has a known orientation (i.e. vertical) then a cycloid grid will give us an unbiased sample of the

population of line orientations on a sphere if the minor axis of the cycloid is parallel to the vertical direction of the section.

Using stereological techniques, the three-dimensional surface density of a component can be estimated from a two-dimensional section. For a VUR section, the estimated surface density of component *Y* in a given reference space is

$$\hat{S}_V(Y, ref) = \frac{2\sum_{i=1}^{n} I_i}{\frac{l}{p}\sum_{i=1}^{n} P_i} \tag{3.1}$$

where *l/p* is the length of the test line per grid point, *I* is the number of intersections of the probe and component *Y* and *P* is the number of points that fall within component *Y* (Howard and Reed, 1998; Baddeley et al., 1986). The estimated volume fraction of component *Y* is

$$\hat{V}_V(Y, ref) = \frac{P_Y}{P_T} \tag{3.2}$$

where P_Y is the number of points that fall within component *Y* and P_T is the total number of points in the reference volume. The estimated surface density and volume fraction are equivalent to the specific surface area with respect to the ice structure (SSA_i) and snow density (ρ) respectively.

The two-dimensional images were analyzed using standard stereological techniques for vertical uniform random sections (Howard and Reed, 1998; Baddeley et

al., 1986). An Interactive Data Language (IDL) (http://www.rsinc.com/) program overlaid a cycloid grid on top of the surface section image (Figure 3.15). The program also divided the image into four quadrants. Enlarged prints of the images were used for the analysis. Manual counts of the number of upper surface of the cycloid probe intersecting with the ice/pore interface and the number of points within the ice were used for the specific surface area (surface density) and snow density calculations.

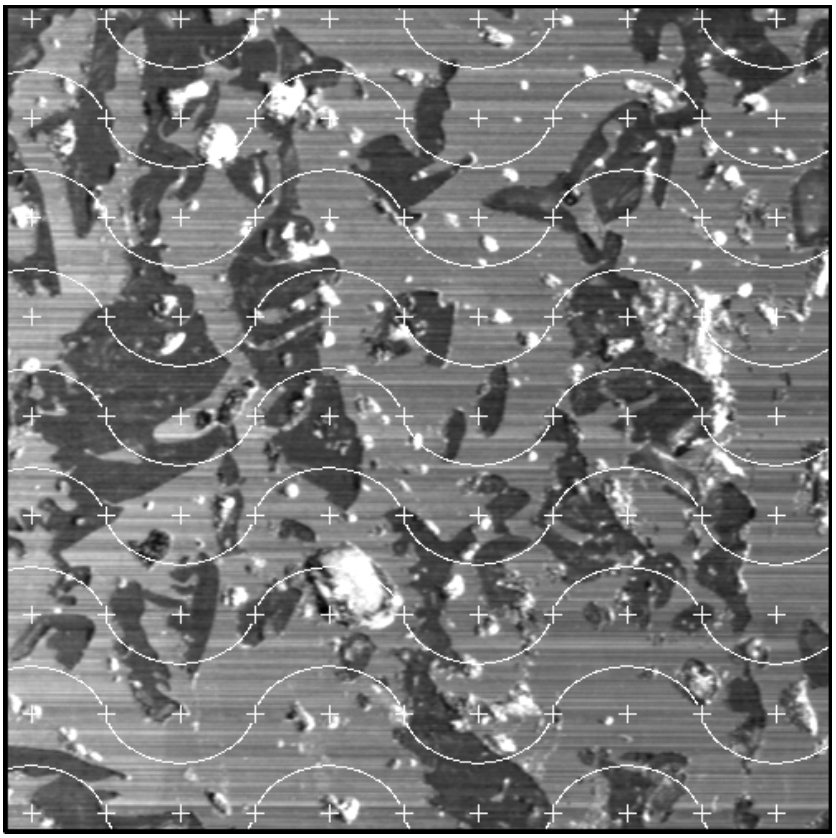

Figure 3.15: Stereological grid on surface sections of snow. The black areas are ice, the gray areas are the pore filler and the white areas are holes in the cast. A cycloid is the arc traced by a single point on a circle as it rolls along a straight line. On this grid, each cycloid begins and ends at the points marked by the cross-hairs.

3.1.3 Three-Dimensional Reconstruction

Images acquired from serial sectioning were converted into three-dimensional micro-structural models with an IDL program. The program took a pre-determined portion of each image. A convolution was performed on the two dimensional image using a center weighted kernel (Figure 3.16) followed by a boxcar average (smoothing). The images were then segmented into black and white model of the ice and pore structure (Figure 3.17). These techniques were employed to remove artifacts (blade streaks) in the images created by the microtome. The images were then stacked into a three-dimensional array and segmented to create a binary array of the ice structure. An erosion/dilation was then performed on the three-dimensional array to remove any remaining portions of the streaks (Figure 3.17).

0	0	0	0	0	0	0
0	0	0	0	0	0	0
0	0	0	0	0	0	0
1	1	1	1	1	1	1
0	0	0	0	0	0	0
0	0	0	0	0	0	0
0	0	0	0	0	0	0

Figure 3.16: The convolution kernel used in the image processing for the three-dimensional reconstruction.

The stack was then processed with Image Processing Language (IPL) (http://www.scanco.ch/). I used IPL to rank the connected structures in the three-dimensional array and remove any unconnected features. I also used intrinsic functions in IPL to scale the array to an element size that could be simulated by the RKS model (Kaempfer et al., 2005), as well as to calculate the specific surface area per unit volume, trabecular

thickness, trabecular spacing, trabecular number and structure model index (SMI). The trabecular parameters and SMI are typically used to characterize bone structures. These parameters are described in Chapter 5.

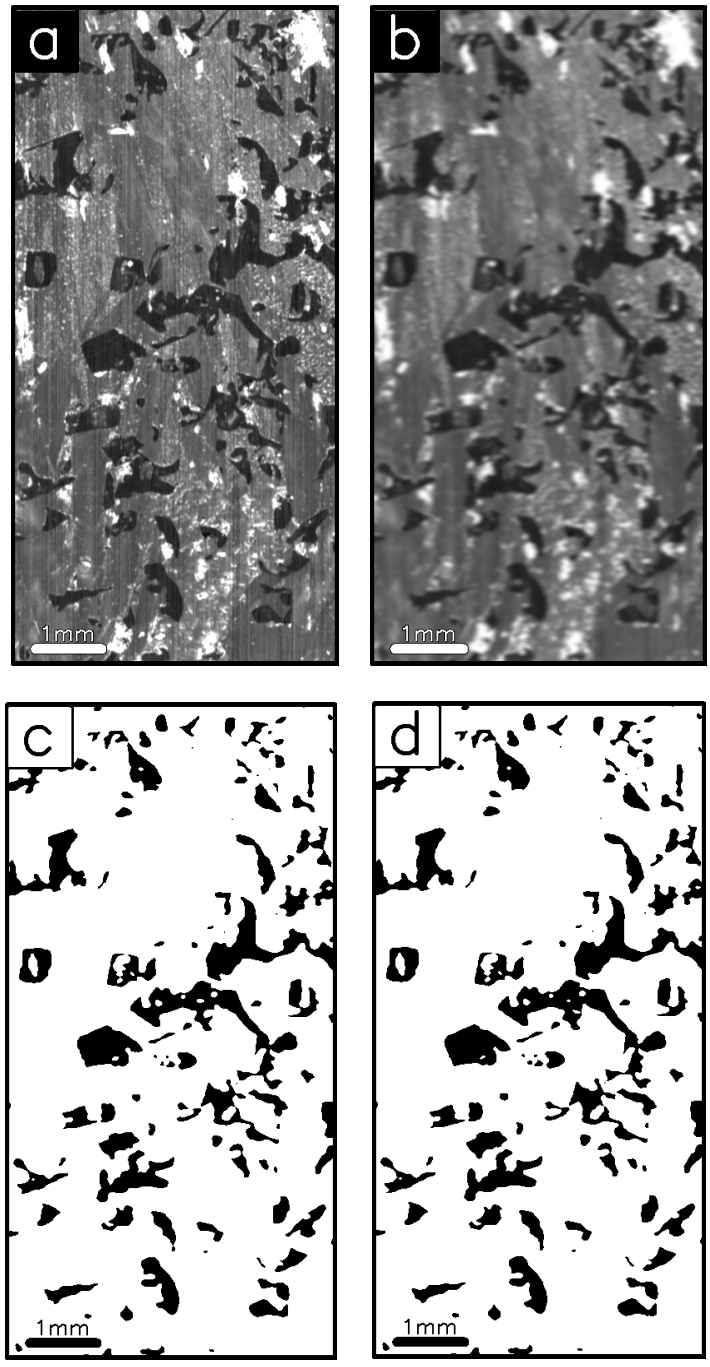

Figure 3.17: The progression of an image during image processing: a) the raw image, b) after the convolution and smoothing, c) the segmented image, d) after an erode/dilate cycle.

3.2 Modeling

3.2.1 van Rietbergen-Kaempfer-Schneebeli Model

I used the finite element model described in Kaempfer et al. (2005) to simulate the temperature distribution within the three-dimensional matrix. The model requires a three-dimensional representation of the ice structure and the thermal conductivity of ice. The structural information was created with the serial sectioning and image analysis techniques described above. I used the thermal conductivity of polycrystalline ice (2.4 W m^{-1} K^{-1}) for the simulations. The model solves the stationary energy conservation equation

$$k_i \nabla^2 T(\vec{x}) = 0 \qquad (3.3)$$

where T is the temperature, k is the thermal conductivity, and x is the location, to determine the temperature distribution throughout the ice matrix. The finite element code was originally developed to simulate elastic deformation in bones (van Rietbergen et al., 1995). Kaempfer et al. (2005) used the physical analogy of Hooke's Law and Fourier's Law to adapt the model formulation to simulate temperature distributions. The model boundary conditions represent the steady-state thermal environment during the experiments, with known temperatures at the upper and lower boundaries and a constant heat flux through the ice structure. One consequence of these boundary conditions is that heat transfer due to the diffusion of water mass through the pore spaces is neglected. Although latent heat exchange from vapor diffusion is an important mechanism, conduction through the ice matrix is the largest contributor to heat transfer in snow.

3.2.2 SNOWPACK Model

SNOWPACK is a one-dimensional numerical model of mass and energy transfer in snow (Bartelt and Lehning, 2002; Lehning et al., 2002a; Lehning et al., 2002b). It includes routines that simulate snow settlement, layering, and grain evolution as well as mass and energy fluxes at the boundaries and within a snow cover. The model is used operationally by the Avalanche Warning Group at the Swiss Federal Institute for Snow and Avalanche Research (SLF) (Lehning et al., 1999), and has also been used in numerous research studies (Lehning and Fierz, personal communication). The model uses a finite element approach to simulate the heat transfer in snow, which includes snow settlement and water vapor fluxes. The model also includes components to represent the movement of liquid water within the snowpack and at the boundaries. Quantities such as heat capacity and thermal conductivity can be prescribed or parameterized.

In this study I used the heat and mass transfer components of the model. No settling of the snow was allowed to occur during the simulations. I provided the model with initial snow parameters including density, grain size, bond size and grain type (Colbeck et al., 1990). I performed paired simulations with two different boundary conditions. First, I used the upper and lower measured temperatures as boundary conditions. These simulations are referred to as the Dirichlet simulations. Second, I used the measured heat flux as boundary conditions (Neumann simulations). For these simulations I also provided the model with an initial temperature.

The model structure in each simulation consisted of twenty four numerical elements, each 45 mm thick. The boundary conditions were supplied to the model and the model results stored in ten minute intervals. The calculation time step for the simulations was one minute.

Chapter 4

THERMOPHYSICAL MEASUREMENTS

4.0 Introduction

The purpose of this chapter is to describe, analyze and interpret the thermophysical measurements made during the experiments. The thermophysical properties of snow covers have broad application from climate science to cold regions engineering. I focused on how the presence of a thin ice layer affected the thermophysical properties and metamorphic process of the snow samples.

I made the same measurements during each of the eighteen experiments and I describe the observations from all of the experiments in this chapter. However, at times the discussion focuses on a set of seven experiments. In addition to the thermophysical measurements, I made microstructural measurements on the surface sections from these experiments. I discuss the results of the microstructure measurements in Chapter 5. The trends in these experiments are discussed separately to aid the comparison and interpretation of the thermophysical and microstructural properties. In this chapter I refer to this sub-dataset as the microstructure dataset.

4.1 Temperature Profile

4.1.1 Profile Shape

Temperature profiles from each experiment show both the difference between the treatment and control samples as well as the temporal evolution of heat transfer through the snow. Figure 4.1 shows the profile pairs for six different experiments. All of the profiles show an element of linearity, but none are completely linear. If conduction through the ice structure was the sole heat transfer mechanism, we should see a linear thermal profile. The profiles departure from linearity could be an indication that other heat transfer mechanisms are contributing to the transfer of thermal energy. Errors in the measurement of each thermocouple's location also contribute to the nonlinear profiles (z error ± 0.25 mm). The error in each temperature measurement is ± 0.7 ºC (see Appendix B). Experiment B from January 6, 2005 has the most linear profile (Figure 4.1c). This experiment contained relatively high density snow (239 kg m^{-3}) with a relatively low initial specific surface area. The conductive heat transfer component in this snow sample may have been larger than in the other experiments.

The transfer of latent heat by the diffusion of water mass is the most likely additional heat transfer mechanism. In snow, convection has been shown to be significant heat transfer mechanism only in shallow and very porous snowpacks (Sturm and Johnson, 1991). It is unlikely that convection played a significant role due to the experimental design and the pore size of the snow. The size of the snow samples is about eight times smaller than the convective cells observed by Sturm and Johnson (1991) and the thermal gradients were 25 to 70% smaller than those used by Powers et al. (1985a, b) and Akitaya (1974). In nature, both free and forced convection (wind

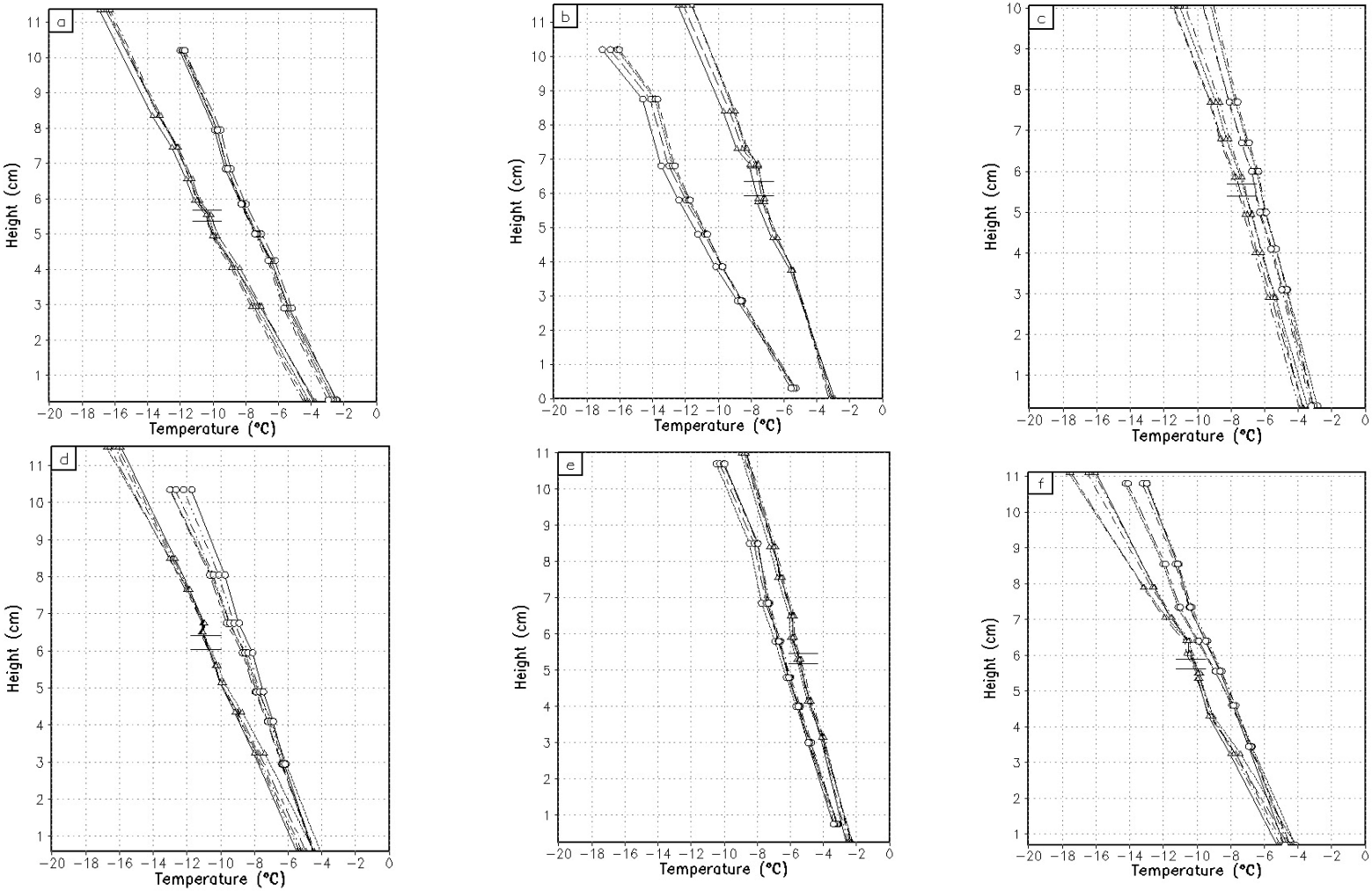

Figure 4.1: Temperature profiles for six experiments, a) March 4, 2005A, b) April 6, 2005A, c) January 6, 2005B, d) March 17, 2005A, e) February 23, 2005B, f) March 25, 2005B. The lines show the temperature profile at the end of each day during the experiment (Day 1 = solid, Day 2 = long dash, Day 3 = short dash, Day 4 = long short dash, Day 5 = dot dash). The location of each thermocouple is marked with circles for the Control sample and triangles for the Treatment sample. The two horizontal lines that cross the Treatment profile indicate the location of the ice layer.

pumping) can occur in snow. However, in the laboratory the snow samples are housed in sealed containers and therefore any convection would be due solely to buoyancy forces. Thus only free convection is possible. The potential for free convection can be evaluated by examining the Grashof number,

$$Gr = \frac{g \beta \Delta T_c l^3 \rho^2}{\mu^2} \qquad (4.1)$$

where g is the acceleration due to gravity, β is the volume coefficient of expansion for the gas (for an ideal gas, $\beta = -\rho(\partial p/\partial T)_P = T^{-1}$), ΔT_c is the temperature difference across on cell, l is the characteristic length of one cell, ρ is the density of the gas and μ is the dynamic viscosity of the gas (Gibson and Ashby, 1997). The Grashof number describes the balance of buoyancy and viscous forces within a fluid or gas. The buoyancy force produces convective cells, but a large viscous force opposes their formation. Holman (2002) suggests convection is an important heat transfer mechanism where the Grashof number is greater than about 1000. By setting Gr = 1000, we can solve for the characteristic length of the convective cell. These laboratory experiments can be evaluated with the following values:

$g = 9.8 \text{ m s}^{-2}$

$\beta = (263 \text{ K})^{-1}$

$\rho_{air\ @\ -10^oC} = 1.25 \text{ kg m}^{-3}$

$\mu_{air\ @\ -10^oC} = 1.68 \times 10^{-5} \text{ N s m}^{-2}$

The characteristic length (l) for 0.01ºC < ΔT_c < 0.2 ºC are shown in Figure 4.2. Under the environmental conditions of the laboratory the minimum cell size for convection is 27 mm., over twice the width of the snow sample. Therefore it is unlikely that convection was a significant heat transfer mechanism at either the pore or sample scale.

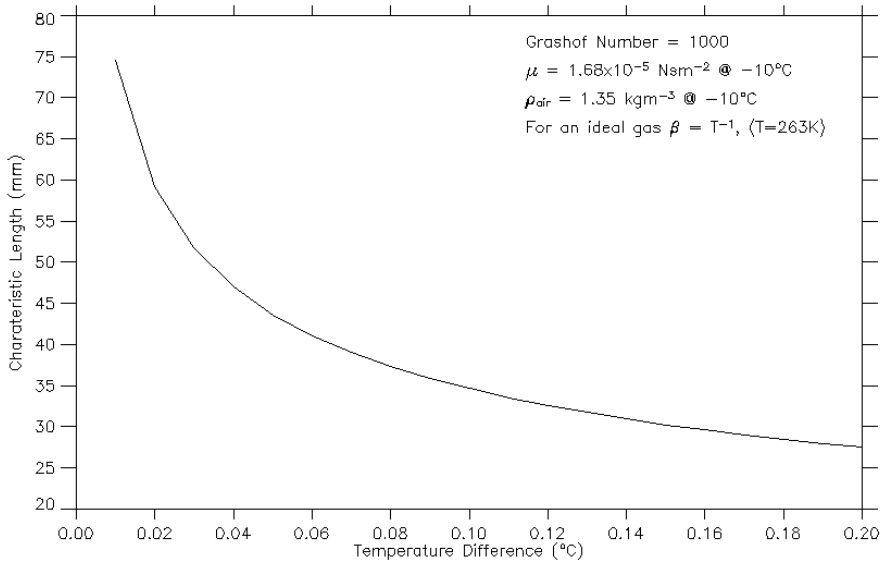

Figure 4.2: Characteristic length needed for significant convection, as determined by the Grashof number, as a function of the temperature difference across the cell.

4.1.2 Treatment vs. Control Samples

The bulk structure of the treatment and control samples was significantly different. However this difference is not evident in the thermal profiles in Figure 4.1. It is nearly impossible to determine which profile is from a layered or homogenous sample by visual inspection. Although the thermal conductivity of the ice layer is nearly one order of magnitude larger than the surrounding snow (k_{ice} = 2.4 W m^{-1} K^{-1}, Petrenko and Witworth, 1999), the signature is lost in the bulk thermal profile. Even when the thermocouples are less than 1 cm apart, it is difficult to see any change in the thermal profile that can be attributed to the presence of an ice layer.

4.2 Bulk Temperature Gradient

The temperature gradient during the experiments ranged from -118 to -60 K m^{-1} (Table 4.1). In eleven of the eighteen experiments the difference between the gradient in the treatment and control samples was less than 20%. The difference was near 30% in three of the experiments and less than 10% in four. The temperature gradient data in the microstructure dataset ranged from -114 to -61 K m^{-1} with a difference of 14 to 31% between the treatment and control samples (Table 4.2). The error in each temperature gradient calculation is ± 2.6 K m^{-1} (see Appendix B).

Table 4.1: Mean bulk temperature gradients for all experiments.

Name	Treatment (K m^{-1})	Control (K m^{-1})	Difference
December 1, 2004 A	-114.2	-88.0	23%
December 1, 2004 B	-78.9	-72.5	8%
December 28, 2004 A	-105.5	-78.8	25%
December 28, 2004 B	-77.2	-70.5	9%
January 6, 2005 A	-87.3	-59.7	32%
January 6, 2005 B	-76.2	-64.5	15%
January 18, 2005 A	-72.0	-77.3	-7%
January 18, 2005 B	-116.0	-99.2	14%
February 23, 2005 A	-118.0	-82.9	30%
February 23, 2005 B	-61.1	-70.8	-14%
March 4, 2005 A	-114.0	-94.2	17%
March 4, 2005 B	-80.5	-68.9	14%
March 17, 2005 A	-105.2	-84.4	20%
March 17, 2005 B	-63.5	-60.7	4%
March 25, 2005 A	-114.4	-88.0	23%
March 25, 2005 B	-75.1	-66.0	12%
April 6, 2005 A	-78.1	-113.1	-31%
April 6, 2005 B	-68.2	-61.4	10%

Note: The percent difference is negative when the location of the treatment and control samples on the heat exchanger was reversed.

Table 4.2: Mean bulk temperature gradients for the experiments included in the microstructure dataset.

Name	Treatment (K m^{-1})	Control (K m^{-1})	Difference
January 6, 2005 B	-76.2	-64.5	15%
February 23, 2005 B	-61.1	-70.8	-14%
March 4, 2005 A	-114.0	-94.2	17%
March 4, 2005 B	-80.5	-69.0	14%
March 17, 2005 A	-105.2	-84.4	20%
March 25, 2005 A	-114.4	-88.0	23%
April 6, 2005 A	-78.1	-113.1	-31%

I performed a paired t-test of the temperature gradients to determine if the mean of the two groups are similar. The t-test is appropriate for these data as the differences of the two groups are normally distributed (Shapiro-Wilks test W = 0.91, p-value = 0.1005). At a significance level of $\alpha = 0.05$ there is evidence to support the hypothesis that the means are significantly different (p-value = 0.0101). The scatter in the data is shown in Figure 4.3 and a linear regression of the data generated a low coefficient of determination $(R^2 = 0.34, \nabla_z T_{treatment} = 0.81 \nabla_z T_{control} + 26.5, p = 0.011)$.

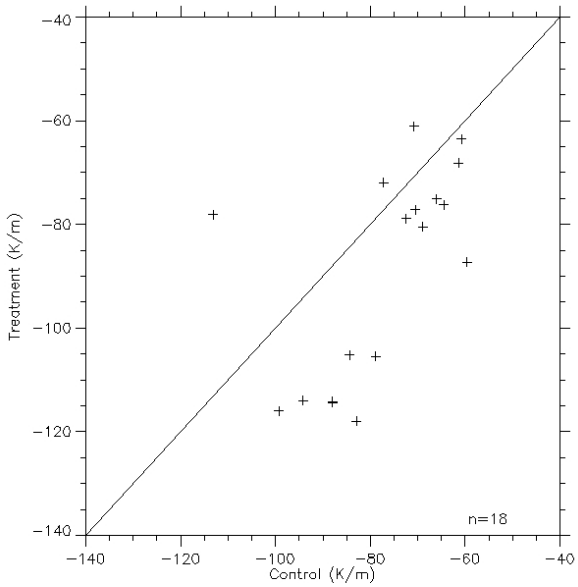

Figure 4.3: Scatter plot of the temperature gradients in the treatment and control samples (p=0.011). The solid line is a one-to-one line for reference.

Although I designed the experimental apparatus to induce a similar gradient in both samples, significant differences developed during some of the experiments. The differences are large and frequent enough that it is difficult to draw any firm conclusions about how the presence of the ice layer affected the bulk temperature gradient of the samples.

4.3 Mean Temperature

The mean sample temperatures from the experiments are shown in Table 4.3 and range from -11 to -5 ºC. In 18 of 21 experiments the mean temperature of the control sample is warmer than the treatment sample (Figure 4.4). In two experiments the difference in the mean temperatures is near 4 ºC, but the mean difference is 1.3 ºC. A linear regression model of the 21 experiments was not significant at α=0.1) (Figure 4.4a). When the experiments where the mean temperature of control sample is colder than the treatment sample are removed the coefficient of determination improves and the model is significant at α=0.05 ($R^2 = 0.67, \overline{T}_{treatment} = 1.4\overline{T}_{control} + 0.92, p < 0.001$).
It is possible that the consistent difference in mean temperature between the treatment and control samples is due to the ice layer. However, it is more likely that it is a result of a systematic bias in the experimental design. The different samples (treatment or control) almost always occupied the same location on the heat exchangers. Although the tests of the heat exchangers show a very small change in surface temperature across the plate, the fluid does cool as it moves through the baffled channels. The control samples were closer to the inflow of the plate and their position likely produced a warmer mean temperature in the sample.

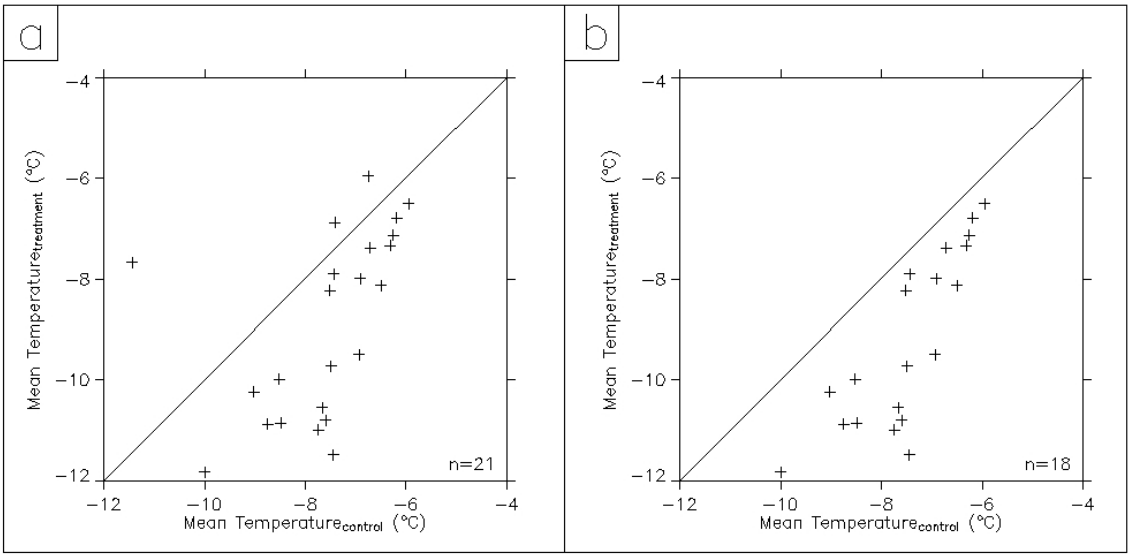

Figure 4.4: Scatter plots of mean temperature in the control and treatment samples: a) all experiments p=0.21, b) all experiments where $\overline{T}_{treatment} < \overline{T}_{control}$, p<0.001. The solid line is the one-to-one line for reference.

Table 4.3: Mean temperature of snow samples.

Experiment	Mean Temperature (°C)		Difference
	Control	Treatment	
December 1, 2004A	-8.52	-9.98	1.46
December 1, 2004B	-7.44	-7.89	0.46
December 11, 2004A	-6.93	-9.49	2.55
December 11, 2004B	-5.94	-6.50	0.55
December 19, 2004A	-7.74	-10.99	3.25
December 28, 2004A	-7.45	-11.48	4.04
December 28, 2004B	-7.41	-6.87	-0.54
January 6, 2005A	-9.99	-11.82	1.83
January 6, 2005B	-6.32	-7.33	1.01
January 18, 2005A	-7.51	-8.23	0.72
January 18, 2005B	-8.75	-10.88	2.13
February 12, 2005A	-7.49	-9.72	2.23
February 12, 2005B	-6.26	-7.13	0.87
February 23, 2005A	-7.59	-10.79	3.20
February 23, 2005B	-6.75	-5.95	-0.81
March 4, 2005A	-7.66	-10.54	2.88
March 4, 2005B	-6.50	-8.12	1.62
March 17, 2005A	-8.48	-10.86	2.38
March 17, 2005B	-6.71	-7.38	0.67
March 25, 2005A	-9.02	-10.24	1.21
March 25, 2005B	-6.90	-7.98	1.08
April 6, 2005A	-11.43	-7.66	-3.77
April 6, 2005B	-6.19	-6.78	0.59

4.4 Heat Flux

During each experiment I measured the heat flux at the upper and lower boundaries of the samples. These measurements ranged from 7 to 27 W m^{-2} and 8 to 30 W m^{-2} at the upper and lower boundaries, respectively (Table 4.4). The heat lost between the heat flux plates ranged from 0 to 33%, but the average loss was 14% (Table 4.4). Only one sample had a negative loss, where the upper heat flux measurement was greater than the lower. In this case the difference between the two measurements was within the measurement error of ± 1.8 W m^{-2} (see Appendix B).

Table 4.4: Mean heat flux at the upper (out) and lower (in) boundaries of all experiments. The adjustment period at the beginning of each experiment has been omitted.

Name	Treatment			Control		
	In (Wm^{-2})	Out (Wm^{-2})	% Loss	In (Wm^{-2})	Out (Wm^{-2})	% Loss
December 1, 2004 A	23.4	21.7	7%	20.8	17.4	16%
December 1, 2004 B	17.8	15.8	10%	16.8	11.6	31%
December 28, 2004 A	13.4	11.7	12%	12.7	10.8	14%
December 28, 2004 B	10.5	8.7	18%	10.9	7.1	35%
January 6, 2005 B	16.9	12.6	25%	13.1	12.3	6%
January 18, 2005 A	18.1	13.6	24%	16.0	11.4	28%
January 18, 2005 B	9.5	7.8	17%	11.2	7.7	31%
February 23, 2005 A	16.3	11.7	28%	12.3	9.0	27%
February 23, 2005 B	9.0	7.1	21%	10.2	8.3	19%
March 4, 2005 A	16.0	12.7	20%	13.6	10.8	20%
March 4, 2005 B	11.6	8.4	30%	8.8	8.6	2%
March 17, 2005 A	26.0	22.3	14%	16.6	18.3	0%
March 17, 2005 B	14.2	14.4	0%	14.1	12.6	10%
March 25, 2005 A	30.7	27.0	11%	19.1	16.3	14%
March 25, 2005 B	16.1	15.1	5%	13.6	13.2	2%
April 6, 2005 A	11.7	10.5	10%	14.9	12.6	15%
April 6, 2005 B	12.4	8.8	29%	10.6	7.9	26%

Table 4.5: Mean heat flux at the upper (out) and lower (in) boundaries of the experiments with good microstructural data. The adjustment period at the beginning of each experiment has been omitted.

Name	Treatment			Control		
	In (Wm^{-2})	Out (Wm^{-2})	% Loss	In (Wm^{-2})	Out (Wm^{-2})	% Loss
January 6, 2005 B	16.9	12.6	25%	13.1	12.3	6%
February 23, 2005 B	9.0	7.1	21%	10.2	8.3	19%
March 4, 2005 A	16.0	12.7	20%	13.6	10.8	20%
March 4, 2005 B	11.6	8.4	30%	8.8	8.6	2%
March 17, 2005 A	26.0	22.3	14%	16.6	18.3	0%
March 25, 2005 A	30.7	27.0	11%	19.1	16.3	14%
April 6, 2005 A	11.7	10.5	10%	14.9	12.6	15%

In each experiment there was an initial adjustment to the thermal environment of the experiment (Figure 4.5). This adjustment occurred during the first few hours of the experiment as the temperature gradient was initially induced in the sample and it transitioned to steady state heat flow. Once the heat flow reached a steady state the heat flux remained nearly constant for the duration of the experiment. The heat flux measurement at the upper boundary was very sensitive to the thermal environment of the cold laboratory. Any disturbance in the cold room (such as opening the door) would reduce the magnitude of the measurement.

4.5 Thermal Conductivity

I used the temperature gradient and heat flux measurements to calculate the effective thermal conductivity (k_e) of the snow samples. Since the measurement system only recorded the heat flux values at the upper and lower boundaries, I was unable to

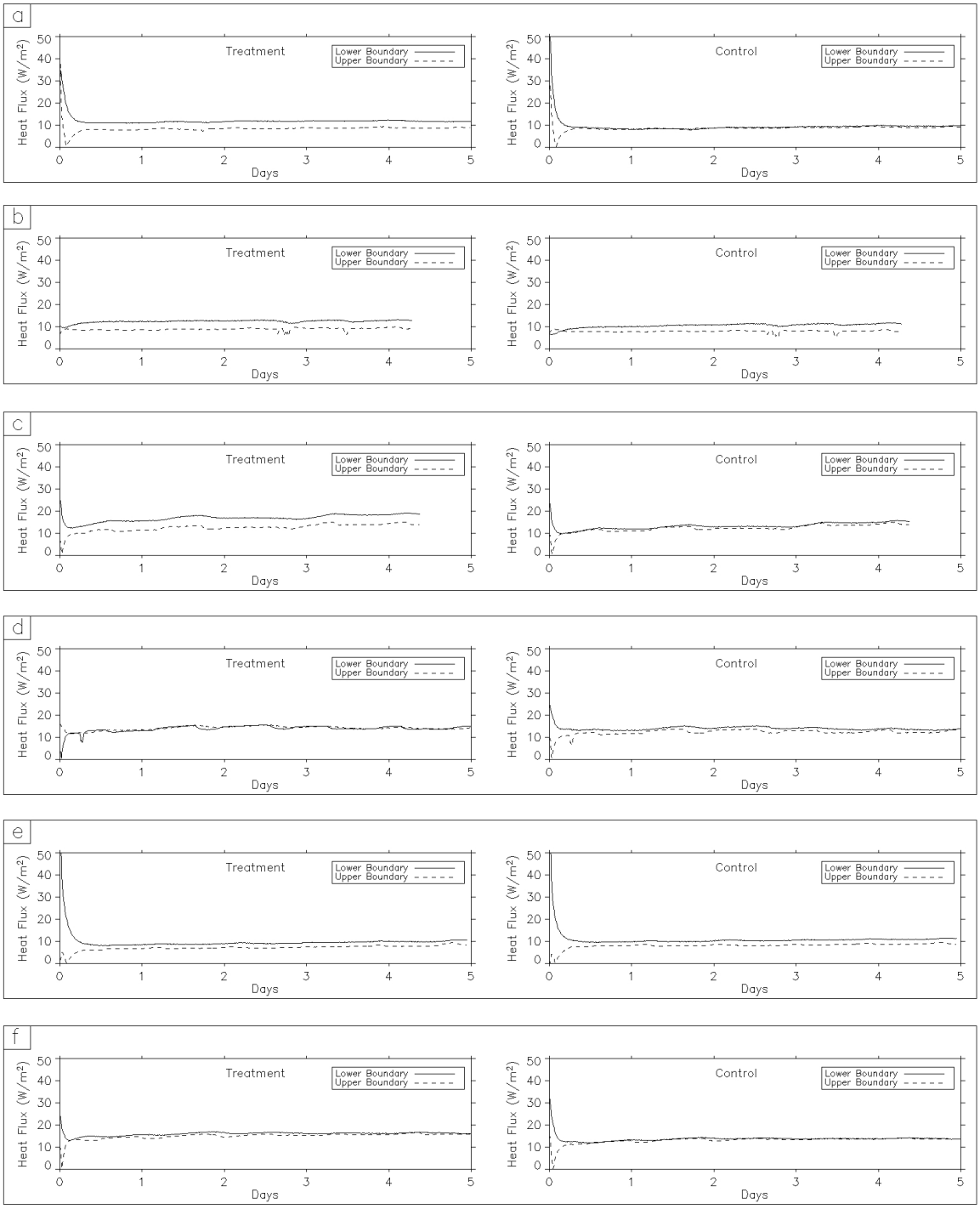

Figure 4.5: The temporal evolution of the heat flux for six experiments, a) March 4, 2005A, b) April 6, 2005A, c) January 6, 2005B, d) March 17, 2005A, e) February 23, 2005B, f) March 25, 2005B. This measurements show the steady-state thermal conditions during the experiments.

calculate the k_e for individual layers. Instead I used average heat flux values and the total temperature gradient to calculate a bulk k_e value (see equation B.10). The error in these calculations is ± 0.013 W m^{-1} K^{-1}. A detailed error analysis of the k_e calculation is presented in section 5.0 of Appendix B. The thermophysical data also allowed me to examine the temporal evolution of k_e during metamorphism.

Values for k_e ranged from 0.08 to 0.265 W m^{-1} K^{-1}. In the microstructural dataset the range was 0.131 to 0.265 W m^{-1} K^{-1}. The effective thermal conductivity increased during every experiment. The average increase in k_e was 22% with a minimum and maximum of 3% and 36% respectively. The lowest value and lowest change occurred in the January 18, 2005 experiment. There were some problems with the heat exchange system during this experiment that resulted in erratic heat flux values. In the microstructure dataset the average increase was 24% (max = 35%, min = 17%). This result is similar to those obtained by Schneebeli and Sokratov (2004).

Many researchers have examined the relationship between the density and effective thermal conductivity of snow (see Sturm et al. (1997) for a review). Although there is a correlation between these two physical parameters, variations in k_e cannot be completely explained by changes in snow density. The relationship between snow density and k_e from the current experiments is shown in Figure 4.6 along with predicted values from a regression equation developed by Sturm et al. Although the k_e values from my study are significantly higher than those predicted by the regression model, both show a general increase in k_e with increasing density. There is one major inconsistency in my data set where samples of the same density have a drastically different value for k_e (Figure 4.6). This discrepancy occurred in the January 18, 2005 experiment. The heating

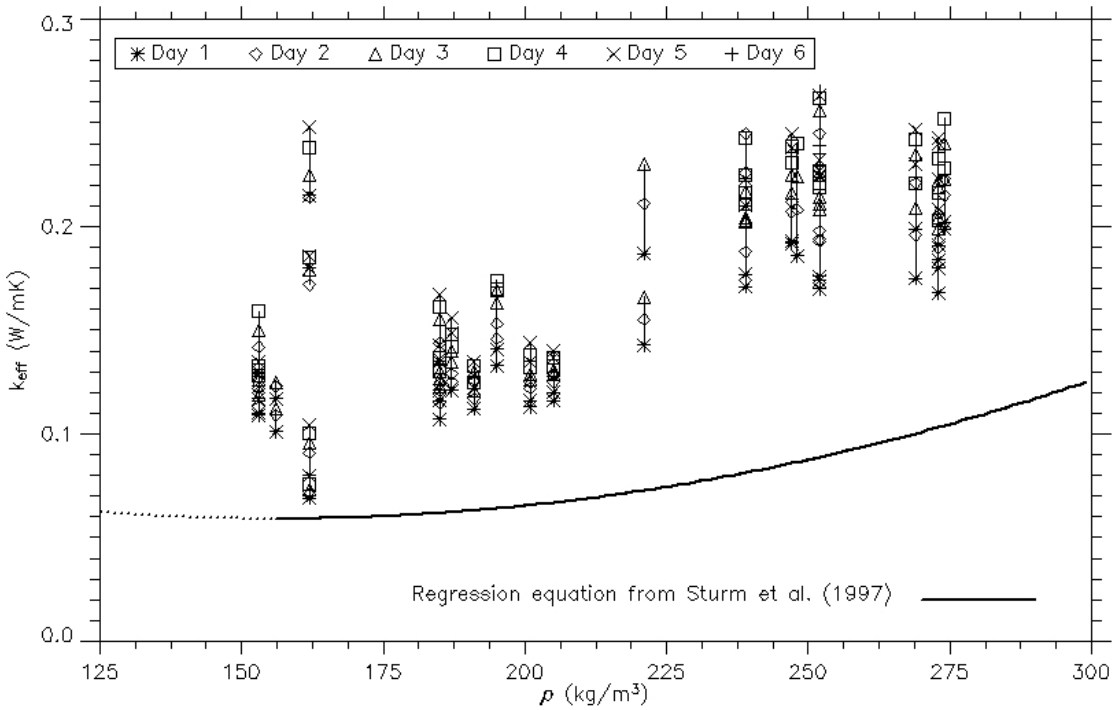

Figure 4.6: Effective thermal conductivity by snow density at each day during each experiment.

system in the heat exchangers malfunctioned during this experiment, resulting in irregular heat flux within the snow samples. The microstructure dataset shows a more consistent trend (Figure 4.7).

There are two plausible explanations for the discrepancy between the values I measured and those predicted by Sturm et al.'s (1997) model. First, much of the data used to develop the regression model had a much higher density than the snow used in my experiments. Their dataset does contain data points in the density range of my experiments but since it is on the low end of the density range the model prediction may not be as accurate for low density snow. Second, Sturm et al. (1997) used measurements from a heated needle probe to calculate k_e. Although they attempted to minimize destruction of the samples during the measurement, it would be impossible not to break

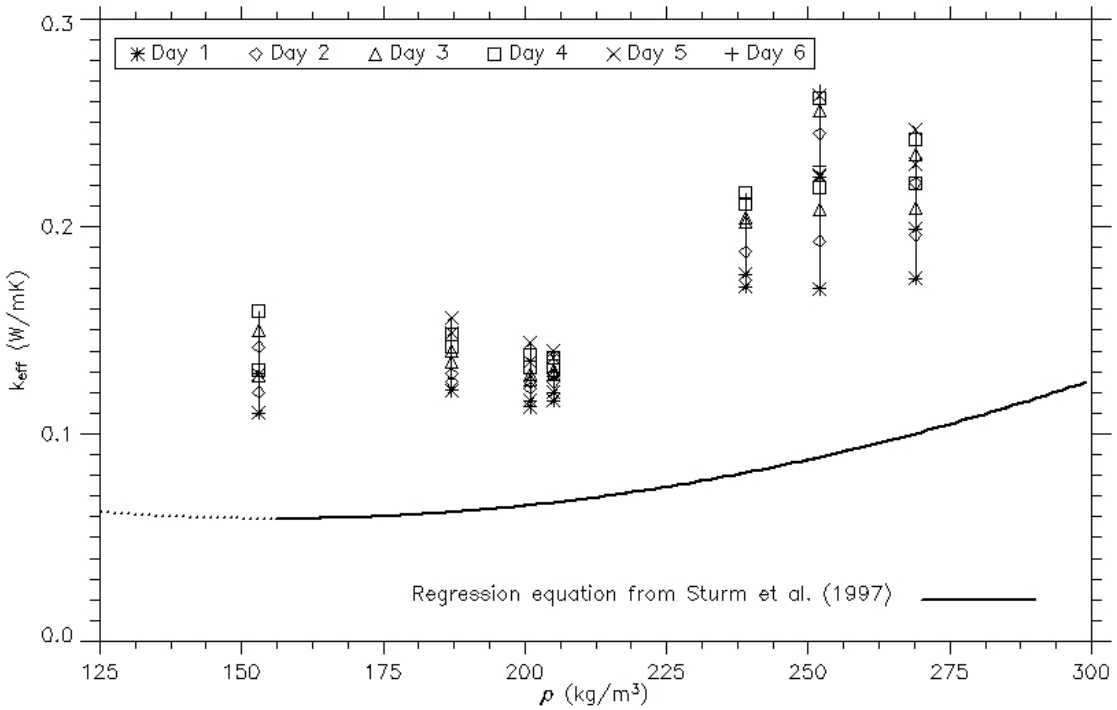

Figure 4.7: Effective thermal conductivity by snow density at each day during the experiments for the microstructural dataset.

the structure directly around the probe. Since the most effective heat transport mechanism in snow is conduction through the ice structure, this method may introduce a systematic error as the structures responsible for the majority of the heat transport are broken when the needle is inserted into the sample.

I performed a simple linear regression of the density and effective thermal conductivity data from the microstructural dataset. These density values were measured with stereological techniques. The details of these measurements are presented in Chapter 5. The model result parameters are shown in Table 4.6. Although the model produced by Sturm et al. (1997) is nonlinear, the coefficients of determination in both models are quite similar ($R^2 = 0.77$, $k_e = 0.73\rho + 0.008$, $p<0.001$ in the current work,

Table 4.6: Parameters from the single-variable linear regression model .

$k_e = 0.73\ \rho + 0.008$		$R^2 = 0.77$	df = 9
	Estimate Standard Error	t value	p-value
Intercept	0.027	0.295	0.775
ρ	0.131	5.533	<0.001

$R^2 = 0.79$ in Sturm et al.(1997)). Given the small dataset generated in this research, these values seem to be quite comparable. The scatter of the data is shown in Figure 4.8.

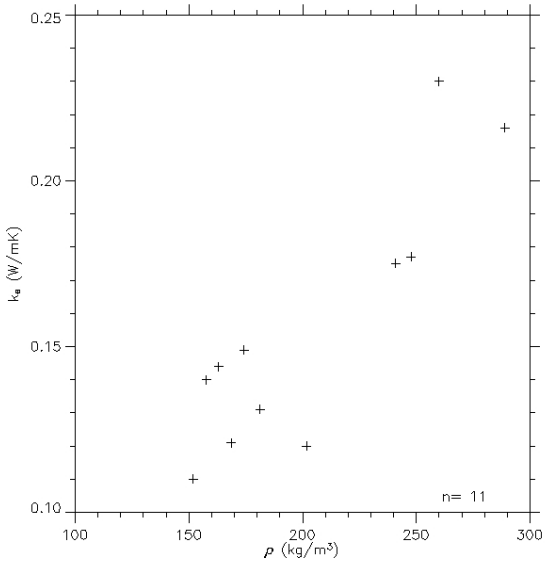

Figure 4.8: Scatter plot of effective thermal conductivity and density from the microstructural dataset.

Previous research has shown that density is loosely correlated to the effective thermal conductivity in snow. However, we also know that the microstructure of the snow has a large effect on k_e. In addition, the character of the microstructure can be very different in snow of similar density. I included the specific surface area and performed a multiple linear regression of the microstructural data to see if the model estimate of k_e

would improve. The model parameters from the multiple regression are shown in Table 4.7. Including specific surface area explained an additional 5% in the variability of the data (adjusted-$R^2 = 0.82$, $k_e = 0.62\rho - 0.002SSA_i + 0.08$, $p<0.001$). With an α of 0.1 we would conclude that it is appropriate to include this parameter in the model (Table 4.7).

Table 4.7: Parameters from the multiple-variable linear regression model.

$k_e = 0.62\rho - 0.002ssa_{-i} + 0.079$		Adjusted $R^2 = 0.82$	df = 8
	Estimate Standard Error	t value	p-value
Intercept	0.040	1.970	0.084
ρ	0.121	5.141	0.001
ssa_{-i}	0.001	-2.160	0.063

Although there is a large amount of scatter in the data (Figure 4.9), this analysis shows that predictions of the effective thermal conductive of snow may be improved by combining density and a measure of the microstructure such as specific surface area. Although the dataset is quite small (n=11), the relationship between SSA_i and k_e appears to be nonlinear. A nonlinear regression model predicts 41% of the variability in k_e ($R^2=0.41$, $k_e=SSA_i^{-0.611}$). Both density and specific surface area can now be obtained fairly easily with field-based measurements (Matzl and Schneebeli, 2006).

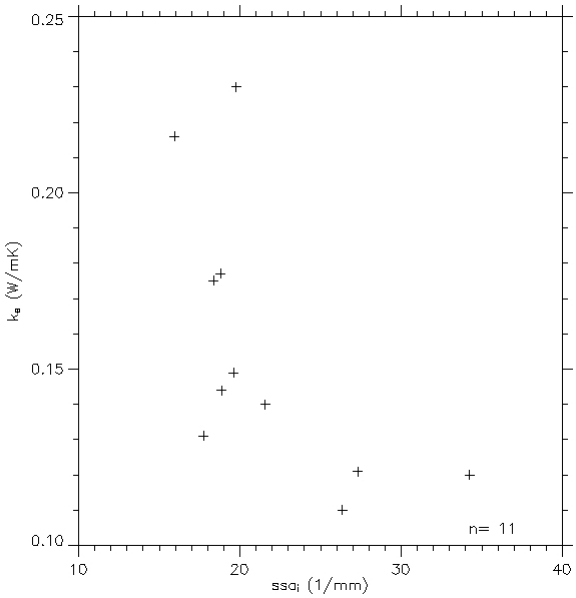

Figure 4.9: Scatter plot of effective thermal conductivity and specific surface area of the ice structure from the microstructural dataset.

4.6 Summary and Conclusions

The thermophysical data collected in these experiments show very interesting trends, but features of the experimental design limit the conclusions we can make from the results. The temperature profiles are generally linear. There is no significant signal from the ice layer in the profiles, although the ice layer clearly affected the microstructure in the snow directly adjacent to the ice layer (as shown in Chapter 5). It is also reasonable to assume that it affected the local temperature gradient. However, this effect was unrecognizable in the bulk temperature distribution and could not be distinguished even when the thermal probes were separated by only one centimeter. Measuring the temperature gradient across the ice layer might require a different type of temperature sensor or a different measurement technique.

The temperature gradients between the treatment and control samples were significantly different. Thus although the samples were constructed from the same type of snow and underwent metamorphism in similar conditions, some differences in the microstructure could be due to differences in the magnitude of the temperature gradient. The absolute value of the temperature gradient in all of the experiments was in excess of 60 K m^{-1}, which is six times the nominal minimum threshold for kinetic growth metamorphism (Armstrong, 1985). Although the transition between equilibrium and kinetic metamorphism is most likely a function of porosity, particle size, mean temperature, and temperature gradient, all of these samples were soundly in the kinetic growth regime during the experiments (Miller, 2002). We do not really know how increasing the temperature gradient affects the crystal growth rates of snow undergoing kinetic growth. Diffusion is a self-limiting process. Faktor et al. (1971) showed that modeled crystal growth rates increased rapidly with increasing temperature difference, but also quickly approached an asymptotic value. Marbouty (1980) found that increasing the temperature gradient produced larger grains in his snow samples (Figure 4.10). The increase in grain size appears to slowly decrease as the temperature gradient increases. However, the temperature gradients in my experiments were larger than those used by Marbouty. The relationship between crystal growth rates and temperature gradient is most likely non-linear.

The heat flux during the experiments reached a steady state after an initial adjustment period. The effective thermal conductivity increased during metamorphism as the connections between ice structures eroded and new connections formed. Under a strong temperature gradient the ice structure changes to optimize one-dimensional heat

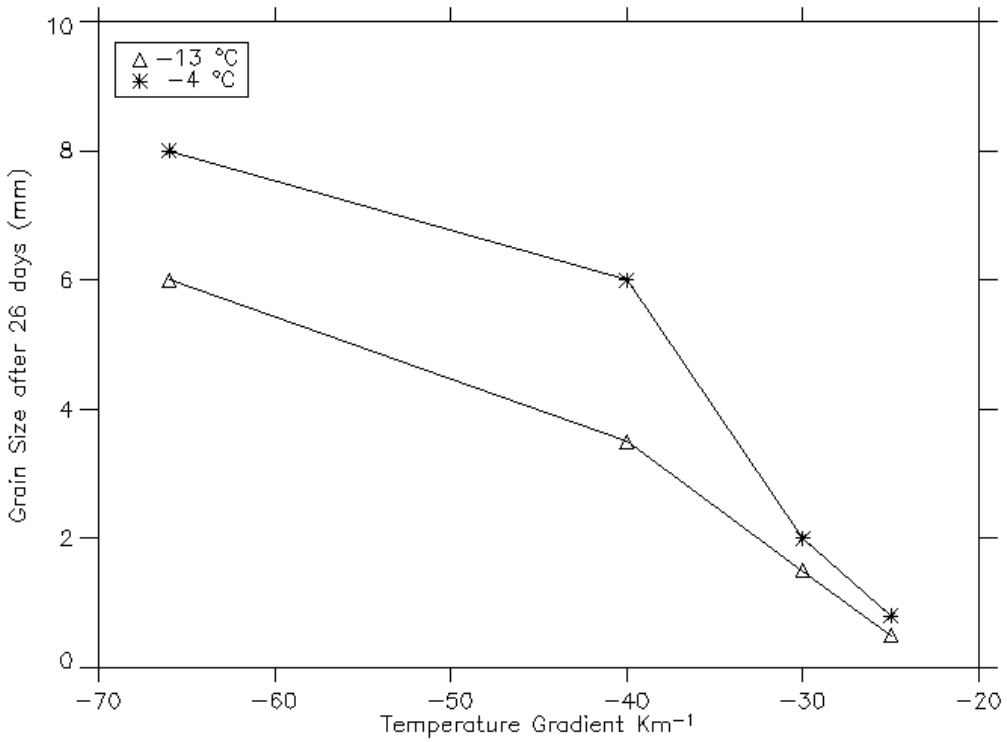

Figure 4.10: Mean grain size and temperature gradient from two different temperature levels in a snow metamorphism experiment (from Marbouty, 1980). The grain size was measured after 26 days of metamorphism.

flow. On average, the effective thermal conductivity increased by 21% during a five day period. Schneebeli and Sokratov (2004) also observed an increase in k_e during metamorphism. To my knowledge this is the only other group that has investigated the temporal evolution of k_e.

The magnitude of the effective thermal conductivity was larger than that predicted by a regression equation developed by Sturm el al. (1997). However the density of the snow samples used in this study are near the lower limit of their density measurements. I observed a similar correlation between density and effective thermal conductivity to those observed in previous studies. By adding specific surface area to the statistical model I was able to improve the correlation by 5%. Matzl (2006)

developed a method for measuring specific surface area that can be used in the field. The present work indicates that by combining a bulk physical parameter such as density with a microstructural parameter we may be better able to determine important thermal properties of snow structures. Although more work is required to increase the confidence of this finding, these results suggests that we can improve our estimates of k_e by recording a second parameter that can also be measured in the field.

Chapter 5

MICROSTRUCTURE

5.0 Introduction

The purpose of this chapter is to describe, analyze and interpret the microstructure of the snow samples at the beginning and end of the laboratory experiments. The discussion includes both quantitative measurements and qualitative observations. The quantitative measurements are from a subset of the total experiments, which I refer to as the microstructure dataset in Chapter 4.

I selected the experiments for the microstructure dataset based on the quality of the thermophysical and image data. In all of these experiments the heat loss from the sides of the insulated boxes was relatively small. In addition, I was able to collect relatively high quality images of the casts with adequate contrast between the ice forms and pore filler. This made automated image processing and three-dimensional reconstruction possible.

I made every attempt to analyze the microstructure with quantitative methods. However, there are some interesting features in these images that were difficult to quantify. Thus, in addition to discussing the measurements, I also discuss qualitative features that appear in the images.

5.1 Stereological Measurements

In this section I discuss stereological estimates of density and specific surface area. All of the measurements are from two-dimensional surface sections of the cast snow samples. I cut the samples parallel to the heat flow axis so that the sections would satisfy the vertical, uniform and random requirement for stereological analysis using cycloid grids (see Chapter 3 for details).

5.1.1 Density

I used two different techniques to measure the density of the snow samples. During the preparation of an experiment I cut a 250 cm^3 section of snow (RIP2 cutter, Snowmetrics) from each block collected from the field. I divided the mass of this section by its volume to calculate the density. I also used stereological methods to calculate the density of the sample casts. The values obtained with the two methods are quite consistent (Figure 5.1) and a linear regression model of the data produced a high coefficient of determination ($R^2 = 0.9$, $\rho_{stereology} = 0.94*\rho_{rip} + 7.5$, p=0.001).

To determine how metamorphism affected the density of the snow samples I compared the mean values of the initial and control samples (Figure 5.2). In the March 04, 2005 experiments the density decreased but in the other six experiments the density increased. The density change was generally much less than 20%, but one sample changed by 28%. A linear regression model of the data explained 67% of the variance in the control sample density (R^2=0.67, $\rho_{control} = 1.1*\rho_{initial} - 14.3$, p=0.02). This result is due in part to the scale of the measurement method. The density profiles for each sample (Figure 5.3) are intertwined indicating that the stereological estimates for the initial and control samples are quite similar.

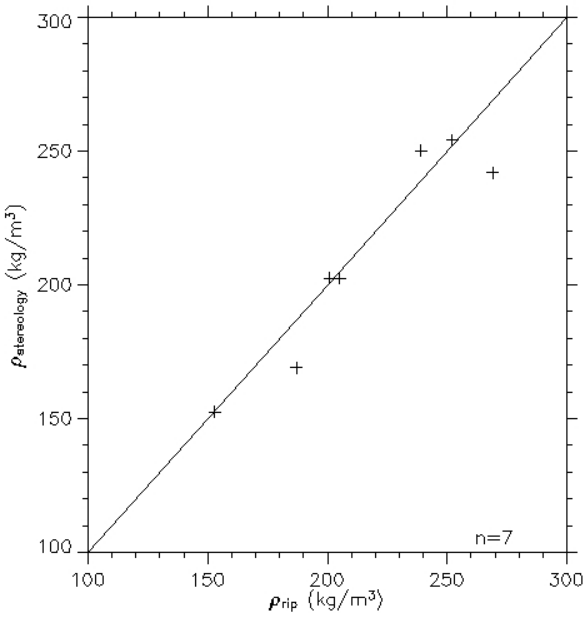

Figure 5.1: Scatter plot of the initial snow density measured with a RIP cutter and stereological methods. The solid line is the one-to-one line for reference. A linear regression model of these data produced a coefficient of variation of 0.9.

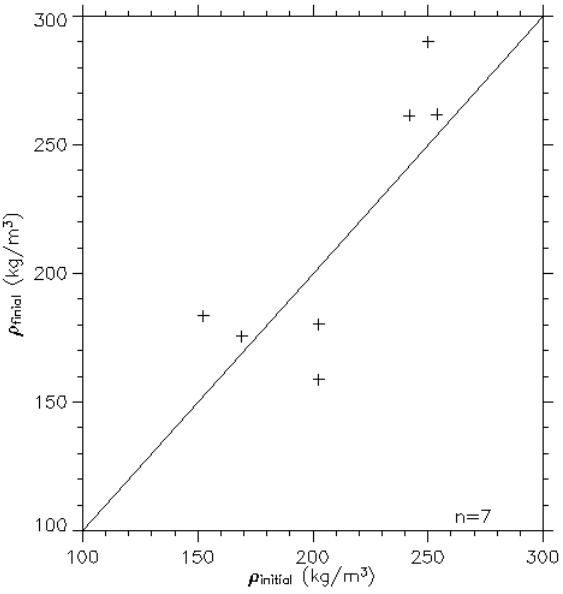

Figure 5.2: Scatter plot of the initial and final sample density measured with stereological methods. The initial density is from the initial cast and the final is from the control sample cast. The solid line is the one-to-one line for reference. A linear regression model of the data produced a coefficient of variation of 0.67.

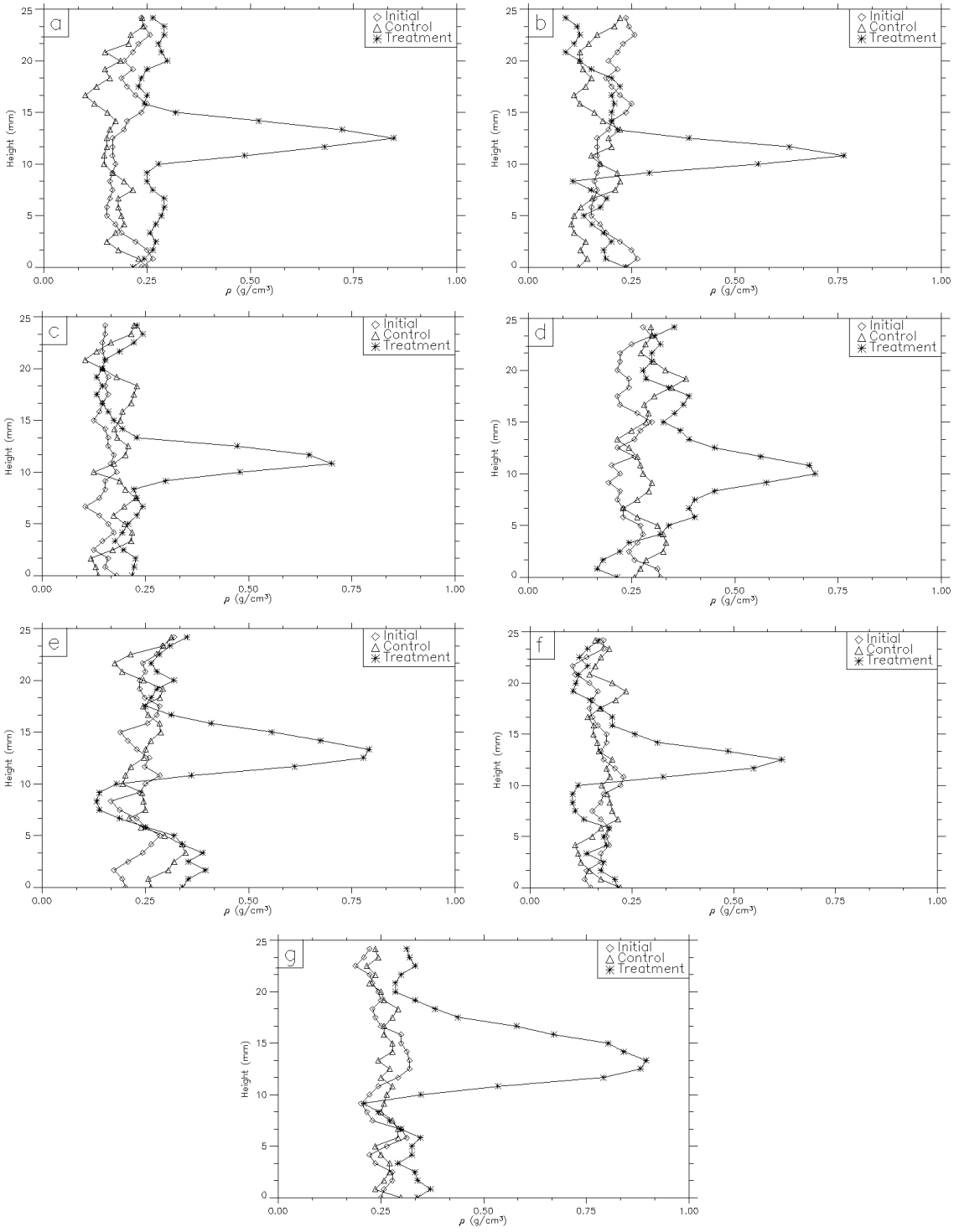

Figure 5.3: Density variation with height from seven experiments. The initial, control and treatment samples appear in the same panel. a) March 4, 2005A, b) March 4, 2005B, c) April 6, 2005A, d) January 6, 2005B, e) March 17, 2005A, f) February 23, 2005B, g) March 25, 2005A.

The density profiles from each experiment are interesting, but the results are not consistent (Figure 5.3). The ice layer is prominent in all the density profiles of treatment samples. There is also a slight, but consistent, decrease in density on both sides of the ice layer in most of the samples (Figure 5.3a,c,e, and g). Since the ice layer was not initially flat, this indicates a substantial change in density around the ice layer. In each experiment repetition the profiles overlap each other indicating that density changes due to metamorphism are within the scatter of the data (Figure 5.3) and due to variations in the initial density and not metamorphism.

5.1.2 Specific Surface Area

The specific surface area is a measure of the surface of an object with respect to its volume. For a porous material we can define the volume as the total volume, or the volume of a single component (i.e. ice). The values that I discuss in this section are the specific surface area with respect to the ice volume (SSA_i).

The SSA_i of the snow samples decreased during metamorphism (Figure 5.4). This result is consistent with the results of previous studies (Schneebeli and Sokratov, 2004). In one experiment (March 17, 2005A) the SSA_i of the control sample increased, but the increase was relatively small (6%).

The SSA_i of the control sample generally decreased more than the treatment sample (Figure 5.4). The calculations include the ice layer, so this result may be more dependent on the presence of the layer than the change due to metamorphism. In two experiments the decrease was larger in the treatment sample. In the January 6, 2005B experiment (ρ = 239 kg m^{-3}, Figure 5.3) the SSA_i values differ by only 0.6 mm^{-1} (18% of

the total change and 3% of the initial value). The difference between the SSA_i values for the treatment and control samples was much larger in the April 6, 2005A experiment. The initial density of the snow used in this experiment was lower than any other repetition (157 kg m^{-3}) and the initial morphology was much closer to precipitation particles (2b) than any of the other experiments.

The decrease in SSA_i during metamorphism is quite prominent in the March 4, 2005 experiments (Figure 5.5a and b). In the rest of the experiments the profiles are more intertwined. The profiles for the February 23, 2005B experiment show a general decrease in SSA_i during metamorphism. The mean values for the initial sample may be skewed by a few points in the profile (Figure 5.5f). Vertically, the SSA_i increases slightly on either side of the ice layer in the treatment samples. This result is consistent in all of the experiments and therefore shows a stronger trend than the density field.

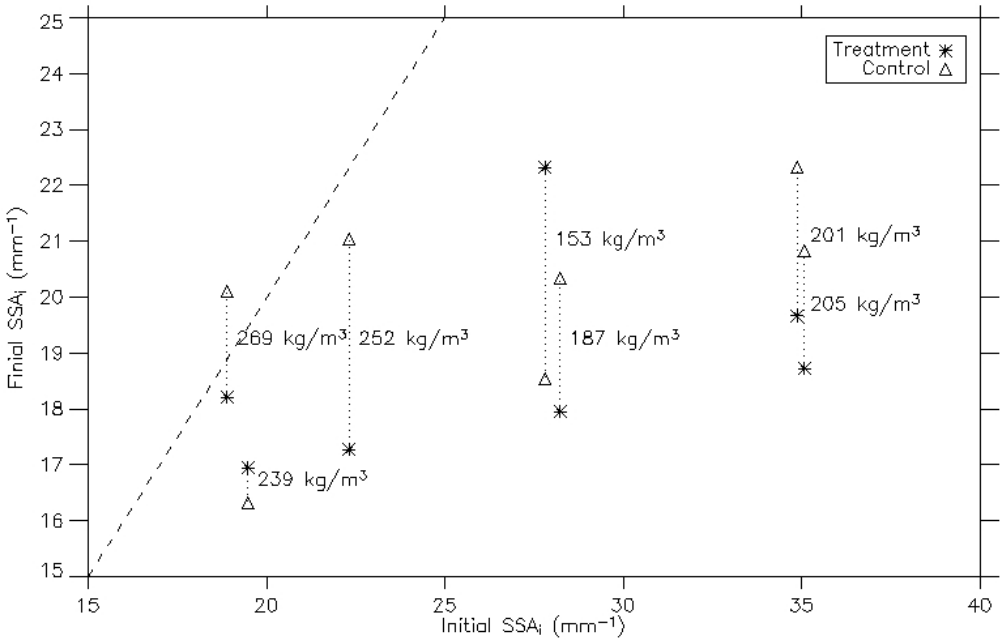

Figure 5.4: The specific surface area with respect to ice volume of the snow samples. The value of the initial cast is listed on the abscissa and the final casts (treatment and control) are on the ordinate. The dashed line is the one-to-one line for reference.

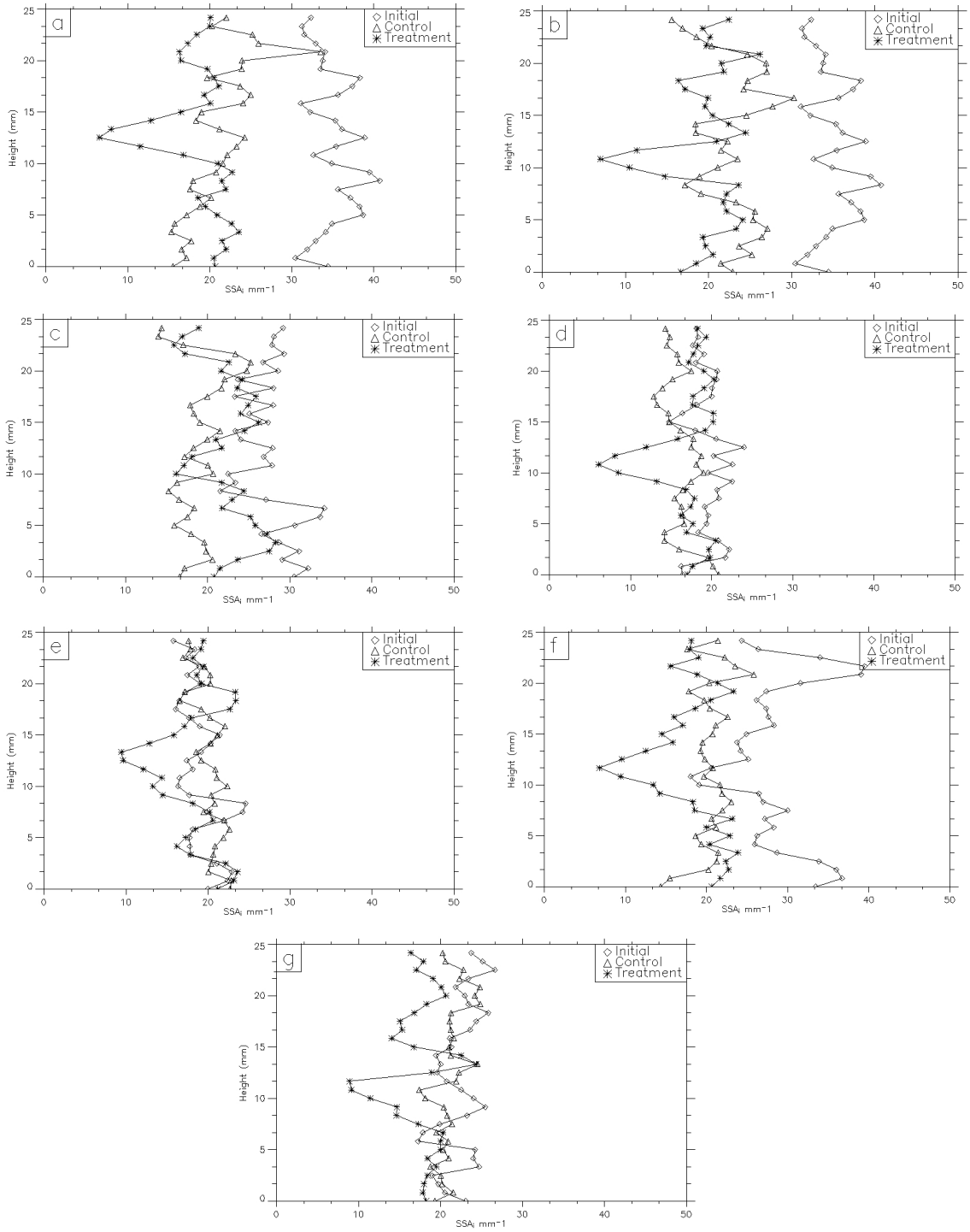

Figure 5.5: Specific surface area variation with height from seven experiments. The initial, control and treatment samples appear in the same panel. a) March 4, 2005A, b) March 4, 2005B, c) April 6, 2005A, d) January 6, 2005B, e) March 17, 2005A, f) February 23, 2005B, g) March 25, 2005A.

5.2 Three-Dimensional Measurements

In this section I discuss values calculated from three-dimensional reconstructions of snow samples. All of the values were obtained from the Image Processing Language (IPL) software package (Scanco, http://www.scanco.ch) (see Chapter 3 for details). The values in this section are from the models of two experiments (January 6, 2005B and March 17, 2005B). There are a total of six samples, two initial casts, two control casts and two treatment casts.

5.2.1 Specific Surface Area

I calculated the specific surface area of the reconstructed samples with IPL routines written by Scanco (see Chapter 3) (Table 5.1). In the January 6, 2005B experiment the SSA_i decreased during the experiment. In the March 17, 2005B samples the SSA_i decreased in the treatment sample and increased in the control sample. This is probably an artifact of the image processing as the calculated SSA_i of the initial sample is quite low for that type of snow (4c, 264 kg m^{-3}).

Table 5.1: Microstructural parameters from the three-dimensional models.

Experiment	Ice volume/ Total volume (mm^{-1})	SSA_i (mm^{-1})	SMI	Trabecular Number (mm^{-1})	Trabecular Thickness (mm)	Trabecular Space (mm)
January 6, 2005B initial	0.081	25.5	2.87	1.04	0.08	0.88
January 6, 2005B control	0.233	12.5	1.4	1.46	0.16	0.52
January 6, 2005B treatment	0.349	8.9	1.74	1.56	0.22	0.42
March 17, 2005B initial	0.224	14	2.5	1.58	0.14	0.49
March 17, 2005B control	0.111	18.9	2.26	1.06	0.11	0.84
March 17, 2005B treatment	0.335	9	1.25	1.51	0.22	0.44

In order to compare the SSA_i values from both the two and three-dimensional analysis, I used a linear regression model (Figure5.6). The model was not significant at the α=0.05 level. The small dataset may contribute to this result. The relationship between the two and three-dimensional values improves slightly with a polynomial model (R^2=0.4, $SSA_{i\text{-}3D} = 0.04(SSA_{i\text{-}2D})^2$, $p<0.001$). There are several possible explanations for this result. First, the three-dimensional models contain more structural elements and thus may include a larger variation in SSA_i. The measurement technique produces a mean value for the entire model, making it difficult to conduct a direct comparison with a two-dimensional slice. Second, the image processing used to segment the ice and pore areas reduced the total ice mass of the sample. This reduction was difficult to quantify, but a careful examination of the images at each step in the process indicated a reduction occurred (Figure 3.12). I made every effort to minimize the effect,

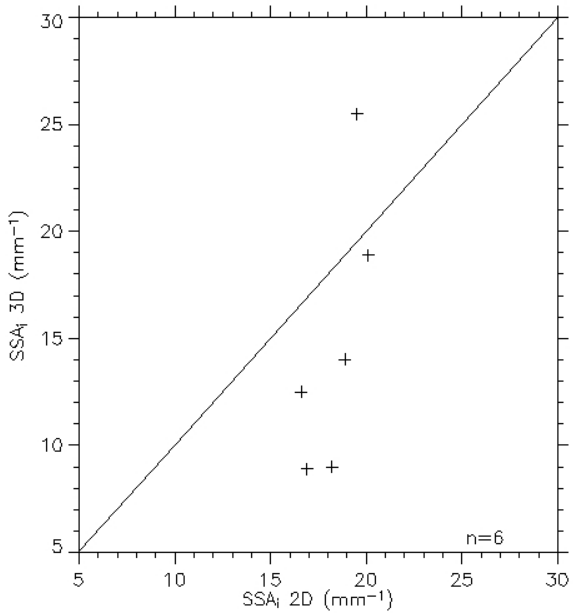

Figure 5.6: Scatter plot of SSA_i values obtained from two-dimensional images (stereology) and three-dimensional models (IPL). The solid line is the one-to-one line for reference.

but it probably contributed to this result. Matzl (2006) compared SSA_i values determined from two and three-dimensional methods and found that they were highly correlated. Although she used a different two-dimensional method, this suggests that the three-dimensional reconstructions were limited by the quality of the original images.

5.2.2 Structure Model Index

The Structure Model Index (SMI) is a parameter developed to describe the microstructure of bones (Hildebrand and Rüegsegger, 1997). The index represents the curvature (convexity) of the structure by quantitatively characterizing a structure as "rod-like" or "plate-like". An ideal plate structure has a value of 0 and an ideal rod structure has a value of 3. A sphere has a SMI of 4. SMI values for my three-dimensional snow models range from 1.4 to 2.9 (Table 5.1). The initial samples have the highest SMI values, indicating that they are more rounded structures. During kinetic growth metamorphism facets develop and the structure become more "plate-like". This transformation is evident in the decrease in SMI values during the experiments. The treatment samples also have a lower SMI value than the control samples as they contain an ice layer, which is obviously a "plate-like" structure.

5.3 Qualitative Microstructural Observations

The microstructural portion of this study was designed to generate and compare quantitative measures of the snow microstructure. Previous researchers have attempted to quantify the grain and bond structure of snow (Kry, 1975; Hansen and Brown, 1986; Edens and Brown, 1991 and 1992), but these efforts were limited to two-dimensional

analyses and rounded snow grains. Faceted snow has a more complicated structure and recent investigations have raised fundamental questions about how we look at the microstructure of snow (Schneebeli, 2000). As a result there are some interesting trends in these images that cannot be quantified with the tools currently available. In this section I discuss some observations of the snow microstructure that have implications for future research, but that I was unable to quantify.

5.3.1 Two-Dimensional Images

During each experiment the snow transformed from its original form (2a or 4c, Colbeck et al., 1990) to a well-developed faceted structure (5a or 5b, Colbeck et al., 1990) (Figure 5.7). The thermal conductions produced a large vapor pressure gradient and water mass and heat flowed vertically through the snow samples. At the end of each experiment the snow contained large faceted structures that were often striated and hollow.

In the treatment samples water vapor deposits on the lower surface of the ice layer. Areas of preferential deposition grew faster than neighboring portions of the ice layer and faceted structures sprouted from its lower boundary (Figure 5.7 and 5.8). In some samples the density of the ice layer and the new ice was different. In some of the images the ice that formed by vapor deposition is visibly differentiated from the artificial ice layer (Figures 5.7, 5.8, 5.9 and 5.10). The metamorphic process formed many and often large connections between the ice layer and the snow below.

While the lower surface of the ice layer was growing the upper surface was eroding. Sublimation at the upper boundary formed a smooth and even surface (Figures

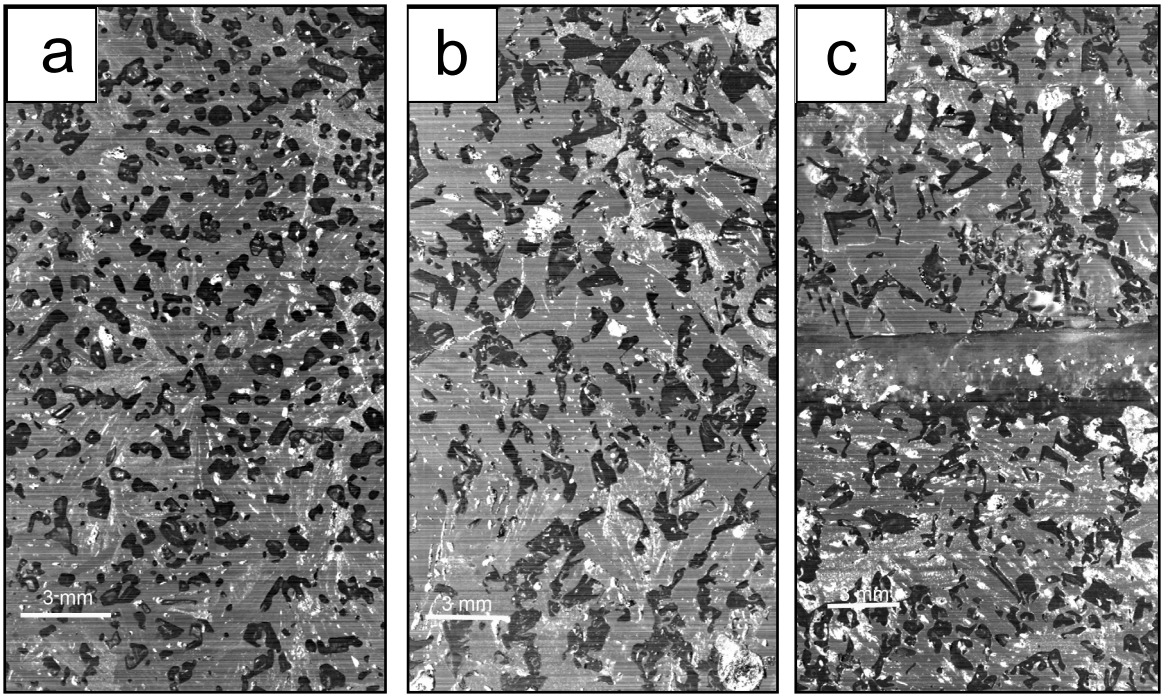

Figure 5.7: Surface sections of the three samples in the March 17, 2005B experiment: a) the initial sample, b) the control sample in the middle, c) the treatment sample. In the sections, the ice structure is black and the pore filler is gray. The white streaks are dimethyl phthalate crystals and in some of the other figures small air holes are visible. This set of images shows the dramatic changes in microstructure that occur during kinetic metamorphism and between the control and treatment samples.

5.7, 5.8, 5.9 and 5.10). The snow structures directly above the ice layer were often larger than their neighbors higher in the sample (Figures 5.8b, d, e and f, 5.9b, and 5.10). In general the connections between the snow above the ice layer were fewer and smaller in size than those below the ice layer (Figures 5.7, 5.8, 5.9 and 5.10). The size differential between particles directly above the ice layer may to be related to the thickness of the ice layer (Figure 5.9). The ice layer seemed to have a very local effect. The effect of the ice layer was limited to structures within two or three particles of the interface.

In many of the experiments, small cavities formed directly above the ice layer (Figures 5.8b, d, e and f, 5.9 and 5.10). These microcavities varied in size, but always formed directly above the ice layer (Figure 5.8). These features were typically several

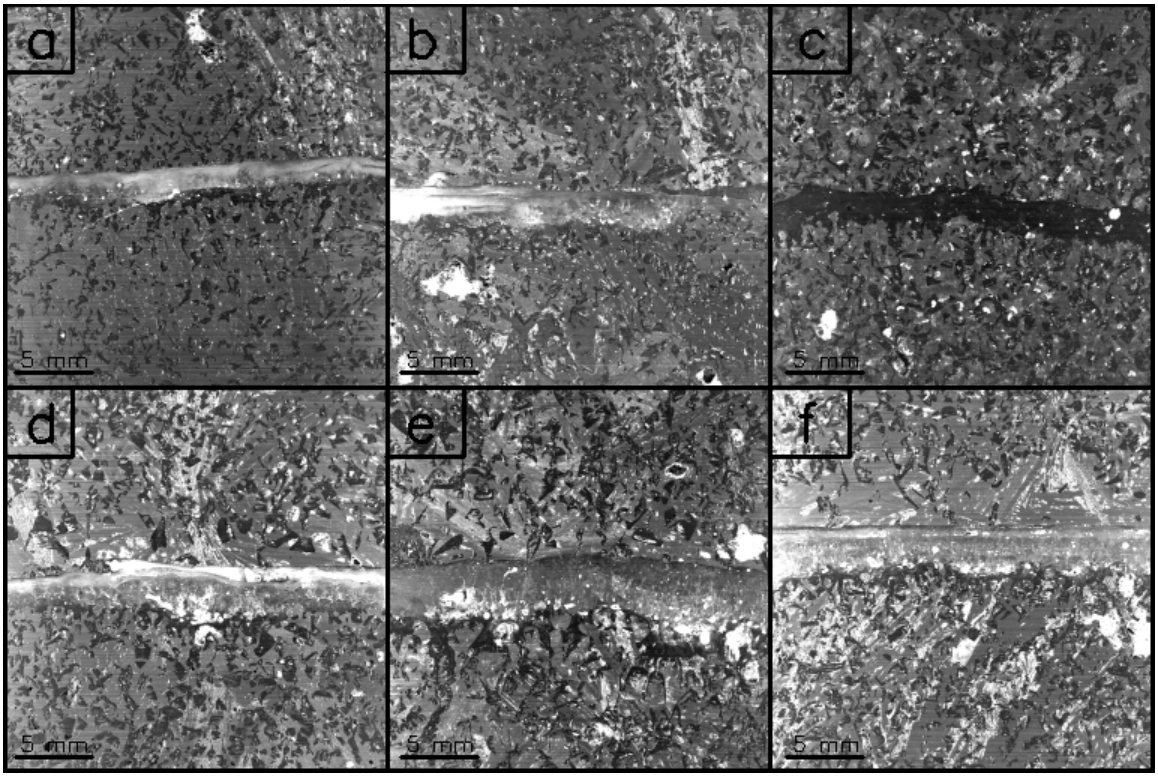

Figure 5.8: Surface sections from six treatment samples: a) April 6, 2005A, b) March 4, 2005A, c) January 6, 2005A, d) March 17, 2005A, e) March 25, 2005A, f) December 1, 2004A.

times larger than the neighboring structures and did not always form in the same location. By examining the serial sections I saw that if you moved horizontally through the structure you would encounter ice at the end of the microcavity. However, another hole was present in a location that contained ice in an earlier section (Figure 5.10).

5.3.2 Three-Dimensional Models

The same microstructural features that appear in the two-dimensional images are also evident in the three-dimensional models. The particles in the initial snow sample structure are relatively small and the edges are typically smooth (Figure 5.11). In contrast the control sample (the same snow after the experiment) has much larger

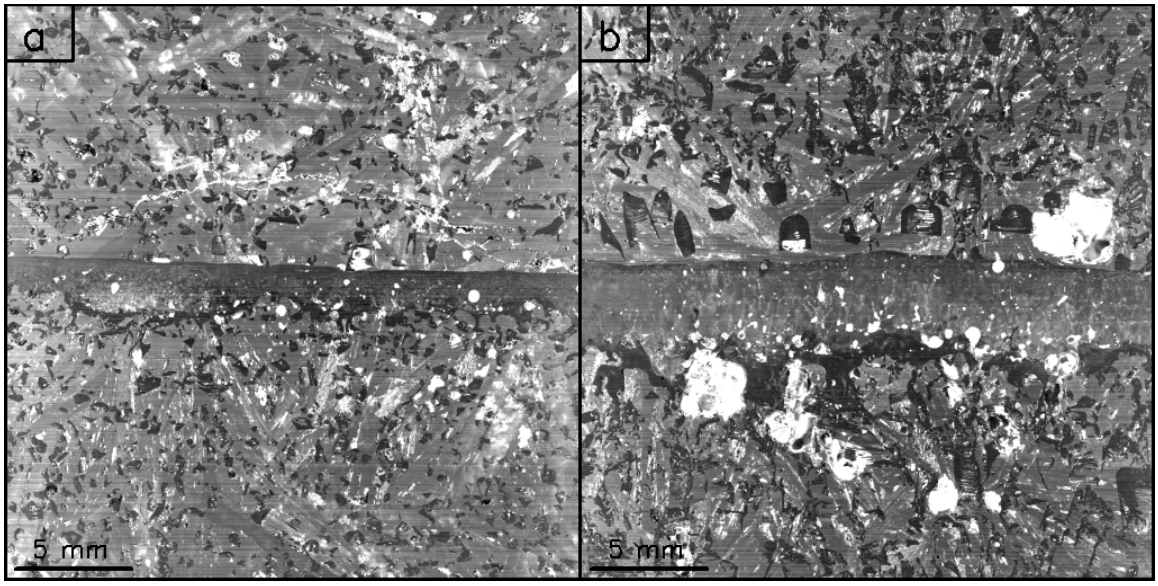

Figure 5.9: Surface sections from a sample with a thinner ice layer (a) and a thicker ice layer (b). Large faceted structures with hollow cups formed directly above the thick ice layer.

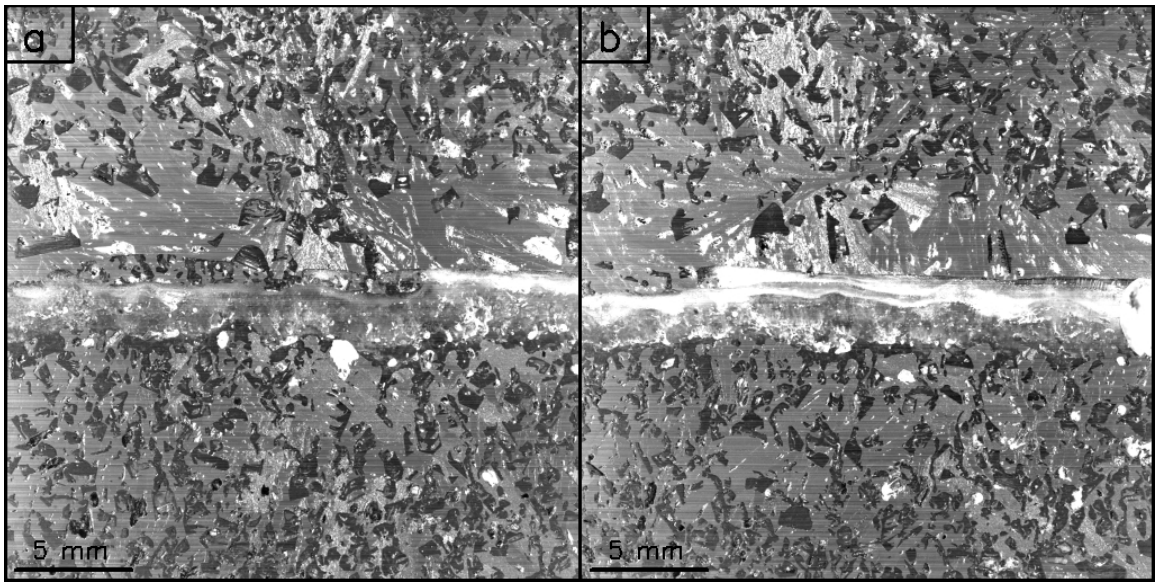

Figure 5.10: Surface sections from the March 19, 2005A treatment sample. Microcavities are visible directly above the ice layer. The region that contains microcavities in panel a) contains ice structures in panel b). The two panels are 6.288 mm apart.

particles with large flat faces (Figures 5.12, 5.13 and 5.14). Some of the structures are striated and with hollow features like the depth hoar crystals that we often see in nature (Colbeck et al., 1990) (Figures 5.12, 5.13, 5.14 and 5.15). Chains of depth hoar crystals, indicating a very well developed kinetic growth structure, also appear in the models (5b, Colbeck et al., 1990) (Figure 5.12).

The three-dimensional models of the treatment samples show similar structures to those I observed in two-dimensions. There are more connections to the snow on the lower side of the ice layer and the connections are generally larger than those on the top. The upper side of the ice layer is generally smooth (Figures 5.15). The particles above the ice layer are generally larger than those directly below. There are also fewer connection points between the structures directly above the ice layer and the layer itself.

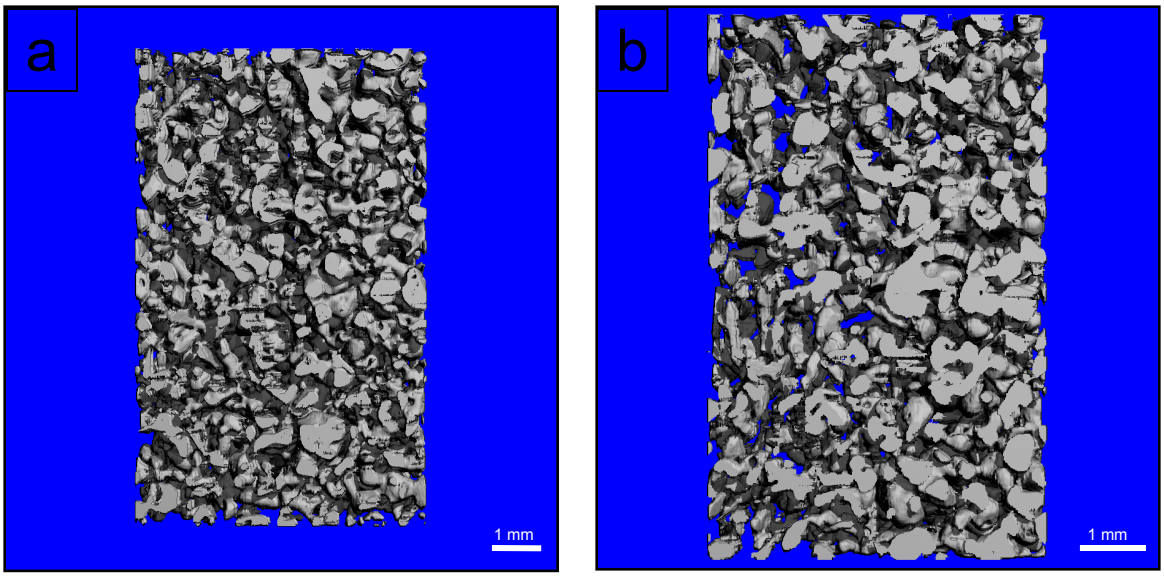

Figure 5.11: Three-dimensional reconstruction of the initial cast from the March 17, 2005 experiment: a) entire reconstruction, b) a narrow section of the model.

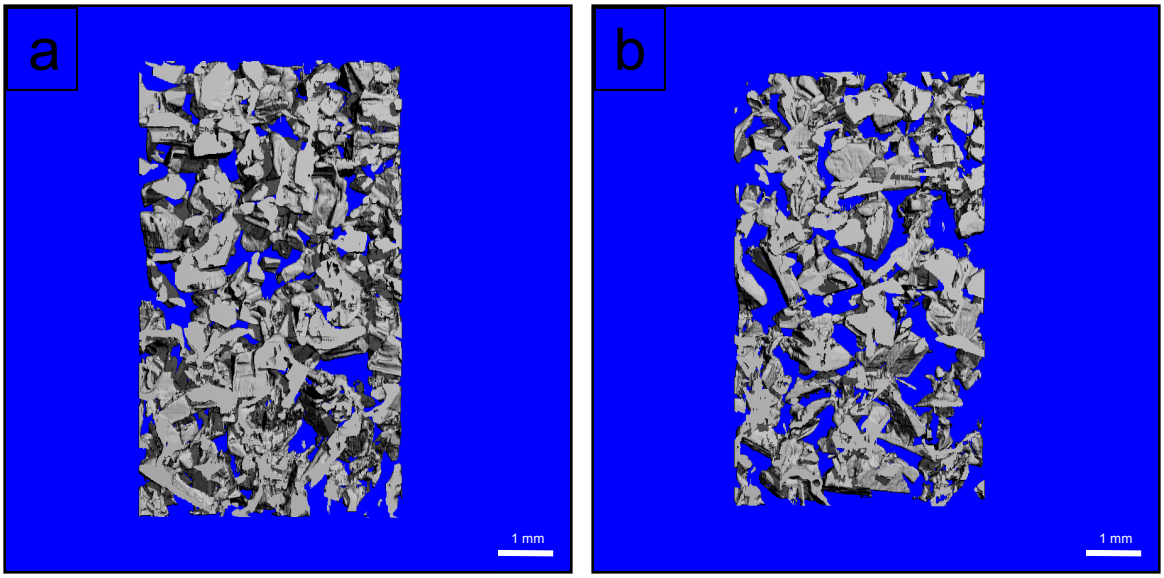

Figure 5.12: Two narrow sections of a three-dimensional reconstruction of the January 6, 2005B control sample. A large range in particle size and the development of kinetic growth forms are visible in the right panel.

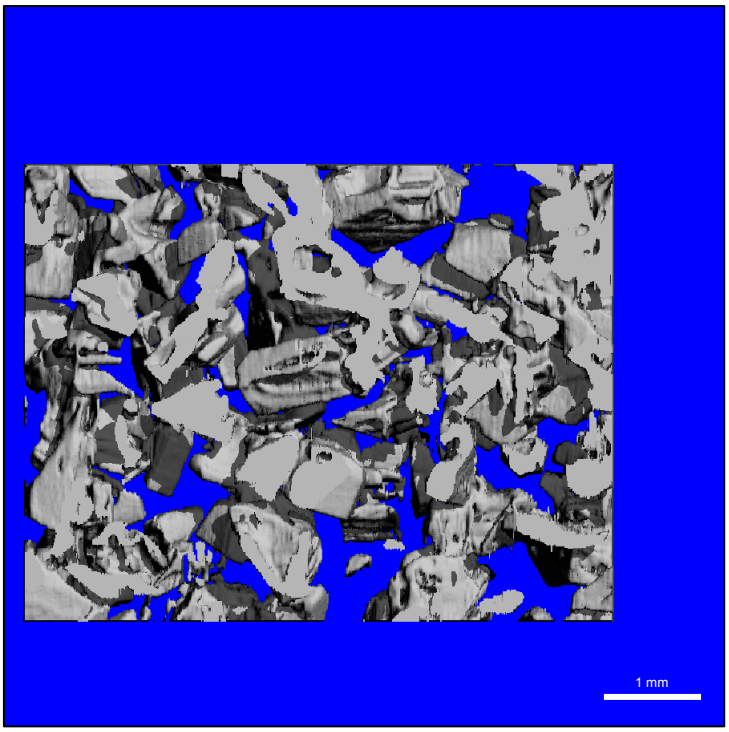

Figure 5.13: Close up view of the three-dimensional reconstruction of the January 6, 2005B control sample.

Air bubbles in the ice layer are visible in the two-dimensional images (Figures 5.7, 5.8, 5.9 and 5.10). Although these features appear to be quite small and round in two-dimensions, in three-dimension they have a horizontal structure (Figure 5.15). These holes in the ice layer probably formed when the ice layer was formed as an artifact of the iterations of water and flash freezing. Although the air pockets impact the heat transfer through the ice layer it is unlikely that they affected the bulk transport through the structure.

5.4 Summary and Conclusions

There have been relatively few studies of snow microstructure that consider kinetic growth forms. Kinetic growth forms are difficult to characterize with quantitative methods as they have complex structures with sharp irregular faces and

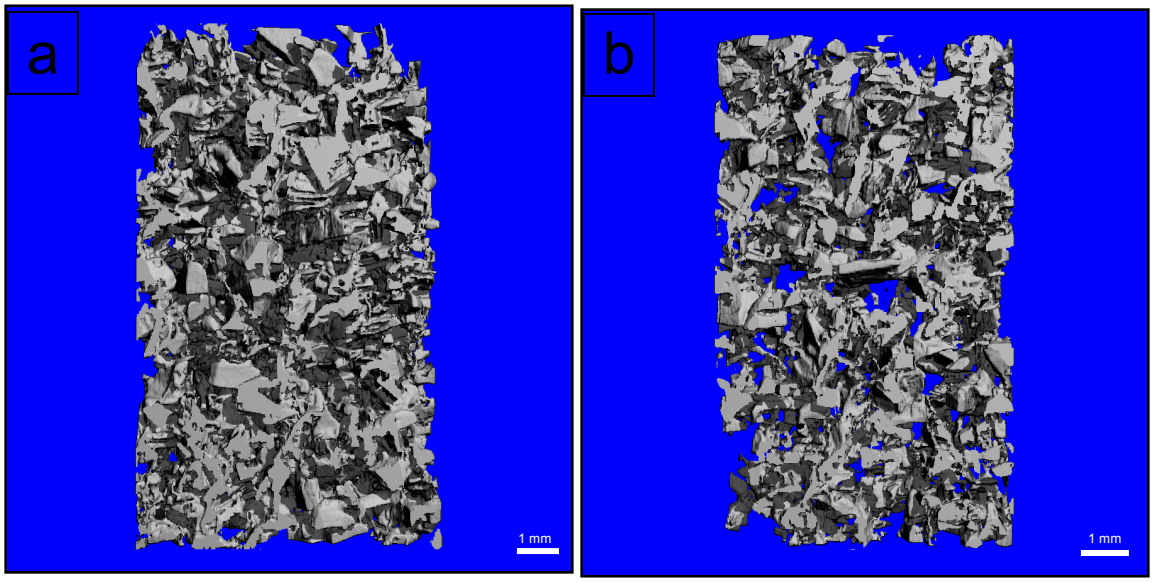

Figure 5.14: Three-dimensional reconstruction of the March 17, 2005B control sample: a) entire reconstruction, b) a narrow section of the model.

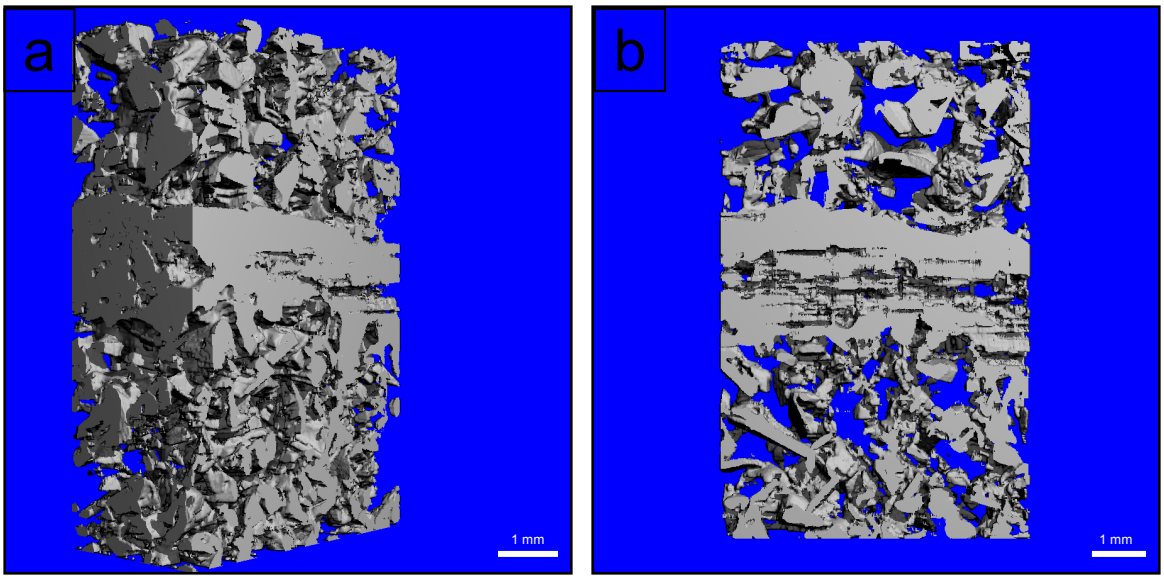

Figure 5.15: Three-dimensional reconstruction of the March 17, 2005B treatment sample: a) entire reconstruction, b) a narrow section of the model.

hollow areas. The trend in microstructural parameters during metamorphism is similar to previous work (Legagneux, 2003; Schneebeli and Sokratov, 2004), although there are only a few microstructural datasets of snow during metamorphism.

The stereological density measurements are well correlated to a common field technique. The density during metamorphism changed more than I expected. Determining the exact error in the stereological measurements is difficult. Thus it is also difficult to determine how much of the scatter in the data is due to the measurement technique. The number of intersections used in the calculations is large enough that the results should be stable (Narita, 1969).

The visual images of the layered structures have important implications. As water vapor deposits on the lower side of the ice layer, the layer begins to grow. Some portions of the ice layer grow faster and these areas eventually extend into and connect to the snow below. Essentially we are looking at a snapshot of the ice layer decomposing. Under these conditions, this process would continue and these extensions would eventually turn into particles. The upper side of the ice layer is eroding and becomes very smooth. The ice layer may actually be moving down in the structure as material attaches to the bottom and is removed off the top. This provides more room in the snow structure for large facets to grow. The particles directly above the layer become larger than their upstairs neighbors and develop large sharp faces and hollow structures. There are fewer connections between the ice layer and the particle directly

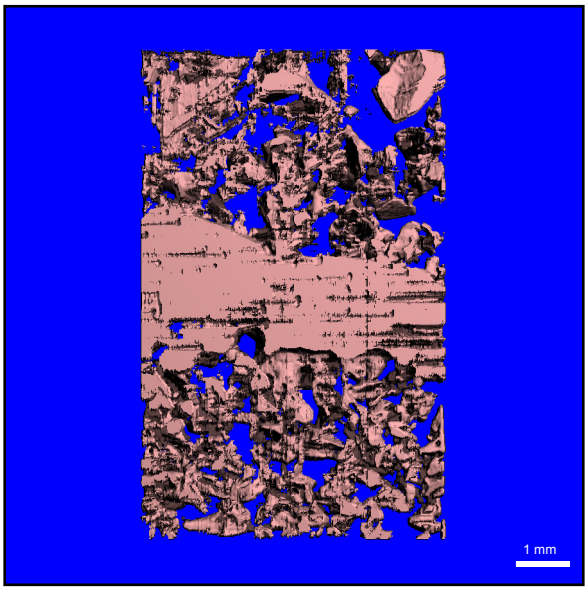

Figure 5.16: A narrow section of the three-dimensional reconstruction of the January 6, 2005B treatment sample.

above creating a mechanical weakness. Although we have observed this process in the laboratory, it would be very difficult to observe structural features of this size with common field techniques.

In snow science it is common practice to characterize the microstructure of an individual snow layer by recording the size and type of the snow grains. We typically measure the length of the "greatest extension" of the grains as a single value or size range (i.e. 4 mm depth hoar or 2-4 mm depth hoar) (Greene et al., 2004). In these models presented here, a large range in particle size still exists after five days under a large temperature gradient. The shape of the particles also represents a wide range of kinetic growth forms, from small facets to large striated and even hollow structures (Figures 5.12, 5.13 and 5.14). This suggests that even in an environment conducive to rapid crystal growth, the structures are both growing and eroding. Very sharp, growing crystals exist alongside smaller rounded and eroding crystals. Although the common field method may be suitable for some applications, it does not give a complete representation in terms of the optical grain size, thermal and probably mechanical properties of the snow microstructure.

Chapter 6

EXPERIMENT SIMULATION

6.0 Introduction

This chapter describes numerical simulations from two different models. I used the SNOWPACK model to simulate the thermal properties and metamorphic evolution of the snow samples and the vanRietbergen-Kaempfer-Schneebeli (RKS) model to simulate the temperature and heat flux in the snow structure at the microscale. Both use a finite-element approach to model the physical processes within the snow. However, the scale of the elements and scope of the models are quite different. SNOWPACK is an operational forecast model that examines heat and mass transport within the snowpack as well as changes in the microstructural properties of the snow. It parameterizes the microstructural properties of the snow based on the conceptual model of snow as a series of grains and bonds. Properties of the each snow layer are empirically determined by the grain class (Colbeck et al., 1990). The RKS model replicates the movement of thermal energy within a static ice structure. It produces a microscale model of the distribution of heat in the structure, but the structure does not evolve through time. Although the simulations are very different in scope and scale, examining the results and comparing them with observed values helps to improve our understanding of snow metamorphism and our ability to simulate processes within a snow cover.

6.1 SNOWPACK Model

Scientists at the Swiss Federal Institute for Snow and Avalnache Research developed SNOWPACK (Lehning et al, 1999; Bartelt and Lehning, 1002; Lehning et al., 2002a and b) building on previous modeling efforts in France (Brun et al., 1992) and the United States (Jordan, 1991; Adams and Sato, 1993). It is a one-dimensional model that simulates vertically oriented processes within the snowpack as well as interactions with the soil and atmosphere. The soil and atmospheric routines provide boundary conditions for the snowpack portion of the model. Typically weather events build layers within the model and those layers evolve based on boundary conditions provided by the soil and atmospheric models.

I initialized the model with measurements from the beginning of each experiment. I turned off the soil portion of the model and set the atmospheric parameters to replicate the cold laboratory environment (i.e. no wind or incoming short wave radiation). I also deactivated the settling routine in the model to maintain the size of the snow sample during the simulation. The model structure in each simulation consisted of twenty four numerical elements, each 45 mm thick, for a total snow height of 10.8 cm. I used a one minute time step and stored the results every ten minutes.

This section I describe two sets of model simulations. For both sets of simulations I provided the model with the initial density, grain size, bond size and grain type. However, the prescribed boundary conditions differ for each set of simulations. The first has Dirichlet boundary conditions where I provided fixed temperature boundary conditions every ten minutes during the simulation. Since the samples in the experiments were in a steady state, I used typical values from the observed evolution as

constant boundary conditions. The second set of simulations has Neumann boundary conditions where the model was provided an initial mean temperature and fixed heat flux at the boundaries during the experiment. I used a typical average (single value) of the upper and lower heat flux measurements from each experiment as both the upper and lower boundary condition.

6.1.1 Temperature Profiles

During the experiments the temperature profile reached a steady state within a few hours. To compare the observed and modeled temperature profiles, I compared the profiles at thirty-three hours (an arbitrary point) into each experiment. The profiles from five experiments and corresponding simulation are shown in Figures 6.1 through 6.5.

Profiles from the April 6, 2005A experiment show the simulated temperature is very close to the observed at the bottom of the snow sample (Figure 6.1). Although the

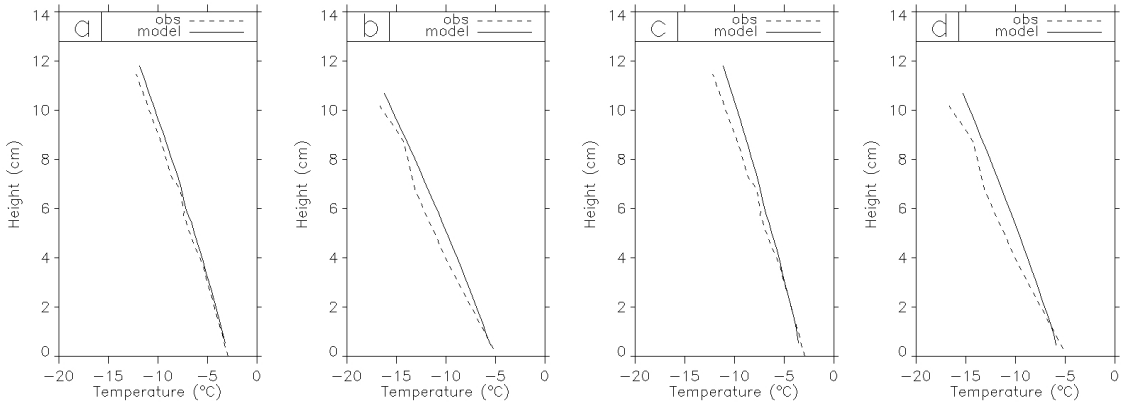

Figure 6.1: Observed and modeled temperature profiles from SNOWPACK 33 hours into the April 6, 2005A experiment: a) treatment sample with Dirichlet boundary conditions, b) control sample with Dirichlet boundary conditions, c) treatment sample with Neumann boundary conditions, d) control sample with Neumann boundary conditions.

slope of the profiles is quite similar, the simulated profiles depart from the observed distribution in the upper portion of the sample. This trend is present in both the Dirichlet and Neumann simulations. There is a similar departure of the simulated from the observed profile in two other Dirichlet simulations (Figures 6.2a and b, 6.3a and b).

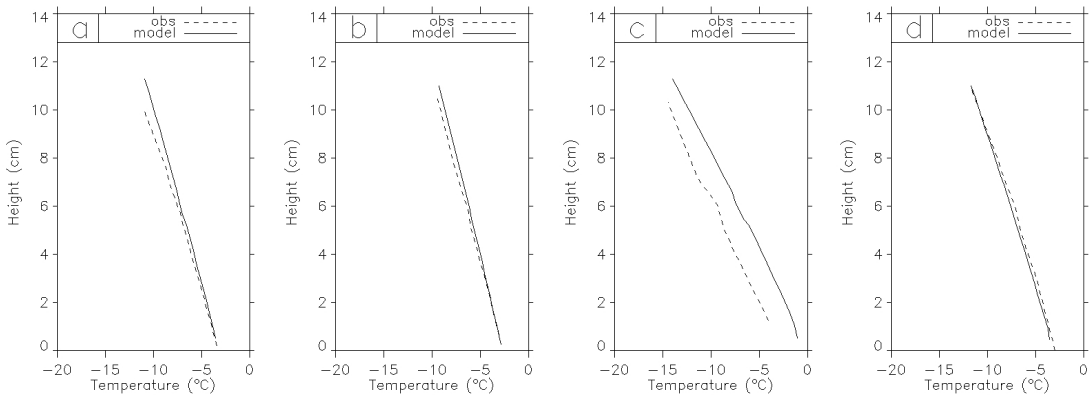

Figure 6.2: Observed and modeled temperature profiles from SNOWPACK 33 hours into the March 17, 2005A experiment: a) treatment sample with Dirichlet boundary conditions, b) control sample with Dirichlet boundary conditions, c) treatment sample with Neumann boundary conditions, d) control sample with Neumann boundary conditions.

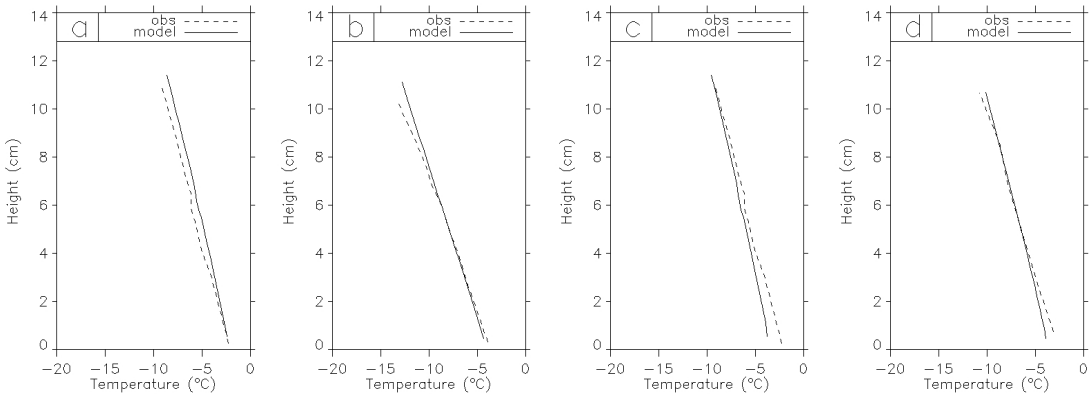

Figure 6.3: Observed and modeled temperature profiles from SNOWPACK 33 hours into the February 23, 2005B experiment: a) treatment sample with Dirichlet boundary conditions, b) control sample with Dirichlet boundary conditions, c) treatment sample with Neumann boundary conditions, d) control sample with Neumann boundary conditions.

The slope and magnitude of the observed and modeled profiles are similar in nearly all of the simulations. The observed and modeled profiles cross in several of the figures (Figures 6.1c and d, 6.2d, 6.3b and d, 6.4b and 6.5a and c). However, the slope is only notably different in Figure 6.5c. In two of the Neumann simulations of treatment samples the magnitude of the temperatures are considerably different than those observed (Figures 6.2c and 6.4c). However, in both cases the slope of the modeled profiles is similar to the observation.

There is no consistent difference between the treatment and control samples in the modeled temperature profiles. This result was discussed in Chapter 4. Even though the ice layer is slightly thicker (~ 1 mm) in the model, there is still no evidence of the layer in the temperature profile (Figures 6.1, 6.2, 6.3, 6.4 and 6.5).

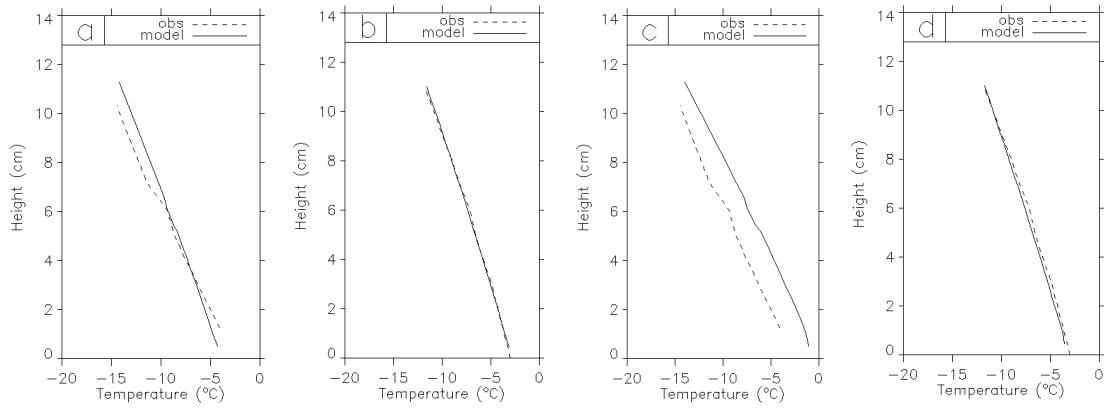

Figure 6.4: Observed and modeled temperature profiles from SNOWPACK 33 hours into the January 6, 2005B experiment: a) treatment sample with Dirichlet boundary conditions, b) control sample with Dirichlet boundary conditions, c) treatment sample with Neumann boundary conditions, d) control sample with Neumann boundary conditions.

6.1.2 Effective Thermal Conductivity

The SNOWPACK model uses an effective thermal conductivity to describe how heat moves through snow. This parameter combines heat conduction through the ice and pore structures as well as latent heat exchange from vapor diffusion across the pores. The effective thermal conductivity in SNOWPACK does not include heat exchange from radiation, which is generally neglected in discussions of heat transfer within a snow cover (see Chapter 1). It also neglects heat transfer by convection, which is appropriate for this application (see Chapters 1 and 4). I calculated an effective thermal conductivity from the temperature and heat flux measurements collected during the experiments. This value represents the transfer of thermal energy by all transport mechanisms. Based on the experimental environment and the nature of the snow in the samples, a direct comparison between the measured and modeled effective thermal conductivities is appropriate.

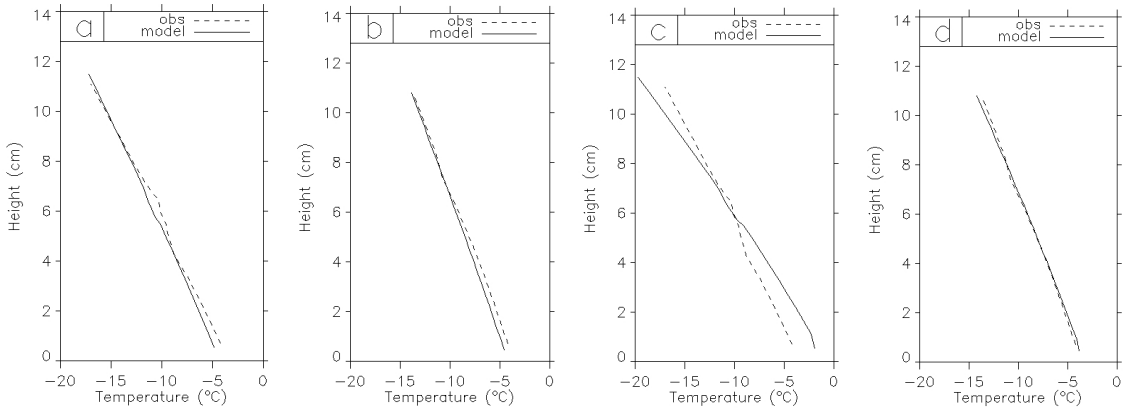

Figure 6.5: Observed and modeled temperature profiles from SNOWPACK 33 hours into the March 25, 2005A experiment: a) treatment sample with Dirichlet boundary conditions, b) control sample with Dirichlet boundary conditions, c) treatment sample with Neumann boundary conditions, d) control sample with Neumann boundary conditions.

Figures 6.6 through 6.10 show the temporal evolution of the observed and modeled effective thermal conductivity (k_e). All of the plots of the observed k_e show an initial adjustment period. This adjustment does not appear in the model plots because I used steady state boundary conditions in the model simulations. The predictions of the magnitude and trend in k_e were closest to the observed values in the experiments containing low density snow (Figures 6.6 and 6.9). The largest departure between the prediction and observation occurs in the treatment samples of the March 17 and 25 experiments (Figures 6.8 and 6.10). The ice layers were slightly thicker in these experiments. Although I have not been able to attribute any changes in the thermophysical parameters to the presence of the ice layer, it is possible that it contributed to the under prediction of k_e by SNOWPACK.

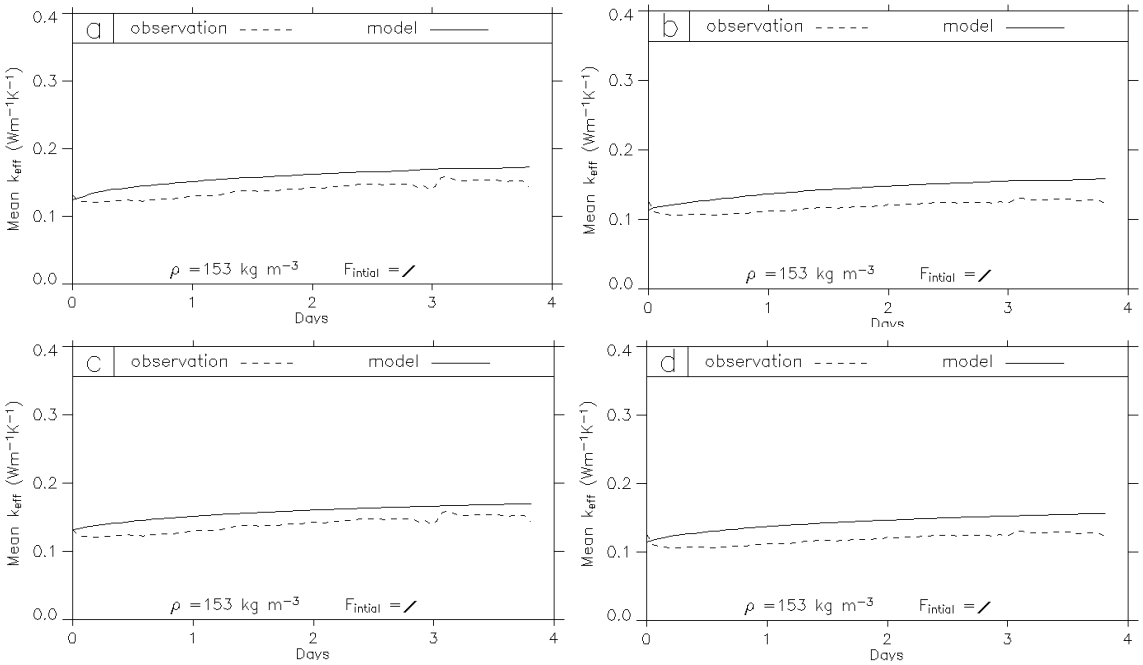

Figure 6.6: Observed and modeled effective thermal conductivity for the April 6, 2005A experiment: a) treatment sample with Dirichlet boundary conditions, b) control sample with Dirichlet boundary conditions, c) treatment sample with Neumann boundary conditions, d) control sample with Neumann boundary conditions.

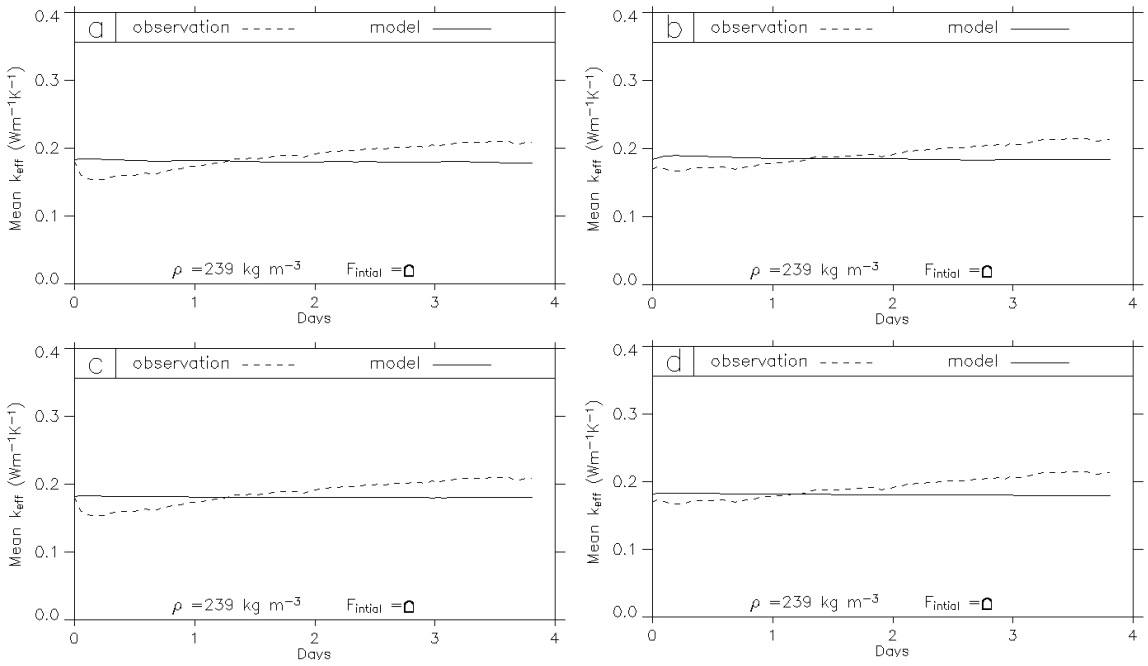

Figure 6.7: Observed and modeled effective thermal conductivity for the January 6, 2005B experiment: a) treatment sample with Dirichlet boundary conditions, b) control sample with Dirichlet boundary conditions, c) treatment sample with Neumann boundary conditions, d) control sample with Neumann boundary conditions.

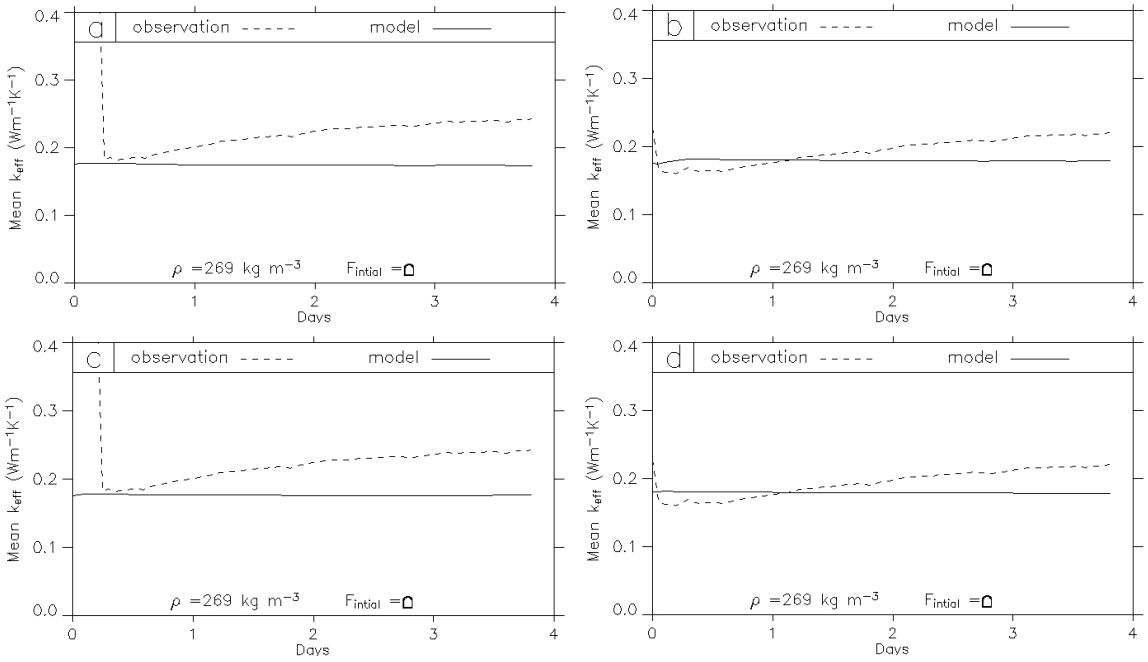

Figure 6.8: Observed and modeled effective thermal conductivity for the March 17, 2005A experiment: a) treatment sample with Dirichlet boundary conditions, b) control sample with Dirichlet boundary conditions, c) treatment sample with Neumann boundary conditions, d) control sample with Neumann boundary conditions.

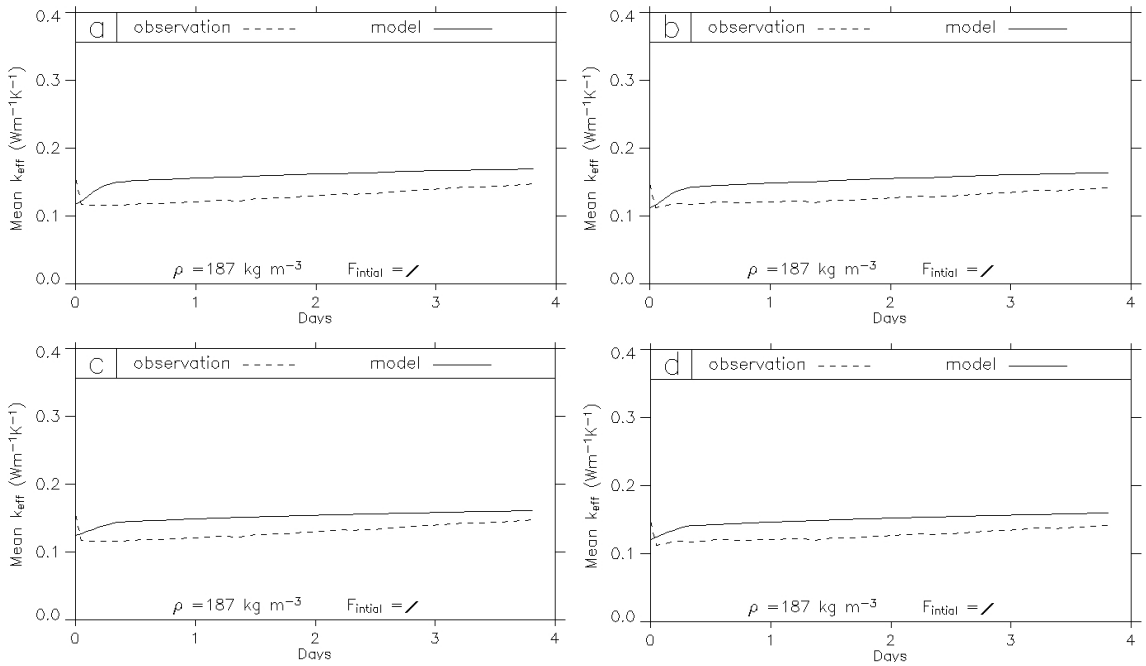

Figure 6.9: Observed and modeled effective thermal conductivity for the February 23, 2005B experiment: a) treatment sample with Dirichlet boundary conditions, b) control sample with Dirichlet boundary conditions, c) treatment sample with Neumann boundary conditions, d) control sample with Neumann boundary conditions.

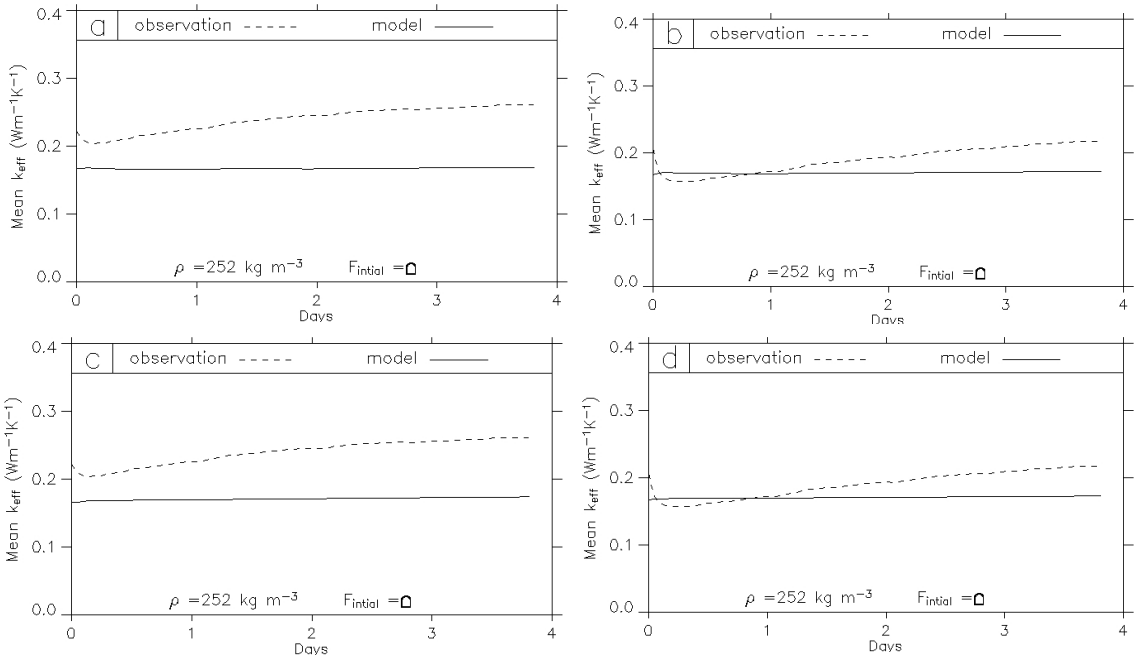

Figure 6.10: Observed and modeled effective thermal conductivity for the March 25, 2005A experiment: a) treatment sample with Dirichlet boundary conditions, b) control sample with Dirichlet boundary conditions, c) treatment sample with Neumann boundary conditions, d) control sample with Neumann boundary conditions.

To examine the magnitude of the modeled and observed effective thermal conductivities, I compared values from the same point in time near the end of the experiments. The predicted values are within 5% of the observed values in eight out of ten of the simulations (Tables 6.1 and 6.2). This result is independent of the type of boundary conditions. The two simulations with an error greater that 5% are the March 17 and 25 treatment samples described above. All of the predicted values are within 10% of the observed values (Tables 6.1 and 6.2).

The effective thermal conductivity increased in every experiment (see Chapter 4). SNOWPACK predicts an increase in k_e in six out of ten of the experiments (Tables 6.3 and 6.4). This result is consistent between the Dirichlet and Neumann simulations. The modeled increase in k_e is generally very close to the observations. In several cases it is within 1% and at most the predicted value differs from the observed by 5% (Tables 6.3 and 6.4).

Table 6.1: Difference between observed and modeled effective thermal conductivity for the Dirichlet simulations. The difference is taken at 80 hours (3 days and 8 hours) into the experiment.

Experiment	Model (W m^{-1} K^{-1})	Observed (W m^{-1} K^{-1})	Obs-Mod%
April 6, 2005A treatment	0.171	0.154	1.7%
April 6, 2005A control	0.156	0.129	2.7%
January 6, 2005B treatment	0.179	0.209	2.9%
January 6, 2005B control	0.184	0.214	3.0%
March 17, 2005A treatment	0.174	0.239	6.5%
March 17, 2005A control	0.179	0.217	3.9%
February 23, 2005B treatment	0.168	0.143	2.5%
February 23, 2005B control	0.162	0.138	2.4%
March 25, 2005A treatment	0.169	0.259	9.0%
March 25, 20005A control	0.172	0.214	4.2%

Table 6.2: Difference between observed and modeled effective thermal conductivity for the Neumann simulations. The difference is taken at 80 hours (3 days and 8 hours) into the experiment.

Experiment	Model ($W\ m^{-1}\ K^{-1}$)	Observed ($W\ m^{-1}\ K^{-1}$)	Obs-Mod%
April 6, 2005A treatment	0.168	0.154	1.4%
April 6, 2005A control	0.155	0.129	2.6%
January 6, 2005B treatment	0.180	0.209	2.9%
January 6, 2005B control	0.180	0.214	3.4%
March 17, 2005A treatment	0.176	0.239	6.3%
March 17, 2005A control	0.179	0.217	3.9%
February 23, 2005B treatment	0.160	0.143	1.7%
February 23, 2005B control	0.158	0.138	2.0%
March 25, 2005A treatment	0.173	0.259	8.6%
March 25, 20005A control	0.172	0.214	4.1%

Table 6.3: Trend from 11 hours to 80 hours in effective thermal conductivity during the experiments and simulations with the Dirichlet boundary conditions.

Experiment	Observed Trend ($W\ m^{-3}\ K^{-1}$)	Modeled Trend ($W\ m^{-3}\ K^{-1}$)	% Change in Observed	% Change in Modeled
April 6, 2005A treatment	0.030	0.028	3.0%	2.8%
April 6, 2005A control	0.022	0.029	2.2%	2.9%
January 6, 2005B treatment	0.048	-0.002	4.8%	-0.2%
January 6, 2005B control	0.042	-0.004	4.2%	-0.4%
March 17, 2005A treatment	0.055	-0.002	5.5%	-0.2%
March 17, 2005A control	0.053	-0.003	5.3%	-0.3%
February 23, 2005B treatment	0.026	0.016	2.6%	1.6%
February 23, 2005B control	0.019	0.018	1.9%	1.8%
March 25, 2005A treatment	0.044	0.002	4.4%	0.2%
March 25, 20005A control	0.052	0.003	5.2%	0.3%

Table 6.4: Trend 11 hours to 80 hours in effective thermal conductivity during the experiments and simulations with the Neumann boundary conditions.

Experiment	Observed Trend ($W\ m^{-3}\ K^{-1}$)	Modeled Trend ($W\ m^{-3}\ K^{-1}$)	% Change in Observed	% Change in Modeled
April 6, 2005A treatment	0.030	0.024	3.0%	2.4%
April 6, 2005A control	0.022	0.025	2.2%	2.5%
January 6, 2005B treatment	0.048	-0.002	4.8%	-0.2%
January 6, 2005B control	0.042	-0.003	4.2%	-0.3%
March 17, 2005A treatment	0.055	-0.001	5.5%	-0.1%
March 17, 2005A control	0.053	-0.002	5.3%	-0.2%
February 23, 2005B treatment	0.026	0.015	2.6%	1.5%
February 23, 2005B control	0.019	0.016	1.9%	1.6%
March 25, 2005A treatment	0.044	0.004	4.4%	0.4%
March 25, 20005A control	0.052	0.003	5.2%	0.3%

There are several methods for assessing the accuracy of the model predictions. We can get a sense for the model's performance by visually comparing the observed and predicted values. I also compared the observed and predicted values at selected times during the experiments. Pielke (2002) outlines a set of statistical comparisons to determine the skill in a model's prediction. I used the root mean square error (RMSE or E), the root mean square error with constant bias removed (E_{UB}) and the standard deviations of the model predictions and observations (σ_{mod} and σ_{obs} respectively). These parameters are calculated with the following equations,

$$E = \sqrt{\frac{\sum_{i=1}^{n} \left[\phi_i - \phi_{i_{obs}}\right]^2}{n}} \qquad 6.1$$

$$E_{UB} = \sqrt{\frac{\sum_{i=1}^{n} \left\{\left(\phi_i - \phi_0\right) - \left(\phi_{i_{obs}} - \phi_{0_{obs}}\right)\right\}^2}{n}} \qquad 6.2$$

$$\sigma = \sqrt{\frac{\sum_{i=1}^{n} \left(\phi_i - \phi_0\right)^2}{n}} \qquad 6.3$$

where n is the total number of data points, ϕ is the predicted value, ϕ_{obs} is the observed value, and ϕ_0 and ϕ_{0obs} are the means of the predicted and observed values respectively. There is skill in the model prediction when all of the following criteria are satisfied:

$$\sigma_{obs} \approx \sigma_{mod} \qquad 6.4$$

$$E < \sigma_{obs} \qquad 6.5$$

$$E_{UB} < \sigma_{obs} \qquad 6.6$$

I consider criterion 6.4 satisfied if the difference between σ_{mod} and σ_{obs} is within 20% of the larger of the two values. None of the Dirichlet or Neumann simulations satisfy all of the criteria (Tables 6.5 and 6.6). There are several cases where E_{UB} is not less than σ_{obs}, but the two values are nearly equal. Although by visual inspection the model seems to have adequately predicted the observations, the statistical evaluation of the model shows no skill in the predictions.

Table 6.5: Statistical determination of model skill in predicting thermal conductivity for the Dirichlet simulations. The values in the table are: E is the root mean square error, E_{UB} is the unbiased root mean square error and σ is the standard deviation. The σ_{obs} » σ_{mod} criterion was satisfied if σ_{obs} - σ_{mod} was no larger than 20% of the larger of the two values. Skill is demonstrated where all three of the criterion are satisfied.

Experiment	Values					Criteria		
	E	E_{UB}	σ_{model}	σ_{obs}	n	$\sigma_{obs} \approx \sigma_{mod}$	$E < \sigma_{obs}$	$E_{UB} < \sigma_{obs}$
April 6, 2005A treatment	0.026	0.019	0.021	0.019	88	yes	no	no
April 6, 2005A control	0.030	0.018	0.020	0.015	88	no	no	no
January 6, 2005B treatment	0.029	0.028	0.018	0.027	99	no	no	no
January 6, 2005B control	0.029	0.027	0.016	0.026	99	no	no	no
March 17, 2005A treatment	0.116	0.093	0.020	0.079	80	no	no	no
March 17, 2005A control	0.037	0.030	0.019	0.029	94	no	no	no
February 23, 2005B treatment	0.033	0.021	0.019	0.019	94	yes	no	no
February 23, 2005B control	0.030	0.019	0.019	0.017	94	yes	no	no
March 25, 2005A treatment	0.082	0.026	0.017	0.028	94	no	no	yes
March 25, 2005A control	0.039	0.029	0.018	0.029	94	no	no	yes

6.1.3 Microstructure Parameters

The SNOWPACK model uses a combination of field based measurements and numerical indices to represent snow microstructure. The metamorphism routines in the model allow the grain and bond dimensions to develop as heat and mass moves through the snow structure. The grain and bond dimensions in SNOWPACK roughly correlate to field measurements. Grain shape is represented by two indices, dendricity and sphericity (Burn et al., 1989 and 1992), that relate to the snow classification used for field

Table 6.6: Statistical determination of model skill in predicting thermal conductivity for the Neumann simulations. The values in the table are: E is the root mean square error, E_{UB} is the unbiased root mean square error and σ is the standard deviation. The $\sigma_{obs} \approx \sigma_{mod}$ criterion was satisfied if $\sigma_{obs} - \sigma_{mod}$ was no larger than 20% of the larger of the two values. Skill is demonstrated where all three of the criterion are satisfied.

Experiment	Values					Criteria		
	E	E_{UB}	σ_{model}	σ_{obs}	n	$\sigma_{obs} \approx \sigma_{mod}$	$E < \sigma_{obs}$	$E_{UB} < \sigma_{obs}$
April 6, 2005A treatment	0.025	0.019	0.020	0.019	88	yes	no	no
April 6, 2005A control	0.029	0.017	0.019	0.015	88	no	no	no
January 6, 2005B treatment	0.029	0.027	0.018	0.027	99	no	no	no
January 6, 2005B control	0.031	0.027	0.015	0.026	99	no	no	no
March 17, 2005A treatment	0.115	0.093	0.020	0.079	80	no	no	no
March 17, 2005A control	0.037	0.030	0.019	0.029	94	no	no	no
February 23, 2005B treatment	0.027	0.019	0.018	0.019	94	yes	no	no
February 23, 2005B control	0.027	0.018	0.018	0.017	94	yes	no	no
March 25, 2005A treatment	0.078	0.026	0.018	0.028	94	no	no	yes
March 25, 2005A control	0.038	0.028	0.018	0.029	94	no	no	yes

observations (Colbeck et al., 1990). Grains with 0.0 dendricity and sphericity are classified as faceted grains (4a) (Lehning et al., 2002). Rounded grains (3a and 3b) have 0.0 dendricity and a sphericity of 1.0. New snow has a sphericity of 0.5 and the dendricity of 1.0. The snow classification in the model contains a primary and secondary grain type for each layer.

All the snow used in these experiments was either decomposing new snow (2a ⟋) or mixed grains (4c ⍾). Under a large temperature gradient the snow metamorphosed into depth hoar (5a ∧ or 5b ⍀). I was unable to examine disaggregated grains at the end of each experiment, so the final grain type is an estimate from the two-dimensional images and three-dimensional reconstructions.

Snow types are usually allowed to develop in SNOWPACK. Initializing the model with existing snow is an unusual application of the model. Thus I had to carefully translate field-based observations into model parameters with the intention of giving the model the best chance for success. The model does not have a snow classification for mixed grains, so most of the simulations began with faceted grains (4a □) or primarily faceted grains with a secondary type of depth hoar (4a/5a □∧) (Table 6.7). Both the grain type and the grain and bond dimensions were selected based on the observed classification and grain size (Tables 6.7, 6.8 and 6.9).

In all of the simulations, the grain type evolved from the initial form into faceted grains and depth hoar or just depth hoar (Table 6.7). This result was consistent regardless of the boundary conditions. In the February 23, 2005B simulations the initial form was faceted grains and depth hoar and the grain type did not change during the numerical experiment. This experiment used relatively low density snow. However, the

Table 6.7: Observed and modeled grain type (Colbeck et al., 1990).

Experiment	Initial Observed	Final Observed	Initial Modeled	Final Modeled Dirichlet	Final Modeled Neumann
April 6, 2005A treatment	⟋	∧	□□	□∧	□∧
April 6, 2005A control	⟋	∧	□□	□∧	□∧
January 6, 2005B treatment	∩	∧	□□	□∧*	□∧
January 6, 2005B control	∩	∧	□□	□∧*	□∧
March 17, 2005A treatment	∩	∧	□∧	∧∧	∧∧
March 17, 2005A control	∩	∧	□∧	∧∧	∧∧
February 23, 2005B treatment	⟋	∧	□∧	□∧	□∧
February 23, 2005B control	⟋	∧	□∧	□∧	□∧
March 25, 2005A treatment	∩	∧	∧∧	∧∧	∧∧
March 25, 20005A control	∩	∧	∧∧	∧∧	∧∧

* The grain form ∧∧ developed in the lower half of the sample.

Table 6.8: Microstructural parameters from the Dirichlet simulations. The grain and bond sizes are in millimeters, but do not directly correspond to field measurements. Dendricity and sphericity are unit-less parameters.

	Experiment	Grain	Bond	Dendricity	Sphericity
Initial	January 6, 2005B treatment	0.8	0.3	0.0	0.1
Final	January 6, 2005B treatment	1.1	0.4	0.0	0.0
Initial	January 6, 2005B control	0.8	0.3	0.0	0.1
Final	January 6, 2005B control	1.1	0.4	0.0	0.0
Initial	March 25, 2005A treatment	1.0	0.4	0.0	0.2
Final	March 25, 2005A treatment	1.3	0.5	0.0	0.0
Initial	March 25, 2005A control	1.0	0.4	0.0	0.2
Final	March 25, 2005A control	1.3	0.5	0.0	0.0
Initial	February 23, 2005B treatment	1.3	0.3	0.0	0.5
Final	February 23, 2005B treatment	1.5	0.5	0.0	0.4
Initial	February 23, 2005B control	1.3	0.3	0.0	0.5
Final	February 23, 2005B control	1.6	0.5	0.0	0.4
Initial	March 17, 2005A treatment	0.9	0.4	0.0	0.1
Final	March 17, 2005A treatment	1.2	0.4	0.0	0.0
Initial	March 17, 2005A control	0.9	0.4	0.0	0.1
Final	March 17, 2005A control	1.2	0.4	0.0	0.0
Initial	April 6, 2005A treatment	1.0	0.2	0.0	0.6
Final	April 6, 2005A treatment	1.3	0.4	0.0	0.5
Initial	April 6, 2005A control	1.0	0.2	0.0	0.6
Final	April 6, 2005A control	1.3	0.4	0.0	0.4

April 6, 2005A experiment also used relatively low density snow and the grain type evolved from faceted grains to depth hoar during the simulations (Table 6.7).

The initial dendricity in all of the simulations was zero. In the model, the dendricity of a layer cannot increase during metamorphism. Therefore it remained zero in all of the simulations (Tables 6.8 and 6.9). The sphericity decreased in all of the simulations and reached zero in all but two of the simulated experiments (Tables 6.8 and 6.9). These experiments (February 23, 2005B and April 6, 2005A) used low density snow. The grain and bond sizes increased in all of the simulations. All of these results occurred in both the Dirichlet and Neumann simulations.

Table 6.9: Microstructural parameters from the Neumann simulations. The grain and bond sizes are in millimeters, but do not directly correspond to field measurements. Dendricity and sphericity are unit-less parameters.

	Experiment	Grain	Bond	Dendricity	Sphericity
Initial	January 6, 2005B treatment	0.8	0.3	0.0	0.1
Final	January 6, 2005B treatment	1.3	0.5	0.0	0.0
Initial	January 6, 2005B control	0.8	0.3	0.0	0.1
Final	January 6, 2005B control	1.1	0.4	0.0	0.0
Initial	March 25, 2005A treatment	1.1	0.4	0.0	0.2
Final	March 25, 2005A treatment	1.5	0.5	0.0	0.0
Initial	March 25, 2005A control	1.0	0.4	0.0	0.2
Final	March 25, 2005A control	1.3	0.5	0.0	0.0
Initial	February 23, 2005B treatment	1.3	0.3	0.0	0.5
Final	February 23, 2005B treatment	1.5	0.5	0.0	0.4
Initial	February 23, 2005B control	1.3	0.3	0.0	0.5
Final	February 23, 2005B control	1.5	0.5	0.0	0.4
Initial	March 17, 2005A treatment	0.9	0.4	0.0	0.1
Final	March 17, 2005A treatment	1.2	0.5	0.0	0.0
Initial	March 17, 2005A control	0.9	0.4	0.0	0.1
Final	March 17, 2005A control	1.2	0.5	0.0	0.0
Initial	April 6, 2005A treatment	1.0	0.2	0.0	0.6
Final	April 6, 2005A treatment	1.3	0.4	0.0	0.5
Initial	April 6, 2005A control	1.0	0.2	0.0	0.6
Final	April 6, 2005A control	1.3	0.4	0.0	0.5

6.2 van Rietbergen-Kaempfer-Schneebeli Thermal Model

The vanRietbergen-Kaempfer-Schneebeli (RKS) model was originally developed to simulate the distribution of elastic stresses in bone structures (van Rietbergen et al., 1995) and snow (Schneebeli, 2004). Kaempfer et al. (2005) adapted the model to simulate the temperature distribution in ice structures. The temperature distribution is produced by conduction through the ice structure. The model does not account for heat transfer through the pore spaces (including heat transported by latent heat exchange). Due to the numerical complexity of the model, I used grid elements of 48 μm. I used fixed temperature boundary conditions based on the observed temperature gradient in each experiment. The domain size of each simulation is shown in Table 6.10.

Table 6.10: Domain dimensions for RKS simulations.

Experiment	X (mm)	Y (mm)	Z (mm)
January 6, 2005B initial	6	6	6
January 6, 2005B control	6	6	6
January 6, 2005B treatment	4	4	9.6
March 17, 2005B initial	6	6	9.6
March 17, 2005B control	6	6	6
March 17, 2005B treatment	6	6	9.6

6.2.1 Temperature Distribution

The temperature difference across 11 cm of snow was on the order of 10 K in the experiments. However the temperature difference in these simulations is less than 1 K (over 6 to 10 mm). Figure 6.11 shows the temperature difference in the reconstruction of the January 6, 2005B initial conditions cast. The sample is warm on the bottom and becomes progressively colder in the upper portion of the modeled sample. The total temperature difference is less than 0.5 K over 6 mm. A vertical thin slice of the model

shows a gradual decrease in temperature from the lower to upper portion of the sample (Figure 6.11b). A similar pattern is evident in the simulation of the March 17, 2005B initial conditions sample (Figure 6.12). The total temperature difference in this simulation is 0.59 K over 9.6 mm.

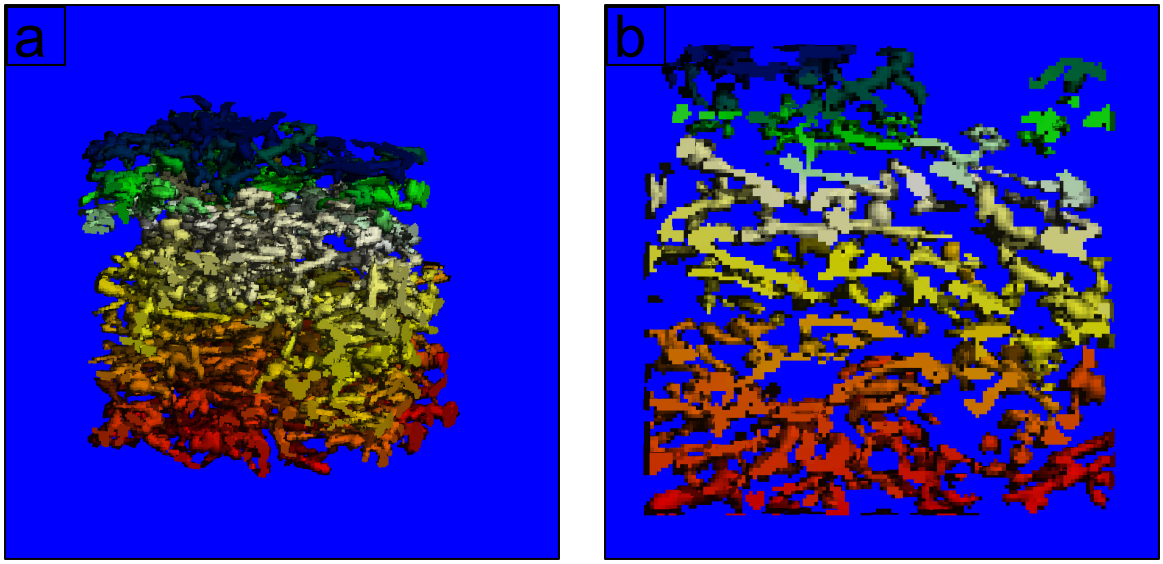

Figure 6.11: Temperature distribution in the initial conditions sample (initial microstructure) from the January 6, 2005B experiment (T deviation 0—0.38 K): a) whole sample, b) thin slice.

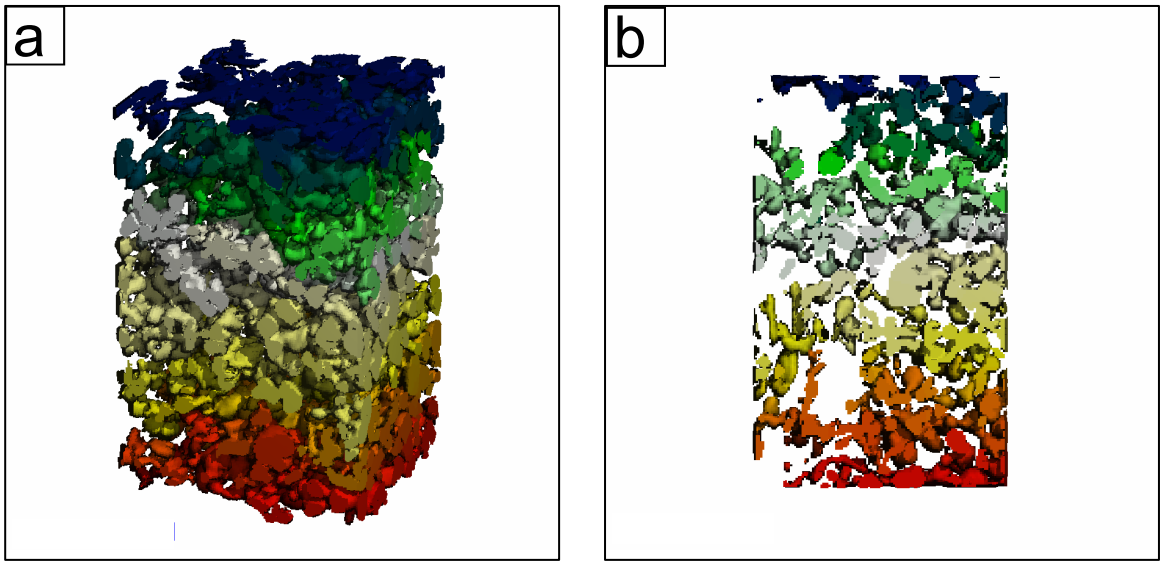

Figure 6.12: Temperature distribution in the initial conditions (initial microstructure) sample from the March 17, 2005B experiment (T deviation 0—0.59 K): a) whole sample, b) thin slice.

As the structure of the samples changes, so does the even distribution of temperature. Initially it is difficult to distinguish between particles and connection points as there is a relatively small difference in their size. After five days under a large temperature gradient the structure changes dramatically forming large particles with relatively small connection points (relative to the size of the particles). As a result there is no longer a gradual change in temperature from the bottom to the top of the sample. Areas with fairly different temperatures exist at the same vertical level in the control samples (Figures 6.13 and 6.14). Pathways that are more efficient at transporting heat develop. Constrictions and "dead-ends" are cooler than adjacent structures (Figures 6.13 and 6.14). This effect is much easier to visualize in the thin slices of the structure (Figures 6.13 and 6.14b), although it is difficult to visualize pathways that extend into or out of the page. There is a step change in the simulated maximum and minimum temperatures increasing *z* within the sample (Figure 6.15). The mean temperature changes steadily (near linear) through the sample (Figure 6.15).

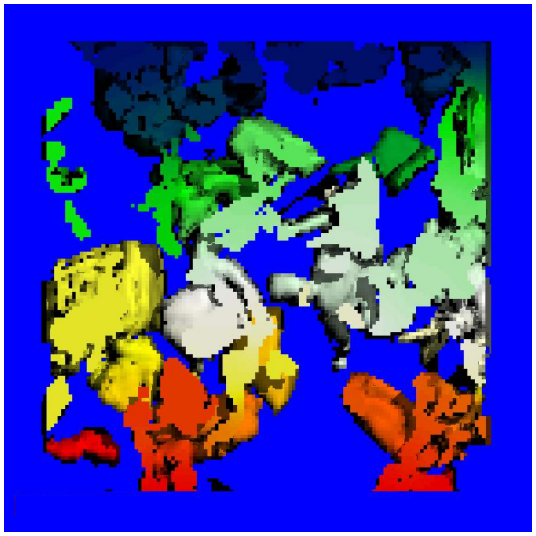

Figure 6.13: Simulated temperature distribution in the January 6, 2005B control sample (T deviation 0—0.38).

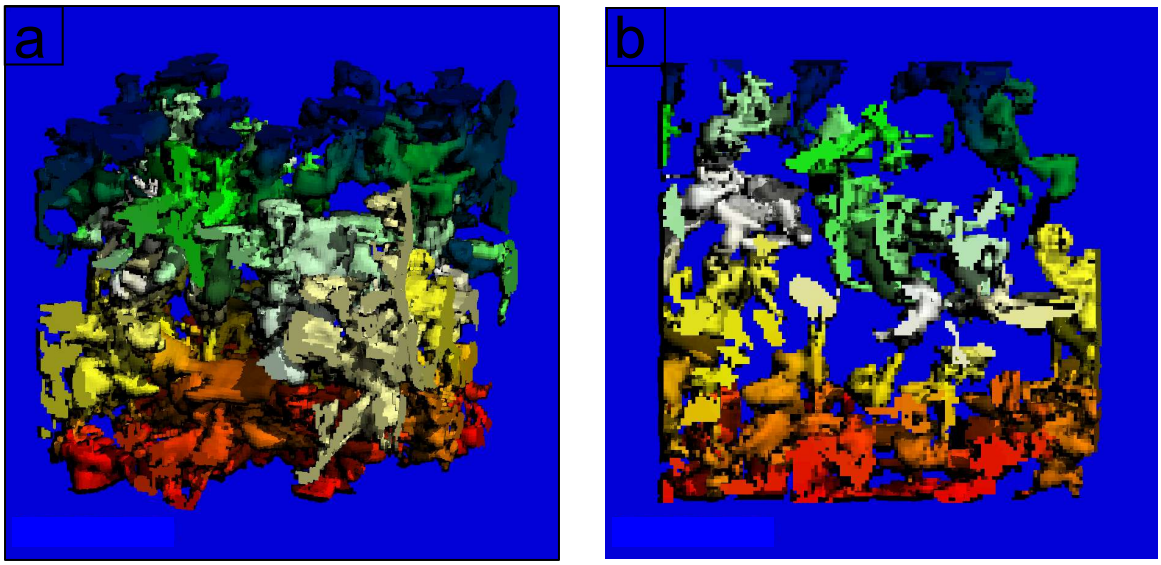

Figure 6.14: Simulated temperature distribution in the March 17, 2005B control sample (T deviation 0—0.37 K): a) whole sample, b) thin slice.

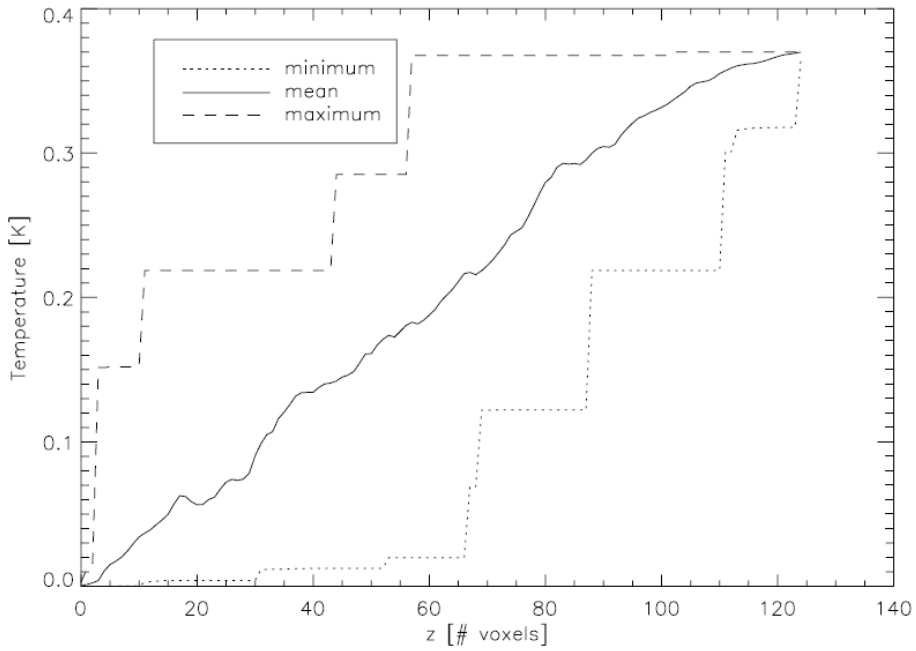

Figure 6.15: Simulated temperature distribution in the March 17, 2005B control sample. The abscissa is the vertical coordinate in the sample (1 voxel = 0.048 mm). The ordinate is the temperature change through the sample.

The ice layer has a large impact on the temperature distribution in the samples. Since the ice is the only heat transport mechanism in the model, the temperature gradient in the ice layer and large connected structures becomes very small (Figures 6.16 and 6.17a). The mean temperature changes steadily (near linear) in the snow above and below the ice layer (Figure 6.17b). However within the ice layer there is a very small, linear, increase in the mean temperature. The maximum and minimum temperatures follow a similar trend. The maximum,

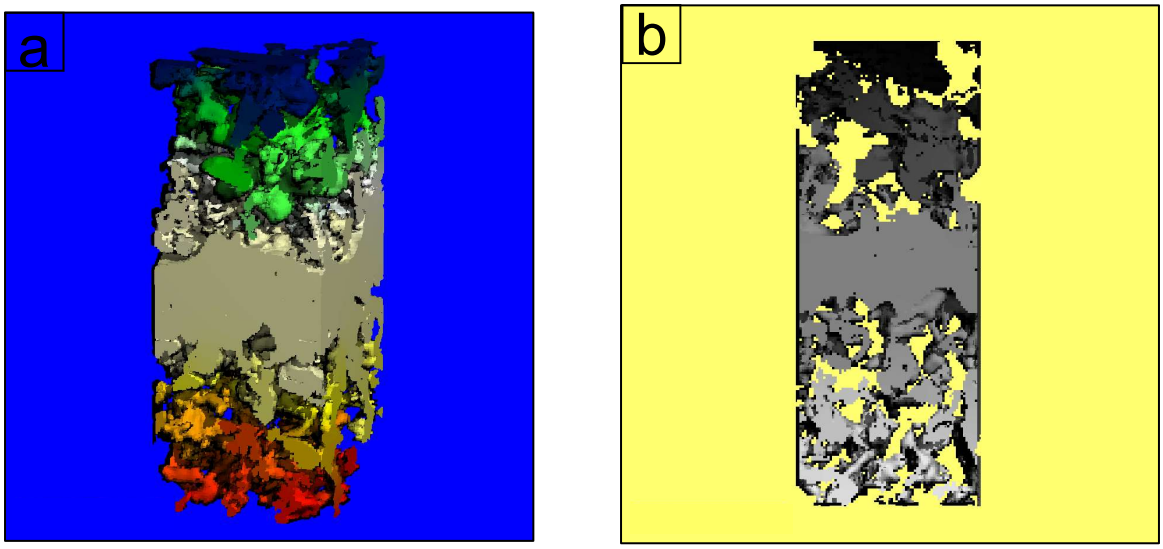

Figure 6.16: Simulated temperature distribution in the January 6, 2005B treatment sample (T deviation 0—0.73 K): a) whole sample, b) thin slice.

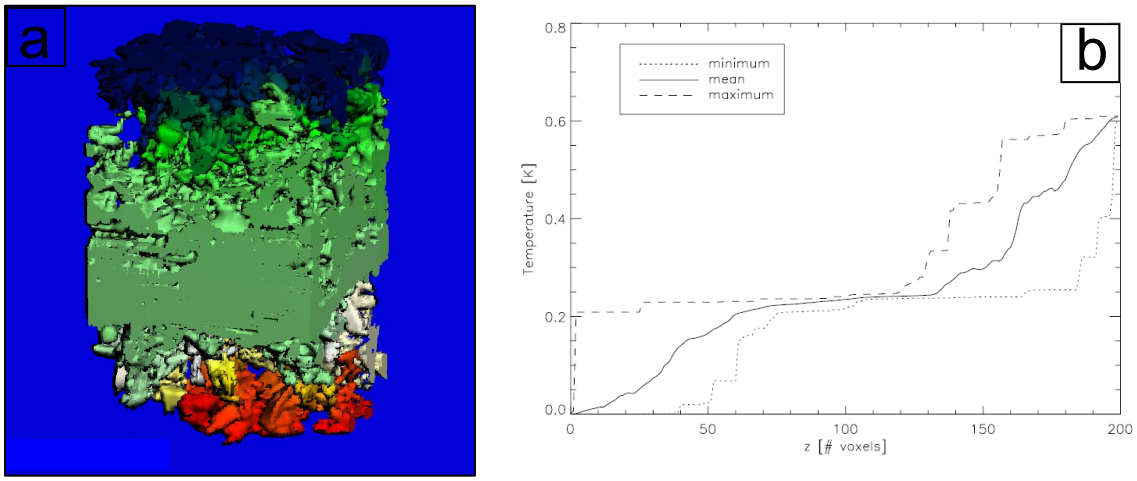

Figure 6.17: Simulated temperature distribution in the March 17, 2005B treatment sample (T deviation 0—0.61 K): a) three-dimensional, b) descriptive values (1 voxel = 0.048 mm).

minimum and mean temperatures converge at the bottom of the ice layer and diverge at the upper boundary (Figure 6.17b).

6.2.2 Temperature Gradient

The RKS model simulations show very high temperature gradients (in excess of 1000 K m^{-1}) in portions of the snow samples. At the beginning of the experiments there are large portions of the structure with a high temperature gradient (Figures 6.18 and 6.19). Although the gradient in the structure is not uniform, there are large areas with a relative small variation in the temperature gradient. This trend is most apparent in the thin slice from the January 6, 2005B experiment (Figure 6.18b).

After several days in the kinetic growth regime the structure reorganizes so that portions are efficiently transporting heat. The simulations of the control samples contain vertical structures with a higher temperature gradient than adjacent particles (Figures

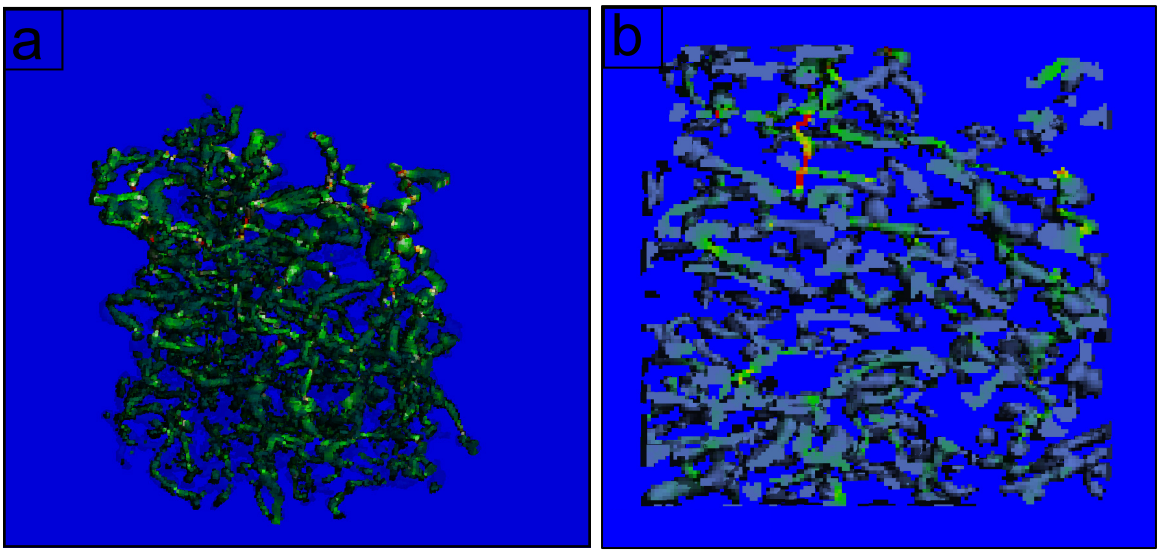

Figure 6.18: Temperature gradient in the initial conditions sample from the January 6, 2005B experiment (0—296 K m^{-1}): a) whole sample, b) thin slice.

6.20a and 6.21). Chains of depth hoar crystals become preferential pathways for heat to move through the snow. Within these structures narrow connections have the highest temperature gradients as the cross-sectional area of the pathway decreases and the heat flux increases (Figure 6.20b). Moving vertically through the sample, the mean temperature gradient is nearly constant (Figure 6.21).

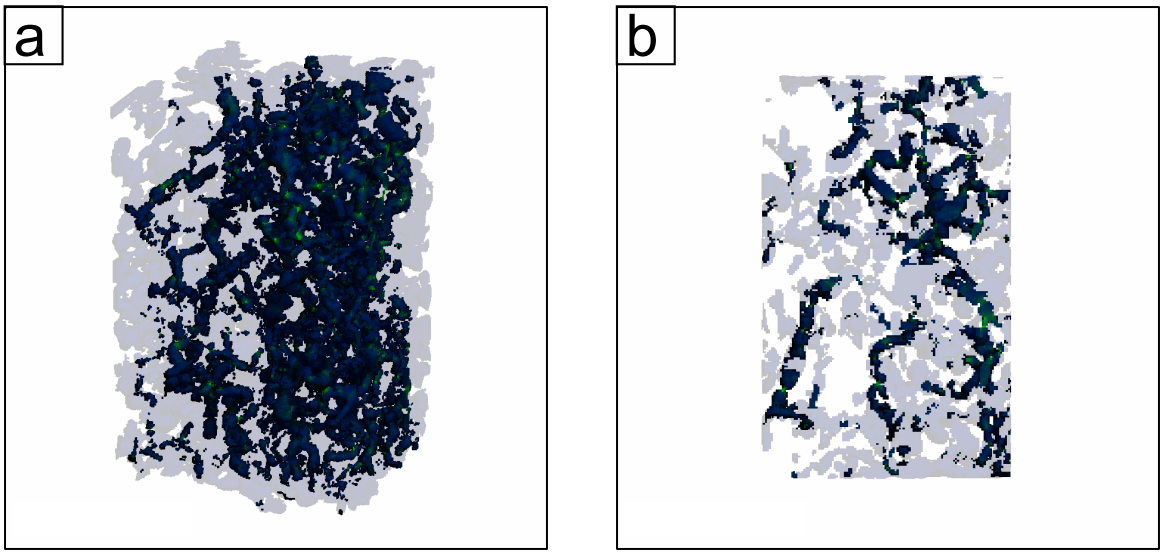

Figure 6.19: Temperature gradient in the initial conditions sample from the March 17, 2005B experiment (0—646 K m^{-1}): a) whole sample, b) thin slice. Areas with a temperature gradient less than 50 K m^{-1} appear in gray.

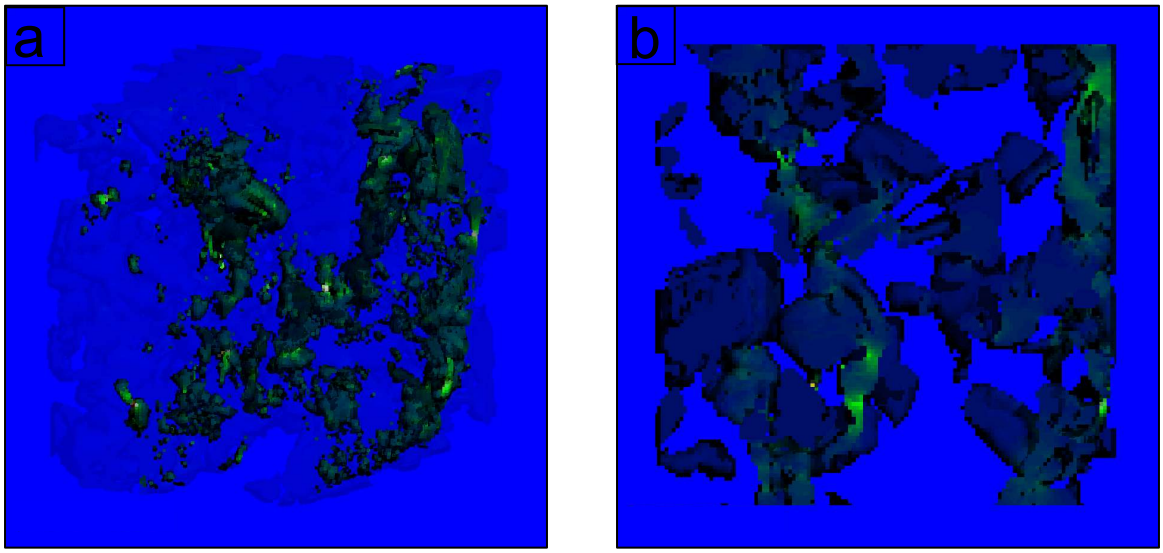

Figure 6.20: Simulated temperature gradient in the January 6, 2005B control sample (0—799 K m^{-1}): a) whole sample with areas less than 50 K m^{-1} in light blue , b) close up of a thin slice. Areas with a temperature gradient less than 50 K m^{-1} appear in gray

The formation of preferential pathways is most apparent in simulations of the treatment samples. Vertical structures with very high temperature gradients extend from above and below the ice layer (Figures 6.22 and 6.23). The ice layer itself has a relatively low gradient with respect to the surrounding structures. The layer contains very few air spaces (pores) and therefore the heat flux through the layer is relatively uniform. The mean temperature gradient is relatively constant in the snow layers above and below the ice layer (Figure 6.24). The gradient changes rapidly at the interface between the ice layer and the snow. There are small areas within the layer with a large temperature gradient. These are probably areas of ice adjacent to air bubbles and as the heat moves around the air space, the heat flux in the ice increases as does the temperature gradient.

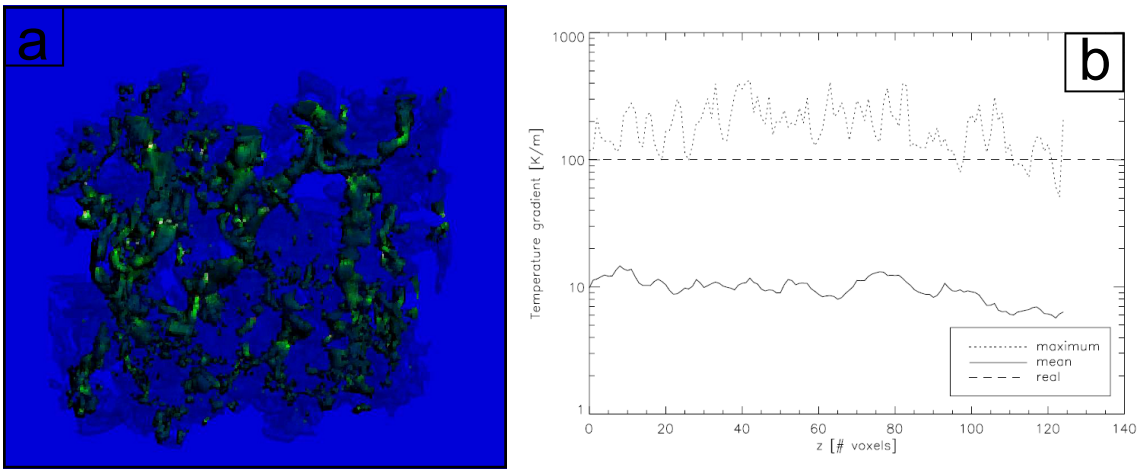

Figure 6.21: Simulated temperature gradient in the March 17, 2005B control sample (0—421 K m^{-1}): a) three-dimensional distribution, b) vertical distribution(1 voxel = 0.048 mm). In the panel on the left areas with a gradient less than 50 K m^{-1} appear in light blue.

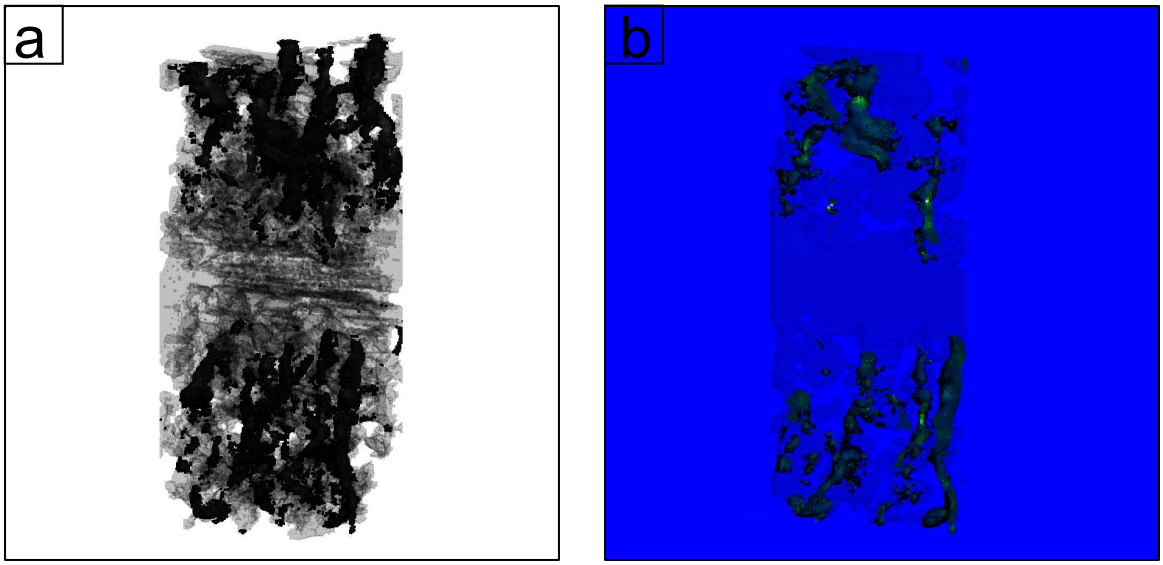

Figure 6.22: Simulated temperature gradient in the January 6, 2005B treatment sample (0 —1329 K m^{-1}). Areas with a gradient less than 50 K m^{-1} appear in light blue. Areas with a temperature gradient less than 50 K m^{-1} appear in gray.

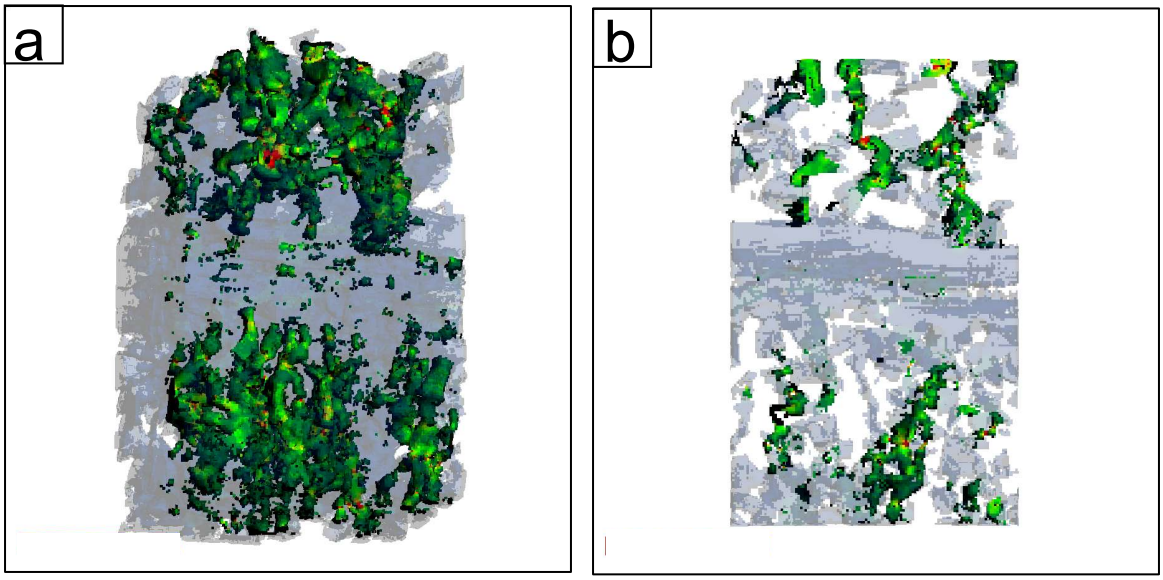

Figure 6.23: Simulated temperature gradient in the March 17, 2005B treatment sample (0—1329 K m^{-1}): a) whole sample, b) thin slice. Areas with a temperature gradient less than 50 K m^{-1} are gray. Areas with a temperature gradient less than 50 K m^{-1} appear in gray.

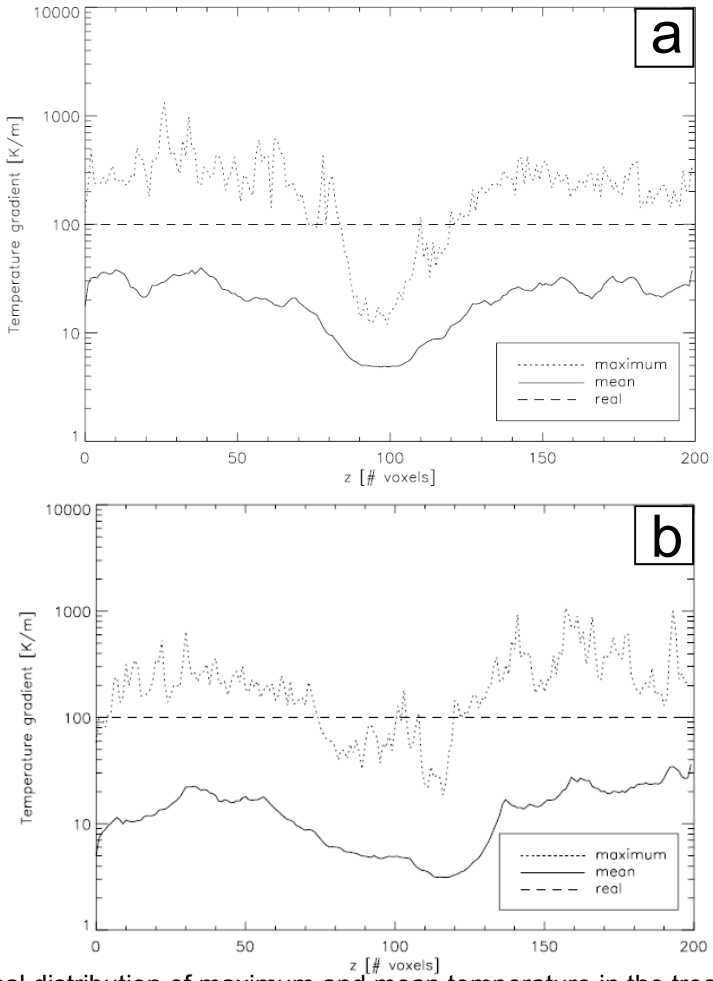

Figure 6.24: Vertical distribution of maximum and mean temperature in the treatment samples: a) January 6, 2005B, b) March 17, 2005B. The abscissa is the vertical coordinate in the sample (1 voxel = 0.048 mm).

6.3 Summary and Conclusions

The simulations in this chapter are from two very different models. SNOWPACK was designed to support operational forecasting programs. It includes representations of the processes that cause the snow structure to change, but processes on the microscale are parameterized. Currently it would be very difficult to build a model that represented processes at the grain scale and also produced information at the layer and snowpack scale needed for avalanche and climate applications. The RKS

model does not attempt to describe the evolution of the structure. Rather it takes an observed structure and simulates how thermal energy is distributed.

The comparison between the SNOWPACK simulations and the observations give us some insight into our ability to replicate processes within the snow. Visually the SNOWPACK simulations are quite similar to the observations. The slope and magnitude of the predicted and observed temperature profiles are similar with a few exceptions. The model did not predict a noticeable difference in the thermal profiles between the control and treatment samples. This result is consistent with the observations presented here and in Chapter 4.

The predictions of effective thermal conductivity are also similar to the observed evolution. The predicted magnitude and trend in k_e were close to the observed values in the experiments with low density snow. In two of the experiments the model did not predict an increase in effective thermal conductivity. I do not have a good explanation for this discrepancy. However, this trend is an important feature that results from snow metamorphism and deserves further investigation. Although visually the evolution in k_e was quite good, statistically the model predictions were without skill in all of the simulations.

The RKS simulations give us some information about processes in the snow that are very difficult or impossible observe. They show how snow metamorphism changes the way thermal energy is transported through the ice fraction of the snow. Initially the transport of heat is relatively even through the snow structure. However, after successive days of kinetic growth large portions of the snow structure have a small contribution to the overall heat transfer and relatively small areas transport most of the

thermal energy. Preferential pathways form parallel to the heat flow. In the control samples, chains of depth hoar crystals form these pathways. In the treatment samples these chains connect to the upper and lower boundaries of the ice layer. The transport of heat is more efficient in the layered sample, which results in lower temperature gradients. Although people have observed chains of depth hoar crystals in the field or many years, these model simulations help us understand how important they are for heat transfer in the snow. The mean temperature in the control sample changes linearly with height. In the treatment sample, the temperature has a linear change in the snow layers, but the mean is a constant value within the ice layer. The mean temperature gradient is constant in the control sample, but there are large changes in the temperature gradient at the interface of the ice and snow layers. Although the change in temperature with height has a clear physical impact on vapor pressure and crystal growth rate, the interpretation of slope of the temperature gradient line is less clear.

Chapter 7

SUMMARY AND CONCLUSIONS

7.0 Conclusions

7.0.1 Thermophysics

These experiments are the first effort to visualize and quantify the effects of a thin ice layer on kinetic growth metamorphism. The temperature profiles and the heat flux data confirmed that the samples were in steady state heat flow. The ice layer did not have a noticeable effect on the thermal profile of each sample at the measured scale. A signature of the ice layer also did not appear in the heat flux measurements. The measured effective thermal conductivities increased during the metamorphic process. This increase appeared to be largest during the first few days of kinetic growth. However, these experiments were not long enough to verify this result (see Schneebeli and Sakratov, 2004). The calculated values of k_e were larger than those predicted by the regression equations from Sturm et al. (1997). A possible explanation is that the snow in these experiments is on the low end of the density range used to develop the regression model. The measurement technique used by Sturm et al. is quite different than the method in this study. My method is limited by heat loss out of the sides of the sample and errors in the location of the thermocouple probes. The needle probe method breaks the snow structure, which is vital to the most important heat transport mechanism, directly around the heat source.

7.0.2 Microstructure

The density measurements obtained in the laboratory correlate very well with the stereological estimates. The specific surface area with respect to the ice volume decreased during kinetic growth metamorphism. I observed a very interesting trend in the microstructure around the ice layers. During kinetic growth metamorphism the upper surface was eroding and became round and smooth. Faceted structures grew from the lower surface as the layer began to transform into depth hoar crystals. At this point in the metamorphic process the solid ice layer was very well connected to the lower snow layer and had fewer connections to the snow above. Microcavities also formed above the ice layer causing the area directly above the ice layer to have less ice per unit volume. These features developed directly above the ice layer and were the height of one or two particles.

7.0.3 Numerical Simulation

The model simulations captured some of the important physical trends observed in the experiments. The SNOWPACK model did an adequate job of predicting the observed temperature profile. The model predictions of the effective thermal conductivity captured the trend in most of the simulations and were very close in magnitude. However, a statistical comparison of the observations and simulations showed no statistical skill in the predictions.

The thermal simulations of the three-dimensional reconstructions showed pronounced changes during the metamorphic process. Initially the temperature within the sample was a function of height, with warm temperatures on the bottom and cool

temperatures on top. During metamorphism the structure changed forming pathways that transported more thermal energy than the surrounding structures. In the control samples these vertical structures were warm on the bottom and transitioned to a cooler temperature near the top of the sample. However, the neighboring structures had less vertical connections and dead ends that disrupted the even vertical temperature distribution. In the treatment samples the ice layer and the vertical structures on either side all reached a similar temperature. Most of the thermal energy was transported through these vertical structures and they developed the largest temperature gradients and crystal chains. Although it has been hypothesized that chains of crystals are important for the vertical transport of thermal energy, to my knowledge these simulations are the first evidence of this phenomena.

7.1 Research Questions

This study was designed to investigate the thermophysical and microstructural effects of kinetic growth metamorphism around a thin ice layer. With the results of this research effort, I can address, if not answer, all of the research questions stated in Chapter 1 (Section 1.3).

1. Is there a consistent effect on the thermophysical properties of the snow sample from the presence of the ice layer?

No. I did not observe a difference in the temperature profiles or heat flux values that could be attributed to the ice layer.

2. Is there a local increase in the temperature gradient due to the ice layer?

No. The slope of the temperature gradient changes at the boundaries of the ice layer, but the magnitude did not increase in the model.

3. Is there a consistent difference between the structures that develop in the homogenous and layered samples?

Yes. Large faceted crystals and vertical chains formed in both samples. The ice layer is a large change in the mesoscale structure of the snow. Even a very thin ice layer has a large effect on the microstructure and makes comparisons difficult. However, microstructure that developed in the treatment samples was very different than the structure of the control samples. The differences are visually distinguishable, evident in the RKS simulations and probably have a large impact on the mechanical properties of the snow.

4. Is there a consistent difference between the structures that develop along the upper and lower interfaces of the ice layer?

Yes. The upper surface of the ice layer became smooth, while faceted structures grew on the lower surface. Microscale cavities formed above the ice layer. Particles were often larger with fewer connections above the ice layer.

5. Can current numerical models of snow metamorphism simulate the evolution in the thermophysical properties we observed?

Yes and no. SNOWPACK often simulated the temperatue profile well, but had trouble with the magnitude and evolution of k_e.

7.2 Summary

The microstructure of snow and how it affects other physical properties impacts research efforts in atmospheric and climate science, hydrology, avalanche science, remote sensing and cold regions engineering. Although it is common to characterize snow with bulk properties such as density and parameters that are easy to measure in the field such as grain size and type, these properties do not directly correlate to the information we need for optical, thermal and mechanical applications. The microstructure of snow is very complex and has a huge impact on many of the properties we strive to describe.

During this study, I developed new methods for studying snow and used techniques from previous research efforts. In most cases we were able to extend the

application of previous methods to snow science or apply them to snow for the first time. Thermocouples in a Teflon frame produced reasonable temperature profiles. By sufficiently insulating the samples, I was able to minimize heat loss during most of the experiments. I was also able to cast fairly large snow samples in dimethyl phthalate with reasonable success. We used these casts to observe serial sections of the snow and by using a weighted convolution kernel, build three-dimensional reconstructions of the structure.

Although I attempted to use quantitative measures to address the research questions, many of the answers came from qualitative observations. There was not a noticeable difference in the thermal properties of the treatment and control samples. The ice layer was so thin that its effect on the thermal field may have been too small to observe with thermocouples.

I did not observe an increase in the temperature gradient around the ice layer. This may be a result of the distance between the thermocouple probes, the sensitivity of the thermocouples, or that no effect exists. The numerical simulations did not show an increased temperature gradient near the layer, but since the model does not include latent heat exchange we can only rule out conduction as the mechanism for this theoretically predicted perturbation.

The nature of the structures on either side of the ice layer was quite different. The difference in the structures was apparent at the scale of our observations. However, the structures were small enough that it would be difficult to observe them with other techniques. Although the structure we observed in this study impacts heat and mass transfer around large density and porosity changes, it also has implications for

mechanical and hydrological applications. Both the nature of the connections and the formation of microcavities help to explain patterns in the mechanical behavior of snow that have been observed for years. Researchers and field technicians have also observed water running along hard layers. The results of this study suggest that although the crust probably acts as a fluid barrier, the structure directly above the crust may also contribute to the formation of preferential flow channels leading to lateral flow.

The modeling results show that numerical simulation of snow metamorphism has evolved, but the parameterizations still have room to improve. The geometry of snow is incredibly complex. In order to develop forecast models some parameterization is absolutely necessary. However, we need more measurements of the physical properties of snow in order to group the key features of snow and develop a more descriptive parameterization. It is possible that combining several different parameters (such as physical and microstructural parameters) will produce a better prediction of key properties. It is encouraging that the predictions of effective thermal conductivity improve by including both density and specific surface area in the regression model.

7.3 Suggestions for Future Research

As a community we need more measurements of the physical properties of snow. The number of thermal conductivity measurements is increasing, but investigations of snow that include measurements in several different categories would help extend our understanding of snow. I suggest we undertake laboratory efforts that include thermal, microstructural and mechanical measurements.

Previous research has focused on metamorphic processes in homogenous snow samples, with only a few investigations of layered snowpacks. This progression was necessary and we have learned a tremendous amount about snow metamorphism from these efforts. However, seasonal snow covers are layered structures and many of the processes we strive to understand occur at the interfaces of these layers. This work addresses a very small portion of the myriad of different interfaces that occur in nature. Thicker ice layers and density changes that do not include a vapor barrier are obvious places to start.

This work examined what happens at layer interfaces that are under a very large temperature gradient. I concentrated on kinetic growth, but we still do not know what occurs when sintering processes dominate. In order to understand persistent weak layers that develop in the snowpack we need to address this question.

There are a countless number of additional questions that were raised during the course of this study. The number of data points obtained in this work is relatively small. Repeating this work would be a worthwhile effort for with each additional effort we slowly extend our knowledge of snow.

LITERATURE CITED

Adams, E.E., and R.L. Brown, 1982: Further results on studies of temperature-gradient metamorphism. *Journal of Glaciology*, **98**, 205-210.

Adams, E.E., and R.L. Brown, 1983: Metamorphism of dry snow as a result of temperature gradient and vapor density differences, *Annals of Glaciology*, **4**, 3-8.

Adams, E.E., and R.L. Brown, 1990: A mixture theory for evaluation heat and mass transport processes in nonhomogeneous snow. *Continuum Mechanics and Thermodynamics,* **2**, 31-63.

Adams, E.E., and A. Sato, 1993: Model for effective thermal conductivity of a dry snow cover composed of uniform ice spheres. *Annals of Glaciology*, **18**, 300-304.

Akitaya, E., 1974: Studies on depth hoar. *Contributions from Institute of Low Temperature Science, Series A*, **26**, 1-67.

Akitaya, E., 1986: Structure of quick hardened snow under temperature gradient. *Low Temperature Science, Series A,* **45**, 11-18.

Alley, R.B., 1986: Three-dimensional coordination number from two-dimensional measurements: a new method. *Journal of Glaciology*, **32**, 391-396.

Alley, R.B., 1988: Concerning the deposition and digenesis of strata in polar firn. *Journal of Glaciology,* **34**, 283-290.

Armstrong, R.L., 1985: Metamorphism in a subfreezing, seasonal snow cover: The role of thermal and vapor pressure conditions, Ph.D. Dissertation, Department of Geography, University of Colorado, Boulder, Colorado.

Arons, E.M., and S.C. Colbeck, 1995: Geometry of heat and mass transfer in dry snow: a review of theory and experiment. *Reviews of Geophysics*, **33**, 463-493.

Atkins, D., and K. Williams, 2000: 50 years of avalanche deaths in the United States. Proceedings of the International Snow Science Workshop, Big Sky, Montana, October, p. 16-20.

Baddeley, A.J., H.J.G. Gundersen, and L.M. Cruz-Orive, 1986: Estimation of surface-area from vertical sections, *Journal of Microscopy*, **142**, 259-276.

Bader, H, R. Haefeli, E. Bucher, J. Neher, O. Eckel, and C. Thams, 1939: Der Schnee und seine Metamorphose. Beitrage zur Geologie der Schweiz Geotechnische Serie, Hydrologie, Lieferung 3, Bern. [English Translation: Snow, Ice, and Permafrost Research Establishment. Translation 14, 1954.]

Bartelt, P., and M. Lehning, 2002: A physical SNOWPACK model for the Swiss avalanche warning Part I: Numerical model. *Cold Regions Science and Technology,* **35**, 123-145.

Bartelt, P., O. Buser and S.A. Sokratov, 2004: A nonequilibrium treatment of heat and mass transfer in alpine snowcovers. *Cold Regions Science and Technology*, **39**, 219-242.

Bell, M.J., 1993: Wind pumping in a snow pack related to atmospheric turbulence. Ph.D. thesis, Chemical and Process Engineering, University of Canterbury, New Zealand.

Brown, R.L., and M.Q. Edens, 1991: On the relationship between neck length and bond radius during compression of snow. *Journal of Glaciology*, **37**, 203-208.

Brown, R.L., P. Bartelt, P.K., Satyawali, and M. Lehning, 2001: Modeling the changes in microstructure of snow during metamorphism. *Cold Regions Science and Technology,* **33**, 91-101.

Brun, E., E. Martin, V. Simon, C. Gendre, and C. Coleou, 1989: An energy and mass model of snow cover suitable for operation avalanche forecasting. *Journal of Glaciology,* **35**, 333-342.

Brun, E., P. David, M. Sudul, and G. Brunot, 1992: A numerical model to simulate snow-cover stratigraphy for operation avalanche forecasting. *Journal of Glaciology,* **38**, 13-22.

Brun, E., E. Martin, and V. Spiridonov, 1999: Coupling a multi-layered snow model with a GCM. *Annals of Glaciology,* **25**, 66-97.

Brzoska, J.B., C. Coleou, and B. Lesaffre, 1998: Thin-sectioning of wet snow after flash-freezing. *Journal of Glaciology*, **44**, 54-62.

Burns, G.W., M.G. Kaeser, G.F. Strouse, M.C. Croarkin, and W.F. Guthrie, 1993: Temperature-Electromotive Force Reference Functions and Tables for the Letter-Designated Thermocouple Types Based on the ITS-90. United States National Institute of Standards and Technology, Monograph 175. pp. 630.

Campbell Scientific, 2000: *CR10X Measurement and Control.* Campbell Scientific, Logan, Utah, www.campbellsci.com.

Carsey, F., 1992: Remote sensing of ice and snow: review and status. *International Journal of Remote Sensing*, **13**, 5-11.

Carslaw H.S., and J.C. Jaeger, 1959: *Conduction of Heat in Solids*. Oxford University Press, Oxford, pp. 510.

Clark, G.K.C., and E.D. Waddington, 1991: A three-dimensional theory of wind pumping. *Journal of Glaciology*, **37**, 89-96.

Cline, D.W., 1997: Snow surface energy exchanges and snowmelt at a continental multitude alpine site. *Water Resources Research*, **33**, 689-701.

Colbeck, S.C., 1983a: Theory of metamorphism of dry snow. *Journal of Geophysical Research*, **88**(C9), 5475-5482.

Colbeck, S.C., 1983b: Ice crystal morphology and growth rates at low supersaturations and high temperatures. *Journal of Applied Physics*, **54**, 2677-2682.

Colbeck, S.C., 1987: A review of metamorphism and classification of seasonal snow cover crystals. In: B. Salm and H. Gubler, (eds.), *Avalanche Formation, Movement, and Effects*, IAHS-AISH Publication No. 162, p. 3-34.

Colbeck, S.C., 1989: Air movement in snow due to windpumping, *Journal of Glaciology*, **35**, 209-213.

Colbeck, S.C., 1991: The layered character of snow covers. *Reviews of Geophysics*, **29**, 81-96.

Colbeck, S.C., E. Akitaya, R. Armstrong, H. Gubler, J. Lafeuille, K. Lied, D. McClung and E. Morris, 1990: *The International Classification for Seasonal Snow on the Ground*. International Commission on Snow and Ice, International Association of Scientific Hydrology. pp. 24.

Colbeck, S.C., and J.B. Jamieson, 2001: The formation of faceted layers above crusts. *Cold Regions Science and Technology*, **33**, 247-252.

Coleou, C., B. Lasaffre, J.B. Brozoska, W. Ludwig, and E. Boller, 2001: Three-dimensional snow images by X-ray microtomography. *Annals of Glaciology,* **32**, 75-81.

Constable, R.T., and R.M. Henkelman, 1991: Contrast, Resolution, and Detectability in MR imaging. *Journal of Computer Assisted Tomography*, **15**, 297-303.

Davis, R.E., J. Dozier, and A.T.C. Chang, 1987: Snow property measurements correlated to microwave emission at 35 GHz. *IEEE Transactions on Geoscience and Remote Sensing,* **GE-25**, 752-757.

Davis, R.E., J. Dozier, and R. Perla, 1987: Measurement of snow grain properties. In: H.G. Jones and W.J. Orville_Thomas (eds.), *Seasonal Snowcovers: Physics, Chemistry, and Hydrology,* p. 63-74, D. Reidel Publishing Company, Dordrecht, Holland.

Davis, R.E., A.W. Nolin, R. Jordan, J. Dozier, 1993: Towards predicting temporal changes of the spectral signature of snow in visible and near-infrared wavelengths. *Annals of Glaciology,* **17**, 143-148.

Davis, R.E., B. Jamieson, J. Hughes, and C. Johnston, 1996: Observations on buried surface hoar-Persistent failure planes for slab avalanches in British Columbia, Canada. Proceedings of the International Snow Science Workshop, Banff, British Columbia, p. 81-85.

Davis, R.E., J.P. Hardy, W. Ni, C. Woodcock, J.C. McKenzie, R. Jordan, X. Li, 1997: Variation of snow cover ablation in the boreal forest: A sensitivity study on the effects of conifer canopy. *Journal of Geophysical Research*, **102**, 29389-29395.

Davis, R.E., B. Jamieson, and C. Johnston, 1998: Observations on buried surface hoar in British Columbia, Canada: Section analyses of layer evolution. Proceedings of the International Snow Science Workshop, Sun River, Oregon, p. 86-92.

Dehoff, R.T., 1983: Quantitative serial sectioning analysis: preview. *Journal of Microscopy,* **131**, 259-263.

de Quervain, M., 1950: Die Metamorphose des Schneekristalls. *Verhandlungen der Schweizerischen Naturforschenden Gesellschaft,* Bd. 130, p. 114-122.

Dominé, F., A. Cabanes, A.S. Taillandier and L. Legagneux, 2001: Specific surface area of snow samples determined by CH_4 adsorption at 77 K and estimated by optical microscopy and scanning electoron microscopy. *Environmental Science and Technology*, **35**, 771-780.

Dominé, F., A. Cabanes and L. Legagneuz, 2002: Structure, microphysics, and surface area of the Arctic snowpack near Alert during the ALERT 2000 campaign. *Atmospheric Environment,* **36**, 2753-2765.

Dominé, F., T. Lauzier, A. Cabanes, L. Legagneux, W. F. Kuhs, K. Techmer, and T. Heinrichs, 2003: Snow metatmorphism as revealed by scanning electron microscopy, *Microscopy Research and Techniques*, **62**, 33-48.

Dozier, J., 1989: Remote sensing of snow in visible and near-infrared wavelengths. In: G. Asrar (ed.), *Theory and applications of optical remote sensing*. p.527, John Wiley and Sons, New York.

Dozier, J., R.E. Davis, and R. Perla, 1987: On the objective analysis of snow microstructure. In: B. Salm and H. Gubler, (eds.) *Avalanche Formation, Movement, and Effects*, IAHS-AISH Publ. No. 162, International Association of Hydrological Sciences, Wallingford, UK, p. 49-59.

Durand, Y., G. Giraud, E. Brun, L. Merindol, and E. Martin, 1999: A computer-based system simulating snowpack structures as a tool for regional avalanche forecasting. *Journal of Glaciology,* **45**, 469-484.

Edens, M.Q., and R.L. Brown, 1991: Changes in microstructure of snow under large deformations. *Journal of Glaciology,* **37**, 193-202.

Edens, M.Q., and R.L. Brown, 1992: The use of computer-based quantitative stereology for studying microstructure of snow. Abstract in the Proceedings of the International Snow Science Workshop, Breckenridge, Colorado, U.S.A., p. 10.

Etchevers, P., Y. Durand, F. Habets, E. Martin, and J. Noilhan, 2001: Impact of spatial resolution on the hydrological simulation of the Durance high-Alpine catchment, France. *Annals of Glaciology,* **32**, 87-92.

Faktor, M.M., I. Garrett, and R. Heckingbottom, 1971: Diffusional limitations in gas phase growth of crystals, *Journal of Crystal Growth,* **9**, 3-11.

Fierz, C., 1998: Field observation and modeling of weak-layer evolution. *Annals of Glaciology*, **26**, 7-13.

Fierz C., and T. Baunach, 2000: Quantifying grain-shape changes in snow subjected to large temperature gradients. *Annals of Glaciology,* **31**, 439-442.

Flin, F., J.B. Brzoska, B. Lesaffre, C. Coleou, and P. Lamboley, 2001: Computation of normal vectors of discrete 3D objects: Application to natural snow images from X-ray tomography. *Image Analysis and Stereology,* **20**, 187-191.

Fohn, P.M.B., C. Camponovo, and G. Krusi, 1998: Mechanical and structural properties of weak snow layers measured in situ. *Annals of Glaciology,* **26**, 1-6.

Fuchs, A., 1956: Preparation of plastic replicas and thin sections of snow. Technical Report No. 41, Snow, Ice and Permafrost Research Establishment, Corps of Engineers, Wilmette, Illinois.

Fuchs, A., 1959: Some structural properties of Greenland snow. Research Report No. 42, Snow, Ice and Permafrost Research Establishment, Corps of Engineers, Wilmette, Illinois.

Gibson, L.J., and M.F. Ashby, 1997: *Cellular Solids: Structure and Properties*, Cambridge University Press, Cambridge, U.K.

Greene, E., and G. Johnson, 2002: Charaterization of a deep slab instability. Proceedings of the International Snow Science Workshop, Penticton, BC October 2002, p. 491-498.

Greene, E., K. Birkeland, K. Elder, G. Johnson, C. Landry, I. McCammon, M. Moore, D. Sharaf, C. Sterbenz, B. Tremper and K. Williams, 2004: *Snow, Weather, and Avalanches: Observational Guidelines for Avalanche Programs in the United States*, American Avalanche Association, Pagosa Springs, Colorado, pp. 136.

Good, W., 1975: Numerical parameters to identify snow structures, In: *Snow Mechanics,* IAHS-AISH Publ. No. 114, International Association of Hydrological Sciences, Wallingford, UK p. 49-59.

Good, W., 1980: Structural investigations of snow; a comparison of different parameter sets. In: E.S. Gelsema and L.N. Kanal (eds.) *Pattern Recognition in Practice*, North-Holland Publishing Company, Amsterdam, p. 161-170.

Good, W., 1982: Structural investigations of snow and ice on core III from the drilling on Vernagtferner, Austria, in 1979. *Zeitschrift Fur Gletscherkunde, und Glazialgeologie,* **18**, 53-64.

Good, W., 1987: Thin sections, serial cuts, and 3-D analysis of snow. In: B. Salm and H. Gubler, (eds.) *Avalanche Formation, Movement, and Effects,* IAHS-AISH Publ. No. 162, International Association of Hydrological Sciences, Wallingford, UK, p. 35-48.

Good, W., 1989: Laboratory techniques for the characterization of snow structures. Proceedings of an International Workshop on Physics and Mechanics of Cometary Materials, Munster, Westfalia, Gremany, p. 147-151.

Gokhale, A.M., and N.U. Deshpande, 1993: Stereology of anisotropic microstructures. Proceedings of the International Conference on Quantitative Microscopy and Image Analysis, Charleston, South Carolina, U.S.A., p. 73-82.

Gow, A.J., 1975: Time-temperature dependence of sintering in perennial isothermal snowpacks In: *Snow Mechanics,* IAHS-AISH Publ. No. 114, International Association of Hydrological Sciences, Wallingford, UK, p.25-41.

Grenfell, T.C., and S.G. Warren, 1999: Representation of a nonspherical ice particle by a collection of independent spheres for scattering and absorption of radiation. *Journal of Geophysical Research,* **104**, 31,697-31,709.

Grenfell, T.C., S.G. Warren, and P.C. Mullen, 1994: Reflection of solar radiation by the Antarctic snow surface at ultraviolet, visible, and near-infrared wavelengths. *Journal of Geophysical Research,* **99**, 18,669-18,684.

Grönemeyer, D.H., and R.B. Lufkin, 2000: *Open Field Magnetic Resonance Imaging*. Springer, Berlin, Germany, pp.304.

Gubler, H., 1978: Determination of the mean number of bonds per snow grain and of the dependence of the tensile strength of snow on stereological parameters. *Journal of Glaciology,* **32**, 434-438.

Gustafsson, D., M. Stahli, P.E. Jansson, 2001: The surface energy balance of a snow cover: Comparing measurements to two different simulation models. *Theoretical and Applied Climatologic,* **70**, 81-96.

Hachikubo, A., 2001: Numerical modeling of sublimation on snow and comparison with field measurements. *Annals of Glaciology,* **32**, 27-32.

Hall, D. K., 1988: Assessment of polar climate change using satellite technology, *Reviews of Geophysics*, **26**, 26.39.

Hansen, A.C., and R.L. Brown, 1986: The granular structure of snow: An inter-state variable approach. *Journal of Glaciology,* **32**, 434-438.

Hidebrand, T., and P. Rüegsegger, 1997: Quantification of bone microarchitecture with the Structure Model Index. *Computer Methods in Biomechanics and Biomedical Engineering*, **1**, 15-23.

Holman, J.P., 2002: *Heat Transfer*. McGraw-Hill, New York, pp. 665.

Howard, C.V., and M.G. Reed, 1998: *Unbiased Stereology: Three-dimensional measurement in microscopy*. Springer, New York, pp. 246.

Incropera, F.P., and D.P. DeWitt, 2002: *Fundamentals of Heat and Mass Transfer*. John Wiley and Sons, New York, pp. 981.

ISA, 1982: *Temperature Measurement Thermocouples*. International Society for Measurement and Control, ISA MC96.1-1982, pp. 72.

Jamieson, B., 2006: Formation of refrozen snowpack layers and their role in slab avalanche release. *Reviews of Geophysics*, **44**, RG2001, doi:10.1029/2005RG000176.

Jamieson, B., T. Geldsetzer, and C. Stethem, 2001: Forecasting for deep slab avalanches. *Cold Regions Science and Technology*, **33**, 275-290.

Jamieson, B., and A. van Hervijnen, 2002: Preliminary results from controlled experiments on the growth of faceted crystals above a wet snow layer. Proceedings of the International Snow Science Workshop, Penticton, British Columbia, Canada, 337-342.

Jamieson, B., and C. Fierz, 2004: Heat flow from wet to dry snowpack layers and associated faceting. *Annals of Glaciology*, **38**, 187-194.

Johnson, J., and M. Schneebeli, 1999: Characterizing the microstructural and micromechanical properties of snow. *Cold Regions Science and Technology*, **30**, 91-100.

Jordan, R., 1991: A one-dimensional temperature model for a snow cover: Technical Documentation for SNTHERM.89. Special Report 91-16, Cold Regions Research and Engineering Laboratory.

Kaempfer, T. U., M. Schneebeli, and S. A. Sokratov, 2005: A microstructural approach to model heat transfer in snow. *Geophysical Research Letters*, **32**, doi:10.1029/2005/GL023873.

Keeler, C.M., 1969: The growth of bonds and the increase of mechanical strength in a dry seasonal snow-pack. *Journal of Glaciology*, **8**, 441-450.

Kerlin, T.W., 1999: *Practical Thermocouple Thermometry*, Instrument Society of America, Research Triangle Park, North Carolina, pp.120.

Kinosita, S, and G. Wakahama, 1959: Thin sections of deposited snow made by the use of aniline. *Low Temperature Science, Series A,* **18**, 77-96.

Kry, P. R., 1975: Quantitative stereological analysis of grain bonds in snow. *Journal of Glaciology*, **14**, 467-477.

Kuroiwa, D., 1975: Mechanics and structure of snow as a dispersed system. In: *Snow Mechanics*, IAHS-AISH Publ. No. 114, International Association of Hydrological Sciences, Wallingford, UK, p.3-15.

LaChapelle, E.R., 1970: Principles of avalanche forecasting. In: Engineering and Avalanche Forecasting and Control. Technical Memo No. 98, National Research Council, Canada, p.106-113.

Leathers, D.J., A.W. Ellis, and D.A. Roberts, 1995: Characteristics of temperature depressions associated with snow cover across the northeast United States. *Journal of Applied Meteorology,* **34**, 381-390.

Legagneux, L., T. Lauzier, F. Domine, W.F. Kuhs, T. Heinrichs and K. Techmer, 2003: Rate of decay of specific surface area of snow during isothermal experiments and morphological changes studied by scanning electron microscopy. *Canadian Journal of Physics,* **81**, 459-468.

Legagneux, L., A.S. Taillandier, and F. Dominé, 2004: Grain growth theories and the isothermal evolution of specific surface area of snow. *Journal of Applied Physics*, **95**, 6175-6184

Lehning, M., P. Bartelt, R.L. Brown, T. Russi, U. Stockli and M. Zimmerli, 1999: Snowpack model cacluations for avalanche warning based upon a new network of weather and snow stations. *Cold Regions Science and Technology,* **30**, 145-157.

Lehning, M, C. Fierz, P. Satyawali, P. Bartelt, and B. Brown, 2002: A physical SNOWPACK model for the Swiss avalanche warning Part II: Snow Microstructure. *Cold Regions Science and Technology,* **35**, 147-167.

Lehning, M, C. Fierz, P. Bartelt, and B. Brown, 2002: A physical SNOWPACK model for the Swiss avalanche warning Part III: Meteorological forcing, thin layer formation and evolution. *Cold Regions Science and Technology,* **35**, 169-184.

Lesaffre, B., E. Pougatch, E. Martin. 1998: Objective determination of snow grain characteristics from images. *Annals of Glaciology,* **26**, 112-118.

Lundy, C.C. and E.E. Adams, 1998: Nondestrutive collection of natural snow specimens for use with CT scan analysis. Proceedings of the International Snow Science Workshop, Sunriver, Oregon, U.S.A., p. 208-213.

Lundy, C.C., M.Q. Edens, and R.L. Brown, 2002: Measurement of snow density and microstructure using computed tomography. *Journal of Glaciology,* **48**, 312-316.

Matzler, C., 2002: Relation between grain-size and correlation length of snow. *Journal of Glaciology,* **48**, 461-466.

Matzl, M., 2006: Quantifying the stratigraphy of snow profiles. Ph.D. thesis, Swiss Federal Institute of technology, Zurich, Switzerland.

Matzl, M. and M. Schneebeli, 2006: Measuring specific surface area of snow by near-infrared photography. *Journal of Glaciology*, **7**, 558-564.

Marbouty, D., 1980: An experimental study of temperature-gradient metamorphism. *Journal of Glaciology,* **26**, 303-312.

McClung, D.M., 1977: Direct simple shear tests on snow and their relation to slab avalanche formation. *Journal of Glaciology*, **19**, 101-109.

McClung, D., and P. Schaerer, 1993: *The Avalanche Handbook.* The Mountaineers, Seattle, p.59.

Miller, D.A., 2002: An integrated microstructural study of dry snow metamorphism under generalized thermal conditions. Ph.D. thesis, Department of Civil Engineering, Montana State University, Bozeman, Montana.

Moore, M.B., 1982: Temperature gradient weakening of snowpacks near rain crusts or melt-freeze layers, unpublished paper, abstract appears in the Proceedings of the International Snow Science Workshop, Bozeman, Montana, October 1982.

Moore, M, G. Ferber, and K. Kramer, 2003: Annual Report 2002-2003. Northwest Weather and Avalanche Center, USDA-Forest Service, Pacific Northwest Region. This report can be found at: http://www.nwac.noaa.gov/ Revised_Final_03.pdf

Murakami, S., and N. Maeno, 1989: Thermal conductivity of snow and snow/metal mixtures. *Low Temperature Science, Series A,* **48**, 13-25.

Nakamura, T., R. Tamura, T. Ohta, and O. Abe, 1998: Experimental study on the spectral reflectance of snow. Proceedings of the International Snow Science Workshop, Sun River, Oregon, p. 214-224.

Narita, H., 1969: Measurement of the specific surface of deposited snow I. *Low Temperature Science, Series A,* **27**, 77-86.

Narita, H., 1971: Measurement of the specific surface of deposited snow II. *Low Temperature Science, Series A,* **29**, 69-79.

Ozeki, T., A. Hachikubo, K. Kose, and K. Nishimura, 2000: NMR imaging of snow. Proceedings of the International Snow Science Workshop, Big Sky, Montana, p. 402-406.

Ozeki, T., K. Kose, T. Haishi, S. Nakatsubo, K. Nishimura, and A. Hochikubo, 2003: Three-dimensional MR microscopy of snowpack structures. *Cold Regions Science and Technology*, **37**, 385-391.

Palais, J.M., 1984: Snow statigraphic investigations at Dome C Antarctica: A study of depositional and digenetic processes. *Ohio State University, Institute of Polar Studies Report 78.*

Palm, E., and M. Tveitereid, 1979: On heat and mass flow through dry snow. *Journal of Geophysical Research*, **84**(C2), 745-749.

Perla, R., 1982: Preparation of section planes in snow specimens. *Journal of Glaciology*, **28**, 199-203.

Perla, R., 1985: Snow in strong and weak temperature gradients. Part II: Section-plane analysis. *Cold Regions Science and Technology,* **11**, 181-186.

Perla, R., and J. Dozier, 1984: Observations of snow structure. Proceedings of the International Snow Science Workshop, Aspen, October 1984, p. 182-187.

Perla, R., and C.S.L. Ommanney, 1985: Snow in strong and weak temperature gradients. Part I: Experiments and qualitative observations. *Cold Regions Science and Technology,* **11**, 23-35.

Perla, R., J. Dozier, R.E. Davis, 1986. Preparation of serial sections in dry snow specimens. *Journal of Microscopy,* **142**, 111-114.

Petrenko, V.F., and R.W. Whitworth, 1999: *Physics of Ice*. Oxford University Press, Oxford, pp.373.

Pfeffer, W.T., and R. Mrugala, 2002: Temperature gradient and initial snow density as controlling factors in the formation and structure of hard depth hoar. *Journal of Glaciology,* **48**, 485-494.

Pielke, R.A. Sr., 2002: *Mesoscale Meteorological Modeling*. Academic Press, New York, p. 464.

Pielmeier, C. and M. Schneebeli, 2003: Stratigraphy and changes in hardness of snow measured by hand, ramsonde and snow micro penetrometer: a comparison with planar sections. *Cold Regions Science and Technology,* 393-405.

Powell, R.L., W.J. Hall, C.H. Hyink, L.L. Sparks, G.W. Burns, M.G. Scroger, and H.H. Plumb, 1974: Thermocouple reference tables based on the IPTS-68. United States National Bureau of Standards, Monograph 125, pp. 410.

Powers, D.J., S.C. Colbeck, and K. O'Neill, 1985a: Thermal convection in snow, CRREL Report 85-9, Cold Regions Research and Engineering Laboratory, Hanover, N.H.

Powers, D.J., K. O'Neill, and S.C. Colbeck, 1985b: Theory of natural convection in snow. *Journal of Geophysical Research*, **90**(B6), 10,641-10649.

Rowe, C.M., K.C. Kuivinen, R. Jordan, 1995: Simulation of summer snowmelt on the Greenland ice sheet using a one-dimensional model. *Journal of Geophysical Research*, **100**, 16265-16273.

Russ, J.C., and R. T. Dehoff, 2000: *Practical Stereology,* Kluwer Academic/Plenum Publishers, New York, pp. 381.

Sato, A., E.E. Adams, and R.L. Brown, 1994: Effects of microstructure on heat and vapor transport in snow composed of uniform fine ice spheres. Proceedings of the International Snow Science Workshop, Snowbird, Utah, U.S.A., p. 176-184.

Sato, A., M.Q. Edens, and R.L. Brown, 1997: Experiment of metamorphism using standard snow. In: T. Nakamura, M. Izumi, and R.L. Sack (eds.), *Snow Engineering: Recent Advances.* Ashgate Publishing, Hampshier, UK, p. 139-142.

Schneebeli, M., 2000: Three-dimensional snow: How snow really looks like. Proceedings of the International Snow Science Workshop, Big Sky, Montana, October, p. 407-408.

Schneebeli, M., 2004: Numerical simulation of elastic stress in the microstructure of snow. *Annals of Glaciology*, **38**, 339-342.

Schneebeli, M., and S.A. Sokratov, 2004: Tomography of temperature gradient metamorphism of snow and associated changes in heat conductivity. *Hydrological Processes*, **18**, 3655-3665.

Schneebeli, M., C. Pielmeier, and J.B. Johnson, 1999: Measuring snow microstructure and hardness using a high resolution penetrometer. *Cold Regions Science and Technology,* **30**, 101-104.

Segal, M., J.R. Garratt, R.A. Pielke, and Z. Ye, 1991: Scaling and numerical model evaluation of snow-cover effects on the generation and modification of daytime mesoscale circulations. *Journal of the Atmospheric Sciences*, **48**, 1024-1042.

Seligman, G., 1936: *Snow Structure and Ski Fields*. International Glaciological Society, Cambridge, 70-72 pp.

Sethi, D.N., P.K. Srivastava, and P. Mahajan, 2002: Image analysis determination of micro-structural parameters of snow and their correlation with snow tensile strength. Proceedings of the International Snow Science Workshop, Penticton, British Columbia, Canada, p. 307-313.

Shi, J., R.E. Davis, and J. Dozier, 1993: Stereological determination of dry-snow parameters for discrete-scatter microwave modeling. *Annals of Glaciology,* **17**, 295-299.

Singh, A.K., 1999: An investigation of the thermal conductivity of snow. *Journal of Glaciology,* **45**, 346-351.

Sommerfeld, R.A., 1976: Classification outline for snow on the ground. RM-48, Rocky Mountain Forest and Range Experiment Station, Fort Collins, Colorado, U.S.A.

Sommerfeld, R.A., 1983: A branch grain theory of temperature gradient metamorphism in snow. *Journal of Geophysical Research,* **88**, 1484-1494.

Sokratov, S.A., 2001: Parameters influencing the recrystallization rate of snow. *Cold Regions Science and Technology*, **33**, 263-274.

Steffen, K., W. Abdalati, and I. Sherjal, 1999: Faceted crystal formation in the northeast Greenland low-accumulation region. *Journal of Glaciology,* **45**, 63-68.

Strack, J.E., R.A. Pielke Sr., and J. Adegoke, 2002: Sensitivity of model-generated daytime surface heat fluxes over snow to land-cover changes. *Journal of Hydrometeorology*, 24-42.

Sturm, M., and J.B. Johnson, 1991: Natural convection in the subarctic snow cover. *Journal of Geophysical Research*, **96**(B7), 11,657-11,671.

Sturm, M., and J.B. Johnson, 1992: Thermal conductivity measurements of depth hoar. *Journal of Geophysical Research,* **97**, 2129-2139.

Sturm, M., J. Holmgren, M. Konig, and K. Morris, 1997: The thermal conductivity of seasonal snow. Journal of Glaciology, **43**, 26-41.

Sturm, M., D. K. Perovich, and J. Holmgren, 2002: Thermal conductivity and heat transfer through the snow on the ice of the Beaufort Sea. *Journal of Geophysical Research*, **107**(C21) 8043, doi: 10.1029/2000JC000409,2002.

Taylor, C.M., R.J. Harding, R.A. Pielke, P.L. Vidale, and R.L. Walko, 1998: Snow breezes in the boreal forest. *Journal of Geophysical Research*, **103**, 23087-23100.

Tremper, B, E. Lees, T. Kimbrough, and E. Greene, 2003: Snow and Avalanches in Utah: Annual Report USDA-Forest Service Utah Avalanche Center 2002-2003. This report can be found at: http://www.avalanche.org/~uac/season_report/SeasonReport02-03.pdf

van Rietbergen, B., H. Weinans, R. Huiskes, and A. Odgaard, 1995: A new method to determine trabecular bone elastic properties and loading using micromechanical finite-element models. *Journal of Biomechanics,* **28**, 69-81.

Verbeek, F.J., 2000: Three-dimensional reconstruction from serial sections. In: R. Baldock and J. Graham (eds.), *Image Processing and Analysis,* Oxford University Press, Oxford, UK, p.153-196.

Voight, B., and 15 others, 1990: *Snow avalanche hazards and mitigation in the United States*. National Academy Press, Washington, D.C., pp. 84.

Walko, R.L., L.E. Band, J. Baron, T.G.F. Kittel, R. Lammers, T.J. Lee, D. Ojima, R.A. Pielke, C. Tayor, C. Tague, C. Trembeck, and P.L. Vidale, 2000: Coupled atmosphere-biophysics-hydrology models for environmental modeling. *Journal of Applied Meteorology*, **39**, 931-944.

Wallace, J.M., and P.V. Hobbs, 1977: *Atmospheric Science: An Introductory Survey*, Academic Press, New York, pp.467.

Watanabe, Z., 1974: A model of making thin sections of deposited snow. *Seppyo*, **36**, 1-4.

Yang, F., A. Kumar, W. Wang, H-M.H., Juang, and M. Kanamitsu, 2001: Snow-albedo feedback and seasonal climate variability over North America. *Journal of Climate*, **14**, 4245-4248.

Yosida, Z., and Colleagues, 1955: Physical studies on deposited snow. I. Thermal properties. *Contributions from the Institute of Low Temperature Science*, 7, 19-74.

Yosida, Z., 1963: Physical properties of snow. In: W.D. Kingery, (ed.) *Ice and Snow: Properties, Processes, and Applications*, MIT Press, Cambridge Mass, p. 485-527.

Appendix A

EXPERIMENTAL PROTOCOL

A.0 Preparation

- Three days before beginning experiment, move snow from storage unit to -10 °C chest freezer
- Fill spray bottles with deionized water
- Get dry ice
- Attach aluminum plates to the bottom of the insulated boxes
- Prepare duct seal for upper aluminum plates
- Cool boxes and plates prior to sample preparation

A.1 Initial cast

- Cool casting fluid to -3 ºC
- Take 9 x 9 x 6 cm block of snow and place it in foil container
- Fill container with casting fluid (~10 min)
- Place container in -35 °C chest freezer

A.2 Sample preparation (2x)

- For each box of snow measure
    - Density (3x)
    - Grain size (3x)
        - Average
        - Maximum
    - Grain type (3x)
    - Photograph grains – this step was dropped after the first few experiments
- Sieve 1 cm of snow into the bottom of the box
- Place lower heat flux plate into the guard and then into the box
- Layered sample
    - Cut 11 x 11 x 5.5 cm block of snow
    - Insert lower portion of thermocouple fork
    - Place sample in the box
    - Build ice layer
        - Insert Plexiglas sleeve
        - Dampen snow with spray bottle, insert plunger, freeze with dry ice (6x)
    - Cut 11 x 11 x 5.5 cm block of snow
    - Insert lower portion of thermocouple fork
    - Place sample in the box

- Control sample
  - Cut 11 x 11 x 11 cm block of snow
  - Insert thermocouple fork
  - Place sample in the box
- Place upper heat flux plate into the guard and then into the box
- Fill the remainder of the box with sieved snow (~ 1 cm)
- Place upper aluminum plate on top of the box and press to seal
- Plug heat flux plates and thermocouple forks in multiplexers

A.3 Cold room experiment

- Seal door
- Turn off defrost cycle
- Data loggers
  - Clear data logger
  - Set up files for current experiment
- Experiment period (5 days)
  - Data was generally collected every 24 hours during the experiment
- End experiment
  - Unseal cold room
  - Defrost as needed (usually 2-3 cycles)

A.4 Casting (4x)

- Cool 1.5 l of casting fluid to -3 °C
- Cut inlet and vent holes with plug cutter (2 of each)
- Remove aluminum plates
- Place silicon caulk on Plexiglas plates and attach to boxes with Quick Clamps
- Place supercooled fluid into casting reservoir and mix until it is -3 °C
- Attach hoses to box
- Fill box with casting fluid until it can be seen in the vent holes (~10 - 15 min)
- Plug holes with duct seal
- Place cast into -35 °C freezer

A.5 Thermocouple location measurement (4x)

- Remove Plexiglas plates from the box
- Cut insulation away from cast
- Remove heat flux plates and guards
- Make vertical cut 3.5 cm from thermocouple fork
- Melt cut face until thermocouple tips are visible
- Measure distance from each tip to lower heat flux plate
- Photograph cut face with thermocouple tips exposed
- Discard cut portion of sample

A.6 Sample storage

- Wrap sample in foil
- Label sample with start date and record the orientation of the sample (mark top)
- Place in -70 °C freezer

Appendix B

Error Analysis

1.0 Thermocouple Measurements

The temperature measurement system consists of a series of type T thermocouples connected to an AM25T multiplexer and a CR10X data logger. The data logger records the voltage within the thermocouple loop. This voltage is proportional to the temperature at the thermocouple junction, which is calculated with a polynomial equation (Powell et. al, 1973; Grant et. al, 1993). This equation is dependent on the voltage in the thermocouple loop and the temperature at the voltage measurement junction. The temperature at the voltage measurement junction is called the reference temperature.

The sources of error for this system are: 1) the error in the measured reference temperature, 2) the error of the thermocouple wire, 3) the error in the calculated temperature from the polynomial equation, 4) the error in the voltage measurement, 5) error induced by temperature gradients between the reference temperature and the thermocouple junction.

1.1 Reference Temperature Error

The AM25T is designed specifically for thermocouple measurements. The wiring panel contains an aluminum bar to minimize the temperature gradient parallel to the panel. There is also a resistance temperature detection sensor (RTD) mounted within the wiring panel to record the reference temperature. The RTD has a measurement error of ± 0.4 ºC.

1.2 Thermocouple Wire

The accuracy of thermocouple wire is rated by the manufacturer as standard or special limits of error (ISA MC96.1-1982). The thermocouple probes used in this study were constructed of special limits of error type T thermocouple wire. The accuracy of this wire is rated at ± 0.5 ºC or within 4% of the measured value. In addition, we tested the wire in compliance with ISO 10012-1, ISO 9001 Section 4.11 and ANSI/NCSL Z540-1-1994. The largest deviation from the test temperature was 0.16 ºC and occurred at -25 ºC.

1.3 Voltage to Temperature Conversion

The voltage in the thermocouple loop is converted to temperature with a high order polynomial equation (Powell et. al, 1973; Grant et. al, 1993). The equations for each thermocouple type are included as intrinsic functions in the Campbell Scientific operating system (Campbell Scientific, 2000). The error in the temperature calculated with the equation for a type T thermocouple within the temperature range of -100 ºC to 100 ºC is ± 0.001 ºC.

1.4 Voltage Measurement

The error in the voltage measured by the CR10X is dependent on the measurement range selected in the data logger's program. I used a range of ± 250 mV for all of the thermocouple measurements. The error in the voltage measurement with a 250 mV range is 0.2% or ± 0.5 mV. At -10 ºC, a voltage error of 0.5 mV equates to an error in the temperature measurement of ± 0.158 ºC.

1.5 Temperature Gradients within the Temperature Measurement System

A temperature gradient along the thermocouple loop can create an additional error in the temperature measurement. To address this source of error, the data logger system was housed in the same cold environment as the experiments. The enclosures for both the data loggers and the multiplexers were also well insulated to reduce temperature fluctuations at the voltage measurement junction during the experiment.

Calculating the exact value of this error requires analyzing the Seebeck coefficient during the experiments. However, this requires the "true" temperature of the thermocouple junction. Without this information, adding a percentage error of 0.25% is generally regarded as a reasonable method of accounting for this effect (Campbell Scientific, 2000). At a measured temperature of -10 ºC, a 0.25% error would be ± 0.025 ºC.

1.6 Total Error in the Thermocouple Temperature Measurements

There are multiple sources of error in the thermocouple temperature measurements. However, each source is independent and therefore the total error is the sum of the individual errors

$$E_T = E_{ref\_temp} + E_{wire} + E_{polynomial} + E_{voltage} + E_{gradien} \quad \text{B.1}$$

$$E_T = 0.4°C + 0.16°C + 0.001°C + 0.158°C + 0.025°C = 0.744 \approx \pm 0.7°C$$

2.0 Thermocouple Location

The location of the thermocouples was measured at the end of each experiment. Once the cast of the sample was complete, the cast was cut vertically near the end of thermocouple probes. The cut surface was applied to an aluminum plate at room temperature so that the surface slowly melted. Once the tips of the probes were exposed, the distance from the lower heat flux plate to each probe was measured with a depth gauge graduated in 0.5 mm increments. A length measurement of (z = 5.5 mm) obtained with this method is within the range 5.25 mm < z < 5.75 mm or 5.5 ± 0.25 mm. The error in the length measurement is E_z = ± 0.25 mm.

3.0 Temperature Gradient

The temperature gradient calculations include error from both the temperature measurement and the measurement thermocouple probe location. The distance between the temperature sensors was measured in millimeters with an accuracy of ±0.25 mm. Therefore the error in Δz is

$$E_{\Delta z} = \sqrt{E_z^2 + E_z^2} \quad \text{B.2}$$

$$E_{\Delta z} = \sqrt{(0.00025\ m)^2 + (0.00025\ m)^2} = 0.00035\ m$$

The error for the absolute temperature measurements was ± 0.7º C. However, in a differential measurement, several sources of error are removed. Since both measurements used to compute the difference use the same reference temperature and

are computed from the same polynomial equation and the probes are constructed from the same spool of wire, the error for the individual temperature measurements is reduced to

$$E_T = E_{voltage} + E_{gradient} \qquad \text{B.3}$$

and the error for the temperature difference is

$$E_{\Delta T} = \sqrt{E_T^2 + E_T^2} \qquad \text{B.4}$$

$$E_{\Delta T} = \sqrt{(0.183°C)^2 + (0.183°C)^2} = 0.2588°C \approx \pm 0.26°C$$

The error in the calculated temperature gradient is

$$E_{\nabla T} = \nabla T \sqrt{\left(\frac{E_{\Delta z}}{\Delta z}\right)^2 + \left(\frac{E_{\Delta T}}{\Delta T}\right)^2} \qquad \text{B.5}$$

Using typical values measured in these experiments of

$$\Delta z = 0.11 \text{ m}$$

$$\Delta T = 10 \text{ K}$$

$$\nabla T = 100 \text{ K m}^{-1}$$

the error in the temperature gradient calculations is

$$E_{\nabla T} = 100 \text{ Km}^{-1} \sqrt{\left(\frac{0.00035 \text{ m}}{0.11 \text{ m}}\right)^2 + \left(\frac{0.26 \text{ K}}{10 \text{ K}}\right)^2} = 2.62 \text{ Km}^{-1}$$

4.0 Heat Flux Measurements

Heat flux values were measured with thermopiles and a CR10X data logger. The thermopiles were calibrated so that heat flux can be directly calculated from the voltage measurement. The sources of error in this system are: 1) the error in the heat flux sensor, 2) the error in the voltage measurement.

4.1 Heat Flux Sensor

We used TNO-PU43 thermopiles. These sensors were factory calibrated to produce heat flux measurements with an error of ±5% (www.tno.nl). At 30 W m^{-2}, the error is ± 1.5 W m^{-2}.

4.2 Voltage Measurement

The error in the voltage measured by the CR10X is dependent on the measurement range selected in the data logger's program. I used a range of ± 25 mV for all of the thermopile measurements. The error in the voltage measurement with a 25 mV range is 0.2% or ± 0.05 mV. The average calibration constant for the 8 sensors was 6.7 W/m^2mV. At 30 W m^{-2}, a voltage error of 0.05 mV equates to an error in the heat flux measurement of ± 0.335 W m^{-2}.

4.3 Total Error in the Heat Flux Measurements

There are multiple sources of error in the heat flux measurements. However, each source is independent and therefore the total error is the sum of the individual errors.

$$E_{heat\_flux} = E_{sensor} + E_{voltage} \qquad \text{B.6}$$

or

$$E_{heat\_flux} = 1.5 \mathrm{Wm}^2 + 0.335 \mathrm{Wm}^2 = 1.835 \mathrm{Wm}^2 \approx \pm 1.8 \mathrm{Wm}^2$$

5.0 Thermal Conductivity

Fourier's conduction equation describes the conductive heat flow in a material,

$$\boldsymbol{q} = k \nabla T \qquad \text{B.7}$$

Where q' is the heat flux vector, k is the thermal conductivity of the material and ∇T is the temperature gradient within the material. In this experiment we assume one-dimensional heat flow, so the equation becomes,

$$q = k \frac{\partial T}{\partial z} \qquad \text{B.8}$$

This relation can be reformed to calculate the thermal conductivity from the heat flux and thermal conductivity.

$$k = q \frac{\partial z}{\partial T} \qquad \text{B.9}$$

Heat is transported through snow by conduction, convection, radiation and diffusion (see Chapter 1). It is very difficult to measure the contribution from each of these components, therefore I calculated an effective thermal conductivity that represents bulk heat transfer within the snow.

$$k_e = q \frac{\partial z}{\partial T} = q \frac{\Delta z}{\Delta T} \qquad \text{B.10}$$

The error in the effective thermal conductivity is

$$E_{k_e} = k_e \sqrt{\left(\frac{E_q}{q}\right)^2 + \left(\frac{E_{\Delta z}}{\Delta z}\right)^2 + \left(\frac{E_{\Delta T}}{\Delta T}\right)^2} \qquad \text{B.11}$$

Using typical values from the experiment of

$$k_e = 0.2 \text{ W m}^{-1} \text{ K}^{-1}$$

$$q = 30 \text{ W m}^{-2}$$

$$\Delta z = 0.11 \text{ m}$$

$$\Delta T = 10 \text{ K}$$

the error in the effective thermal conductivity measurement is

$$E_{k_e} = 0.2 \text{Wm}^{-1}\text{K}^{-1} \sqrt{\left(\frac{1.8 \text{Wm}^{-1}}{30 \text{Wm}^{-1}}\right)^2 + \left(\frac{0.00035 \text{m}}{0.11 \text{m}}\right)^2 + \left(\frac{0.26 \text{K}}{10 \text{K}}\right)^2} = 0.01309 \text{Wm}^{-1}\text{K}^{-1} \approx 0.013 \text{Wm}^{-1}\text{K}^{-1}$$